

Alma Mater Studiorum - Università di Bologna

DOTTORATO DI RICERCA IN
CHIMICA

Ciclo 35

Settore Concorsuale: 03/C1 - CHIMICA ORGANICA

Settore Scientifico Disciplinare: CHIM/06 - CHIMICA ORGANICA

A GLASSFUL OF GRAPHENE: GRAPHENE-BASED MATERIALS FOR DRINKING
WATER REMEDIATION

Presentata da: Antonio Bianchi

Coordinatore Dottorato

Luca Prodi

Supervisore

Marco Bandini

Co-supervisore

Magda Monari

Esame finale anno 2023

“O è acqua o è unto!”

[It's either water or grease!]

- Claudia

INDEX

Index	5
List of Acronyms & Abbreviations	7
List of Publications	11
PREFACE: De Legibitate Litterarum Scientificarum	13
PART 1: Introduction	17
1.1 “Tell me of the waters of your homeworld, Usul”	17
1.2 A water issue	17
1.3 Unwanted guests: emerging contaminants	20
1.4 Tapping our resources: Point-of-use purification	23
1.5 Nanotech for big change: entering graphene and related materials	24
1.6 In GO we trust: graphene oxide and adsorption	28
1.7 Implementing nanotechnologies in water purification	29
1.8 Aim of this thesis	31
Bibliography	34
PART 2: Core-Shell System	41
2.1 Double trouble, single solution: adsorptive membranes	41
2.2 Benefits of “core-shell” strategy	42
2.3 An important limitation	43
Bibliography	45
Core-shell graphene oxide-polymer hollow fibers as water filters with enhanced performance and selectivity	47

PART 3: Ion Transport	67
3.1 She sells GO sheets by the seashore: graphene and desalination	67
3.2 HF-GO for ion transport	69
Bibliography	72
Ion Migration Control <i>via</i> Electric Field Modulation in a Core-Shell	
3D GO-Polymer Water Treatment Device	73
PART 4: Coextrusion	95
4.1 The “coextrusion” strategy	95
4.2 New materials for new challenges	98
4.3 Strategy and industry	100
Bibliography	101
Graphene oxide-polysulfone hollow fibers membranes with synergic	
ultrafiltration and adsorption for enhanced drinking water treatment	103
CONCLUSIONS & PERSPECTIVES	129
ACKNOWLEDGMENT	133
APPENDIX 1: Supplementary Information for:	
Core-shell graphene oxide-polymer hollow fibers as water filters with	
enhanced performance and selectivity	135
APPENDIX 2: Supplementary Information for:	
Graphene oxide-polysulfone hollow fibers membranes with synergic	
ultrafiltration and adsorption for enhanced drinking water treatment	155

List of Acronyms & Abbreviations

AAS

Atomic Absorption Spectroscopy

ADWT

Advanced Drinking Water Treatment

AOP

Advanced Oxidation Processes

BSA

Bovine Serum Albumin

CIPRO

Ciprofloxacin

CNR

National Council of Research

CNT

Carbon Nanotubes

CVD

Chemical Vapor Deposition

DWD

Drinking Water Directive

EC

Emerging Contaminants

EDTA

Ethylenediaminetetraacetic Acid

EIS

Electrochemical Impedance Spectroscopy

EOC

Emerging Organic Contaminants

ESI

Electronic Supporting Information

FITC

Fluorescein Isothiocyanate

FS

Filtering Surface

GAC

Granular Activated Carbon

GNP

Graphene Nanoplatelets

GO

Graphene Oxide

GRM

Graphene and Related Materials

HF

Hollow Fibers

HF-GO

Hollow Fibers coated with Graphene Oxide

HPLC-UVHigh-Performance Liquid Chromatography coupled with Ultraviolet Spectroscopy

ICP-OESInductively Coupled Plasma Optical Emission Spectroscopy

ISOFInstitute for Organic Synthesis and Photoreactivity

K_fFiltration Coefficient

K_{ow}Octanol-Water Partition Coefficient

LLDPLiquid-Liquid Displacement Porometer

MFMicrofiltration

MWMolecular Weight

NFNanofiltration

NMPN-Methyl Pyrrolidinone

NPNanoparticles

OFLOXOfloxacin

P-LOQTypical Limit of Quantification

PESPolyethersulfone

PFASPer/Polyfluoroalkyl Substances

POEPoint-of-Entry

POUPoint-of-Use

PSUPolysulfone

Q_{max}Adsorption Capacity

rGOReduced Graphene Oxide

RhBRhodamine B

ROReverse Osmosis

RSDRelative Standard Deviation

SEM

Scanning Electron Spectroscopy

SERSSurface-Enhanced Raman Spectroscopy

SISupporting Information

TMDTransition Metal Dichalcogenides

UFUltrafiltration

UPLC-MS/MSUltrahigh Performance Liquid Chromatography coupled with Mass Spectroscopy

XRDX-Ray Diffraction

List of publications

Core-shell graphene oxide-polymer hollow fibers as water filters with enhanced performance and selectivity

Bianchi, A.; Kovtun, A.; Zambianchi, M.; Bettini, C.; Corticelli, F.; Ruani, G.; Bocchi, L.; Stante, F.; Gazzano, M.; Marforio, T. D.; Calvaresi, M.; Minelli, M.; Navacchia, M. L.; Palermo, V.; Melucci, M.

Faraday Discussions, 2021,227, 274-290; DOI 10.1039/C9FD00117D

Graphene oxide-polysulfone hollow fibers membranes with synergic ultrafiltration and adsorption for enhanced drinking water treatment

Bianchi, A.; Zambianchi, M.; Khaliha, S.; Tunioli, F.; Kovtun, A.; Navacchia, M. L.; Salatino, A.; Xia, Z.; Briñas, E.; Vázquez, E.; Paci, D.; Palermo, V.; Bocchi, L.; Casentini, B.; Melucci, M.

Journal of Membrane Science, 658, (2022), 120707; DOI 10.1016/j.memsci.2022.120707

Graphene oxide nanosheets for drinking water purification by tandem adsorption and microfiltration

Bianchi, A.; Khaliha, S.; Kovtun, A.; Tunioli, F.; Boschi, A.; Zambianchi, M.; Paci, D.; Bocchi, L.; Valsecchi, S.; Polesello, S.; Liscio, A.; Bergamini, M.; Brunetti, M.; Navacchia, M. L.; Palermo, V.; Melucci, M.

Separation and Purification Technology, 300, (2022), 121826; DOI 10.1016/j.seppur.2022.121826

Scalable synthesis and purification of functionalized graphene nanosheets for water remediation

Mantovani, S.; Khaliha, S.; Favaretto, L.; Bettini, C.; Bianchi, A.; Kovtun, A.; Zambianchi, M.; Gazzano, M.; Casentini, B.; Palermo, V.; Melucci, M.

Chemical Communications, 2021,57, 3765-3768; DOI 10.1039/D1CC00704A

Defective graphene nanosheets for drinking water purification: Adsorption mechanism, performance, and recovery

Khaliha, S.; Marforio, T. D.; Kovtun, A.; Mantovani, S.; Bianchi, A.; Navacchia, M. L.; Zambianchi, M.; Bocchi, L.; Boulanger, N.; Iakunkov, A.; Calvaresi, M.; Talyzin, A. V.; Palermo, V.; Melucci, M.

FlatChem, 29, (2021), 100283; DOI 10.1016/j.flatc.2021.100283

Facile high-yield synthesis and purification of lysine-modified graphene oxide for enhanced drinking water purification

Mantovani, S.; Khaliha, S.; Marforio, T. D.; Kovtun, A.; Favaretto, L.; Tunioli, F.; Bianchi, A.; Petrone, G.; Liscio, A.; Palermo, V.; Calvaresi, M.; Navacchia, M. L.; Melucci, M.

Chemical Communications, 2022, 58, 9766; DOI 10.1039/d2cc03256b

PREFACE

De Legibitate Litterarum Scientificarum

- On the legibility of scientific literature

When I started my career in research, not many years ago (say, during my master's thesis), I used to have some issues in reading scientific articles. Almost everything of what I read was difficult to comprehend, uselessly long, or unavoidably boring. After some years in the job, I have read a fair amount of articles, essays, reports, manuals, presentations, and so on, and I can say with a certain security that... nothing has truly changed. Reading scientific articles still requires an effort that other English texts do not demand from me, and coffee is often the sole mean allowing me to finish them.

At some point, in my research group, we considered writing a review. Just like every other person in my generation, the first thing I did was searching on Google “how to write a scientific review”, and in the chaos of blogs, webpages, and posts, I discovered something interesting. It seems that I am not the only one finding it difficult to read scientific papers. Indeed, a share of the scientific community believes that the average paper is written pretty badly. I am not referring to the technical content (i.e. the “quality of the science” researched in the articles), but to the stylistic choices behind the text. The majority of scientific literature follows a specific style of writing, which R. A. Lanham baptized *The Official Style*.¹ This is an extremely formal, old-fashioned style, packed with passive voices, acronyms, long sentences, and with the most flat, colourless, and impersonal prose as possible. This leads to long and boring texts, seldom difficult to comprehend even by people trained in the subject.

Thankfully, there is a movement in the scientific community pushing toward the abandonment of The Official Style, in favour of a lighter, more appealing style, which gives priority to legibility rather than formality. To put it another way, writing “with the reader in mind”. The focal points of this philosophy are the following.²

- 1) Remove *is* forms and limit passive voices, in favour of active verbs (not “this device is capable of performing the act of filtering”, but “this device filters”);
- 2) Use as little acronyms as possible (“comparing rGO with GAC on RhB adsorption *via* UPLC-MS/MS analyses for Q_{\max} detection”);
- 3) Get to the point quickly (“[*five lines of data, procedures, acronyms, subordinates, and appositions*] were studied”);
- 4) Vary the length of the sentences (it sound counterintuitive, but it is important).

This is not just a matter of aesthetics, because more and more studies correlate easiness of reading with higher citations.³⁻⁶ If an article is more accessible (given the technical content), it is more likely to be quoted. Shorter, more compelling titles attract the attention of the reader, and may be the reason for the article is chosen between similar papers. The first title of this thesis was “Development of graphene oxide-based composite materials for advanced drinking water purification technologies”, a formal, impersonal title, which would never allow this thesis to be remembered more than a day. Changing the title to a more modern “A Glassful of Graphene” was an easy choice. The same applies to the title of each paragraph in the introductory text of each part. I am certainly no great writer, but I wrote this thesis with “the reader in mind”, hoping that no one will need coffee to reach the end of it.

Following the philosophy of putting legibility in front of formality, I decided to spread this thesis with text boxes containing my personal thoughts on the topic of the main text, or experiences that arose from studying such subjects. They have...

... this shape.

If the reader does not like this kind of informal intrusions, he/she is free to ignore them. They are not necessary to the academic purpose of this thesis. However, if the reader is interested in a more all-around analysis of how this PhD came to be, I hope they will be a pleasant reading.

Bibliography

1. Lanham, R. A., *Revising Prose*. University of California, 1979, Scribner.
2. Wilke, C. O. Avoiding the official style. <https://clauswilke.com/blog/2015/08/26/avoiding-the-official-style/>.
3. Di Girolamo, N.; Reynders, R. M., Health care articles with simple and declarative titles were more likely to be in the Altmetric Top 100. *J. Clin. Epidemiol.* **2017**, *85*, 32-36.
4. Freeling, B.; Doubleday, Z. A.; Connell, S. D., Opinion: How can we boost the impact of publications? Try better writing. *Proc Natl Acad Sci U S A* **2019**, *116* (2), 341-343.
5. Freeling, B. S.; Doubleday, Z. A.; Dry, M. J.; Semmler, C.; Connell, S. D., Better Writing in Scientific Publications Builds Reader Confidence and Understanding. **2021**, *12*.
6. Hillier, A.; Kelly, R. P.; Klinger, T., Narrative Style Influences Citation Frequency in Climate Change Science. *PLOS ONE* **2016**, *11* (12), e0167983.

PART 1

INTRODUCTION

1.1 “Tell me of the waters of your homeworld, Usul”

One of the book sagas I love the most is the sci-fi masterpiece *Dune*, by Frank P. Herbert.¹ In *Dune*, an interplanetary conspiracy revolves around the monopoly over a substance, called *melange*, which is the foundation of the entire economy of the galaxy. The desert planet of Arrakis is the only source of this substance in the universe, and so tortures, injustice, war, slavery, any kind of wicked behaviour is perpetrated on the planet by the governors, in order to maintain their privilege. Arrakis is fully covered in sand and would be a cruel and unforgiving place to live in even without human malice. Local tribes spend the majority of their energies and lives seeking for water and striving for survival. There is so little water on the planet that when a member of the tribe dies, the water of the body is distilled, the body dried, and the precious liquid is given back to the community. So, to sum up, while the most expensive and devastating wars are fought over a source of power, people crave for the most fundamental need: water. At this point, it does not sound like science fiction anymore.

1.2 A water issue

It is known that the world is facing a water crisis. This is a dual problem: on the one hand, there is a problem of scarcity, and on the other hand, there is a problem of pollution. The *Sustainable Development Goals Report 2022*^{2,3} displaces a dreadful scenario: at 2020, 2 billion people (26% of world population) lack safely managed drinking water; 3.6 billion people (46%) lack

safely managed sanitation; 2.3 billion people (29%) lack basic hygiene. The current rate of progress is bound to quadruple, in order to achieve the goals set for 2030. However, this is not a recent problem. Societies all around the world have managed water resources badly for centuries. In the last 300 years (since the beginning of the industrial era), 80% of natural wetlands have disappeared. In addition to that, more recent crises are worsening the situation: covid-19 pandemic has deeply damaged supply chains, global trade, and isolated communities; the conflict in Ukraine has caused food, fuel and fertilizer prices to skyrocket; and 2022 is witnessing an unprecedented heat wave, which is inducing droughts and heavy hydric stress even in areas traditionally safe from these calamities.

It is mandatory to increase the effort to lower the average pollution levels in water bodies. Only 70% of the wastewaters produced in high-income countries are treated before being released to the environment, and this value dramatically falls to 8% for wastewaters produced in low-income countries. Worldwide, this means that 80% of wastewaters are released to the environment without an adequate treatment. ⁴

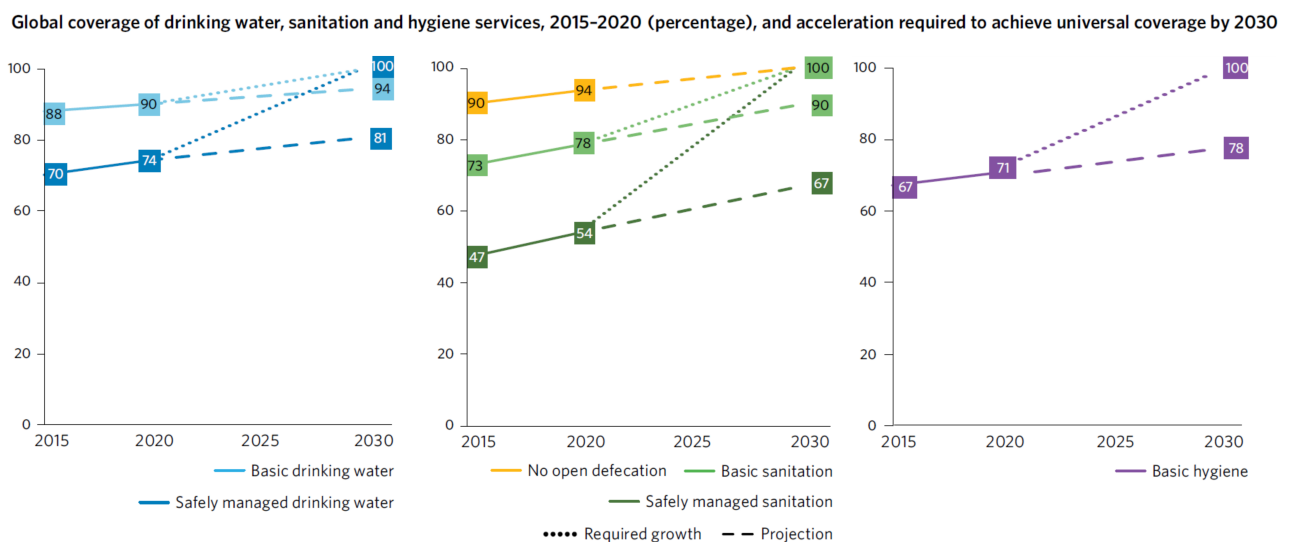


Figure 1 Worldwide situation of drinking and sanitation water use. ²

Thankfully, United Nations endeavour to achieve the Sustainable Development Goals is orienting global policies toward a coordinated effort aimed at the resolution of these problems, even though the possible agency of each country depends deeply on its economic and political stability. The achievement of goal 6, which states to “ensure availability and sustainable management of water and sanitation for all”, is not only a fundamental target *per se*, but it is also necessary to secure other extremely important objectives, such as food security, health, poverty reduction, human rights, and ultimately, peace.

European Union policies about water are consistent with the ones promoted by the United Nations. At the end of 2020, the European Commission promulgated the new Drinking Water Directive 2020/2184,⁵ which represents an important step in the history of water management in this continent. This directive introduces standards aimed at the protection of human health from negative effects of contaminated water resources for human consumption, and the guarantee of its healthiness and cleanliness. Water must contain no microorganisms and parasites, nor substances which quantity or concentration can constitute a risk for human health. It also introduces a risk-based approach to the monitoring of water bodies and distribution lines, designed to identify risks and dangers in the system, and to elaborate the most efficient and cost-effective solution to the problem. Last but not least, the new directive facilitates the access to the information and data on monitoring and evaluation for the public and the scientific community.

The new directive imposes the limit values to a great variety of substances, elements, and microorganisms, which are considered pollutants for water and dangerous for human health. Several of these limit values have been updated since the previous directive (98/83/EC⁶), but many others have been standardized for the first time in this occasion (such as for the infamous poli- and perfluoroalkyl substances, known as PFAS). The degree of quality that the Drinking Water Directive 2020/2184 requires is such that the European Union is aiming at granting the

highest quality water in the world. The European Union is therefore at the forefront in tackling the “water issue”.

1.3 Unwanted guests: emerging contaminants

When approaching the drinking water subject, it takes very little time to meet the term ‘emerging contaminants’ (EC). EC are chemicals or microorganisms usually not monitored in the environment but with a known or suspected adverse effects on ecology and/or human health.⁷ This term traditionally refers to agricultural and industrial chemicals, but now indicates a vast and articulated family of substances and microorganisms (more than 1’000), such as pharmaceuticals, pesticides, herbicides, personal care products, surfactants, endocrine-disrupting compounds, hormones, antibiotics, intestinal enterococci, and Escherichia Coli.⁸⁻¹⁰ These substances can be easily found in rivers, surface and groundwater, municipal wastewater, and in the worst cases, even drinking water and food sources.¹¹ Several EC have been observed at ppb and ppm levels¹² in surface waters all throughout Europe.⁸

One of the main characteristics of *emerging* contaminants is being emerging, indeed, which means that the scientific community has a relatively limited knowledge of their toxicology and environmental effects. This is due to several factors, like the impossibility to test them in municipal water systems, or the fact that by-products may be produced during their permanence in water bodies, or the arise of synergies due to mixtures of compounds.

One of the most concerning features of EC is that conventional drinking water treatment plants (the facilities that provide potable water for big communities) are usually very effective in removing macroscopic solids, organic matter, microorganisms and pathogens, but ineffective in removing EC.¹³⁻¹⁹ Bar-screening, grit removal, peroxidation, coagulation & flocculation, sedimentation, disinfection, sand- and granular activated carbon filtration represent the

traditional (and thus the most common) technologies for water purification, but they are not designed and optimized for this kind of “non-traditional” pollutants. The removal of specific EC requires energy and chemicals consumption, especially at the low concentration at which EC are usually found in raw water, which leads to higher treatment costs and environmental impacts. The technologies employed for the removal of these molecules are known as advanced drinking water treatment (ADWT) processes. They can be roughly divided into three categories: advanced oxidation processes, membrane processes, and adsorption.⁹

Advanced oxidation processes (AOP) exploit the elevated oxidant potential of hydroxyl radicals ($\text{HO}\cdot$; 2.8 V) to chemically deteriorate pollutants.²⁰ The classification of AOP depend on the method used to generate the radical: chemical, sonochemical, photochemical, and electrochemical. The most used radical generators include hydrogen peroxide (H_2O_2), ozone (O_3), UV light, photocatalysts, and their combinations.²¹ While the use of AOP may be highly effective in the degradation of pharmaceuticals, it is noteworthy that their efficiency is limited by the low concentration of target substances in water, the possibility to generate reaction intermediates and by-products, and the relatively high costs when large installations are considered.²⁰

Membrane processes take advantage of semipermeable materials that allow the discrimination between water and other substances: water crosses the membrane (becoming the *permeate*), while substances are retained and concentrated at the membrane surface (giving the *retentate*). Selectivity and efficiency of the membranes depend on the material they are composed of, which define pore size, hydrophilicity and surface charge. Metal, ceramics, glasses, and most of all, polymers may be used to produce membranes²² for water purification.

The driving force of the separation may be used to classify membranes, thus giving pressure driven processes (micro-, ultra-, nanofiltration and reverse osmosis); electric potential gradient (electrodialysis); and concentration gradient (forward osmosis²³). The type of membrane

needed in each situation depends on several parameters, primarily selectivity toward specific pollutants and their concentration in water. The main disadvantage of this technology is that pollutants are not degraded, but transferred from the matrix to the surface of the membrane and concentrated, thus the disposal of the retentate requires additional treatments. On the other hand, membrane processes are easy to implement and operate, have modular design, small energy and chemicals consumption.

Adsorption processes exploit porous, high-surface materials for trapping EC in their structure. They are extremely common processes, thanks to the balance between efficiency, cost-effectiveness, and ease of use. The adsorption capacity of the adsorber depends on several factors, such as density, pore size, active surface area, surface chemistry, and operational parameters (pH, temperature, contact time, etc.). Silica gel, zeolites, alumina, and most of all activated carbon are among the most exploited adsorbers.²⁴ A great research effort was put in enhancing the adsorption efficiency of these materials, which lead to the development of nanoadsorbers, on engineered nanomaterials, meaning materials with at least one dimension in the range 1-100 nm.²⁵ Graphene and its related materials, the protagonists of this work, fall in this latter category; we will talk about them briefly.

ADVANCED DRINKING WATER TREATMENTS

Advanced Oxidation Processes	Membrane Processes	Adsorption Processes
<ul style="list-style-type: none"> ✓ Rapid reaction rates Small footprint No sludge production No concentrated waste 	<ul style="list-style-type: none"> ✓ Low costs Simple devices High selectivity Small footprint 	<ul style="list-style-type: none"> ✓ Low costs Simple devices Easy operability
<ul style="list-style-type: none"> ✗ Relatively high costs Low selectivity Complex operability Byproducts 	<ul style="list-style-type: none"> ✗ Fouling Concentrated waste 	<ul style="list-style-type: none"> ✗ Low selectivity High waste production

Figure 2 Pros and cons of advanced drinking water treatments.

1.4 Tapping our resources: Point-of-use purification

As we mentioned in the previous paragraph, current drinking water treatment plants are inefficient in the removal of EC from water. This is not due to an intrinsic limit of this kind of facility, but to the rapidity that characterizes the insurgence of the EC issue.

Drinking water treatment plants are huge and expensive structures and usually work non-stop to provide water to tens to hundred thousands of people. Their technological progress is extremely slow, because the implementation of research is heavily time- and money-consuming, doubtlessly²⁶ too sluggish to face every new EC that may start infesting the water bodies they treat.

In addition to that, many people all over the world do not have access to municipal water suppliers, or need some other form of augmentation of water security. For example, 84% of all water systems in the USA serve small communities (<500 people) and in most cases treat groundwater. 79% of USA violations of contaminant levels regulation can be attributed to these systems. In emerging mega-cities and developing countries (especially in China and India), water delivery may be intermittent and often require in-site storage (e.g. rainwater harvesting). For these reasons, the market of point-of-use water treatment devices is growing (>\$20 billion per year).

Point-of-use (POU) systems are small and relatively cheap (in the range \$10² and \$10³ per unit) which can be installed on the water supply lines, directly on the tap or dispenser, performing the purification *in situ* where water is ultimately used. The high turnover of replacement parts, the high sales volumes, the small scale, and the low cost make remarkably easy to implement new technologies in POU systems. This market is therefore an optimal environment for research on water purification.

POU systems represent also a springboard for the transfer of new technologies from small scale to larger scales. While POU purifies water right before its pouring, point-of-entry (POE) systems treat water at the entrance of a building (houses, hospitals, factories, etc.) and serve every tap in it. POE systems exploit the same technology of POU systems, but treats higher volumes of water.

1.5 Nanotech for big change: entering graphene and related materials

Among the options for the enhancement of drinking water purification systems, nanotechnology is one of the most promising.²⁵ The term *nanotechnology* implies the use of materials with at least one dimension in the range 1-100 nm. This is a well-established field of knowledge, from which chemistry has been picking up inspiration and resources for its development for at least 50 years now. Some renowned examples are titanium dioxide²⁷, iron (hydro)oxide,²⁸ MXenes,²⁹ and metal-organic frameworks³⁰ (known as MOF), transition metal dichalcogenides (TMD),³¹ and other 2D crystalline materials (such as borophene, germanene, 2D silica, etc.).

These last materials, 2D nanomaterials, are particularly fascinating, thanks to their characteristics, which enable a vast array of applications in several fields. For instance, they possess an elevated superficial area, as high as thousands of m² per gram, which is extremely attractive for the development of nanoplatforms.³² Electrical mobility is a fundamental factor in the development of advanced conductors and semiconductors. Non-nanostructured materials with thousands of cm²/Vs are extremely rare, but several nanomaterials reach (and overcome) this threshold, e.g. the field-effect carrier mobility for electrons of few layered black phosphorus was estimated at about 1'000 cm²/Vs.³³ The intrinsic flexibility of 2D nanomaterials makes them excellent options for the development of flexible electronics and

sensors, which is a difficult terrain for traditional semiconductors and metal-based strain sensors, due to their rigidity and fragility.³⁴ Additionally, some 2D nanomaterials have been reported with tunable band gap³⁵ and exceptional semiconducting properties.³⁶ Additionally, they may express peculiar optical properties when few layers or monolayers are reached, such as optical transparency (which is appealing to the development of optical sensors),³⁷ and X-ray attenuation, which may find great applications in the radiotherapy or phototherapy of cancer,³⁸ and bioimaging.³⁹ Last but not least, 2D nanomaterials display excellent mechanical strength and can sustain heavy stress, with Young's moduli included between 150 and 400 10⁹ Pa.^{40, 41}

To those familiar with scientific dissemination, the term nanotech will immediately recall the famous lecture *There is plenty of room at the bottom*, given by Richard P. Feynman in 1959. At those who do not know this incredible character, I suggest reading the book "Surely you are joking, Mr. Feynman!".⁴² Nobel Prize in physics in 1965, full professor at the Massachusetts Institute of Technology, worked at the Manhattan Project along with Oppenheimer, Fermi and Bohr, he was also a portraitist, a burglar, and a bongo drummer. An interesting reading indeed.

An influential family of nanomaterials is represented by the allotropes of carbon. The reader may be familiar with fullerenes and carbon nanotubes; scientific literature is plenty of interesting applications and studies about these materials, especially nanotubes, in all sort of fields.^{43, 44} In the last decade though, the most prominent member of this family has been graphene.

Graphene is a bidimensional, one-atom thick layer of sp² hybridized carbon organized in a hexagonal lattice.⁴⁵⁻⁴⁸ Since the first time it has been isolated (study that granted Andre Geim and Konstantin Novoselov the Nobel Prize in Physics 2010),⁴⁹ graphene led to a huge and shared research effort to understand its properties. These are indeed astonishing: ultrahigh charge mobility (10⁵ cm²/Vs), high specific surface area (2600 cm²/g), ultrahigh Young's

modulus (10^{12} Pa), optical transparency (98%), intrinsic flexibility, good biocompatibility, and high electrical and thermal conductivity, just to cite a few.⁵⁰⁻⁵⁶

The “honeycomb” structure that characterizes graphene is the foundation for a galaxy of different nanomaterials, with extremely varied characteristics, known as graphene related materials (GRM). It is possible to produce 0D materials (such as graphene quantum dots), 1D materials (nanotubes), and 3D materials (the stacking of graphene layers gives graphite, and its folding in a sphere gives fullerenes). Even more interesting are its 2D derivatives (meaning the materials that maintain its sheet-like structure). Graphene nanoplatelets⁵⁷ (GNP) are nanoparticles made of stacks of graphene with thickness in the range 1-15 nm and radii up to hundreds of microns, they may be treated as nanoparticles in several applications; defective graphene maintains the same structure of graphene, but its surface is scattered with holes and defects,^{58 59} that make it look like a net and modify its conductivity; fluorographene⁶⁰ is a perfluorinated lattice of sp^3 carbon, which is highly susceptible to nucleophilic substitution and reductive defluorination, thus behaving as a highly reactive precursor of modified graphene; and other exotic-sounding variations, such as graphone,⁶¹ graphyne,⁶² and graphdiyne.⁶³

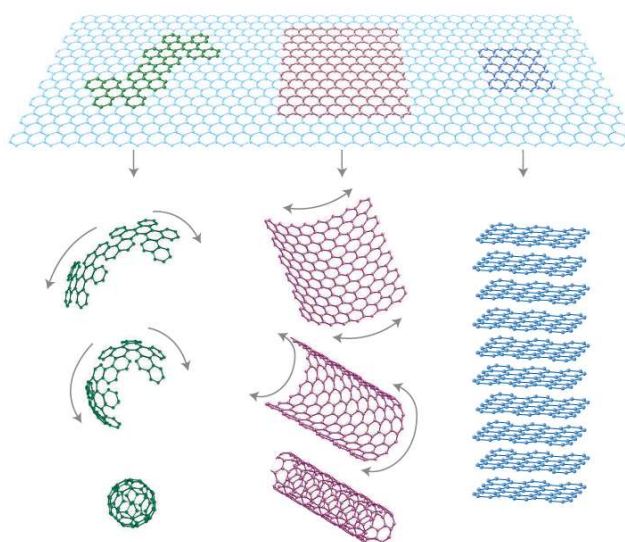


Figure 3 1D, 2D, and 3D geometries of graphene and related materials.⁶⁴

Unfortunately, for what concerns the main subject of this work (water purification), graphene and all of these materials share a common limitation: they are highly hydrophobic, and thus tend to aggregate in water, vastly hindering the active surface exploitable for water treatment. This leads us to the most important GRM for the present work, which is graphene oxide. Graphene oxide (GO) possesses the same 2D structure of pristine graphene, but its surface is populated with non-aromatic areas containing a variety of oxygenated functional groups.⁵⁰ The number of these areas depends on the oxygenation ratio (C/O) and on the chemical procedure exploited for its production. Epoxides and hydroxides represent the majority of the functional groups on the surface of the sheets, while carboxylic and carbonyl groups are the most frequent on the edges of the sheets. These edge groups are the main actor in GO water dispersibility. GO possesses a highly articulated chemical reactivity.⁶⁵ *In primis*, its oxidized functionalities endow it with potential both as green oxidant and solid organic acid, and permit a high number of covalent modifications based on oxygen reactivity.⁶⁶⁻⁷⁰ GO can undergo nucleophilic substitution, redox reactions, electrophilic addition, and condensation.⁷¹ The aromatic structure may also be exploited to bond GO with other molecules, such as organo- and photocatalysts, and enables vicinity-driven synergistic interactions.⁷²

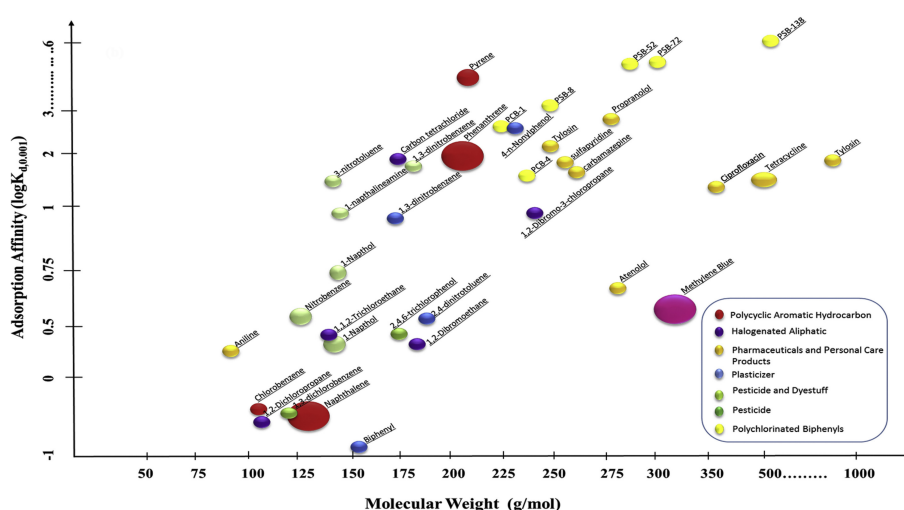


Figure 4 Graphene oxide (GO) structure and its adsorption affinity toward several classes of pollutants. The size of each circle represents the number of studies in literature.⁷³

1.6 In GO we trust: graphene oxide and adsorption

Despite such an interesting reactivity, GO main feature for the sake of this study is its adsorption efficiency. Adsorption is defined by IUPAC as “*an increase in the concentration of a dissolved substance at the interface of a condensed and a liquid phase due to the operation of surface forces*”.⁷⁴ In other words, it describes the adherence of atoms and molecules dispersed in a media to a heterogeneous surface (where the bonding energy is not thoroughly fulfilled). The materials performing the adsorption is called *adsorber* and the substance being adsorbed is called *adsorbate*. Humanity has exploited adsorption for water purification for millennia, with sand and activated carbon as its main players. Even nowadays, these two materials play a role in water purification, from the most rudimental systems to the most complex and advanced facilities (POU, POE, or water purification plants whatsoever). In industry, adsorbents are classified by their composition: oxygen-containing compounds (such as silica gel), polymer-based compounds (such as chitosan), and carbon-based materials (first of all activated carbon). GO is a high-surface oxygenated carbonaceous material suitable for the preparation of polymeric composites; thus its potential in this field is evident.⁷⁵⁻⁷⁸

The secret to GO versatility in water adsorption is the large number of different interactions that it can perform.^{73, 79} The aromatic regions on the surface of GO can adsorb organic molecules with an extended π core and a compatible geometry;⁸⁰ oxygenated groups with lone electron pairs (i.e. carboxyl, epoxy, and hydroxyl) can coordinate electron deficient species in water, such as cationic heavy metals; hydroxyl groups can establish hydrogen bonds with suitable molecules; hydrophobic substances may seek adsorption on GO while in a aqueous media; and complex structures may find the right combination of some or all of these interactions that maximizes their adsorption.⁸¹

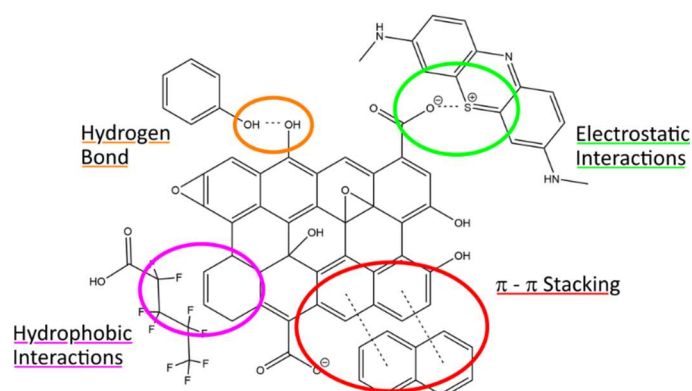


Figure 5 Graphene oxide (GO) may take advantage of several interactions to adsorb pollutants from an aqueous environment.

1.7 Implementing nanotechnologies in water purification

Even if nanotechnologies are not the sole option for POU enhancement, they offer features that are difficult or even impossible to achieve with traditional chemicals or bulk materials. The improvement of selectivity and efficiency is not the only benefit of nanotechnologies, because they permit reactions and processes which are precluded to traditional technologies (such as carbocatalysis^{72, 82} or PFAS adsorption⁸³⁻⁸⁵).

There are fundamentally two ways to integrate nanotechnologies in water purification: bulk use, and embedding them into matrixes. Both of these strategies possess pro and cons, and take into consideration several parameters (such as kinetics, processability in the media, production costs, etc.), but arguably the two most important parameters are 1) the percentage of exploitable surface (to be more specific, the number of adsorption active sites per unit of surface area⁸⁶), and 2) cost and complexity of recovery after treatment. These two parameters are so fundamental because they represent the main concern of two crucial problems in the development of water purification devices, which are respectively 1) maximizing efficiency, and 2) avoiding secondary contaminations.

Maximizing efficiency is a pretty straightforward need. At mass, volume, or cost parity (depending on priority), the higher the purification efficiency of a system, the higher its added market value is. This is not a negligible aspect, because the cost of GRM is still relatively high, if compared with more traditional materials. At Q4 2022, the average cost of graphene spaces from US\$/g 10 to 1000. This value highly depends on the quality of the material (meaning mainly the amount of monolayer mass contraposed to multilayer mass) and the procedure exploited for the production. For example, the two main techniques used in graphene production are GO reduction and chemical vapor deposition (CVD). GO can be reduced at different degrees up to almost total reduction,^{87, 88} giving a material called reduced GO (rGO) with a >99% reduction degree (C/O > 200). This material is very similar to graphene, but is not as good as pure graphene for certain applications (first of all, graphene conductivity has approximately 10^8 S/m,⁸⁸ while rGO has approximately 10^{4-5} S/m^{21, 89}). For what concerns GO (the material we will see the most in this work), its cost is in the range 1-10 US\$/g. For a comparison, granular activated carbon, the benchmark for adsorption in water treatment, has an average cost in the range 1-10 US\$/kg.⁹⁰ Despite being difficult to have a precise estimation of GMR costs (due to the growing number of bulk GRM producers, new technologies, etc.), the trend is that their cost is lowering with the passing of the years.^{88, 91-93}

The reader could be less familiar with the concept of *secondary contamination*, but it likely represent the most important risk posed by the application of nanotechnologies to water purification.⁹⁴ With secondary contamination, we mean the transfer of material from the purification system to the already treated water (for example, if a filter containing nanomaterials releases them in water during its operative life). There are several strategies to face this problem,⁹⁵ but the most competitive is likely to attach or embed nanomaterials to macroporous hierarchical structures, i.e. the production of composite materials that ideally maintain the positive aspects of the nanomaterials, providing them characteristics that annul

their negative aspects. In reality, this kind of solution is indeed effective in preventing secondary contaminations, but bring with it other problematic features, such as hindering mass transport, blocking external stimuli (i.e. light for photoreactivity), or limiting access to the abovementioned exploitable surface area. Thus a strong research effort^{51, 52, 96, 97} is put in finding the best solution aimed at the optimization of these aspects, meaning finding the best compromise for each application. The present thesis work is positioned in this framework.

1.8 Aim of this thesis

This thesis comes from the participation of the Institute for Organic Synthesis and Photoreactivity of the Italian National Research Council (CNR-ISOF) in a European project promoted by the Graphene Flagship, called *Graphil*.⁹⁸

The Graphene Flagship^{99, 100} (together with the Human Brain Project) represent the first generation of Future and Emerging Technologies (FET) Flagships.¹⁰¹ These large-scale, science-driven and mission-oriented community initiatives are funded by the European Commission and aimed at a profound advancement of technological knowledge and growth. The Graphene Flagship was funded in 2013 and is about to be completed by 2023; it brings together 22 countries, 170 partners between universities, research facilities and companies, and invested € 1 billion in research on GRM, with the aim of generating both fundamental knowledge and industrial applications based on these innovative materials. Among the countless projects that the Graphene Flagship cradles, 11 are Spearhead projects, industry-led projects aimed at developing graphene-enabled prototypes into commercial applications. *Graphil* is one of these projects and its mission is the development of compact graphene-based water filters for drinking water purification.

CNR-ISOF (which is the research leader in *Graphil*) and Medica s.p.a. (which is the industrial leader) had already collaborated¹⁰²⁻¹⁰⁴ on the upcycling of industrial wastes obtained during

the production of hollow fibers. The main strategy was attach GO to the scraps obtained during the production of hollow fibers-based blood filters, and use them as adsorbers in water purification. This first success posed the bases for *Graphil*, which is oriented not toward the upcycling of wastes, but toward the development and marketing of brand new graphene-based products. From this assumption, the main focus of my research focused on the development of composite materials based on the implementation of GO into one of Medica s.p.a. products, polymeric hollow fibers. I pursued two different strategies aimed at this, which tackle the compromise between giving new positive features to the hollow fibers and not losing the already assessed ones from two opposite points of view. I also studied the potential of the materials obtained with these two approaches in fundamental studies and real water treatment applications.

In *part 2*, we will see the synthesis of a core-shell composite, obtained coating polyethersulfone hollow fibers with GO, and the theorization of a synergic effect occurring during filtration. The coating strategy maximizes exploitable surface area, sacrificing water permeability.

In *part 3*, we will see a more fundamental study performed on this very core-shell system, aimed at deepening the comprehension of ion transport inside GO membranes.

In *part 4*, we will see the development of coextruded GO-polysulfone hollow fibers and their application in real POU filtering devices. The coextrusion strategy maximizes water permeability, sacrificing exploitable surface area.

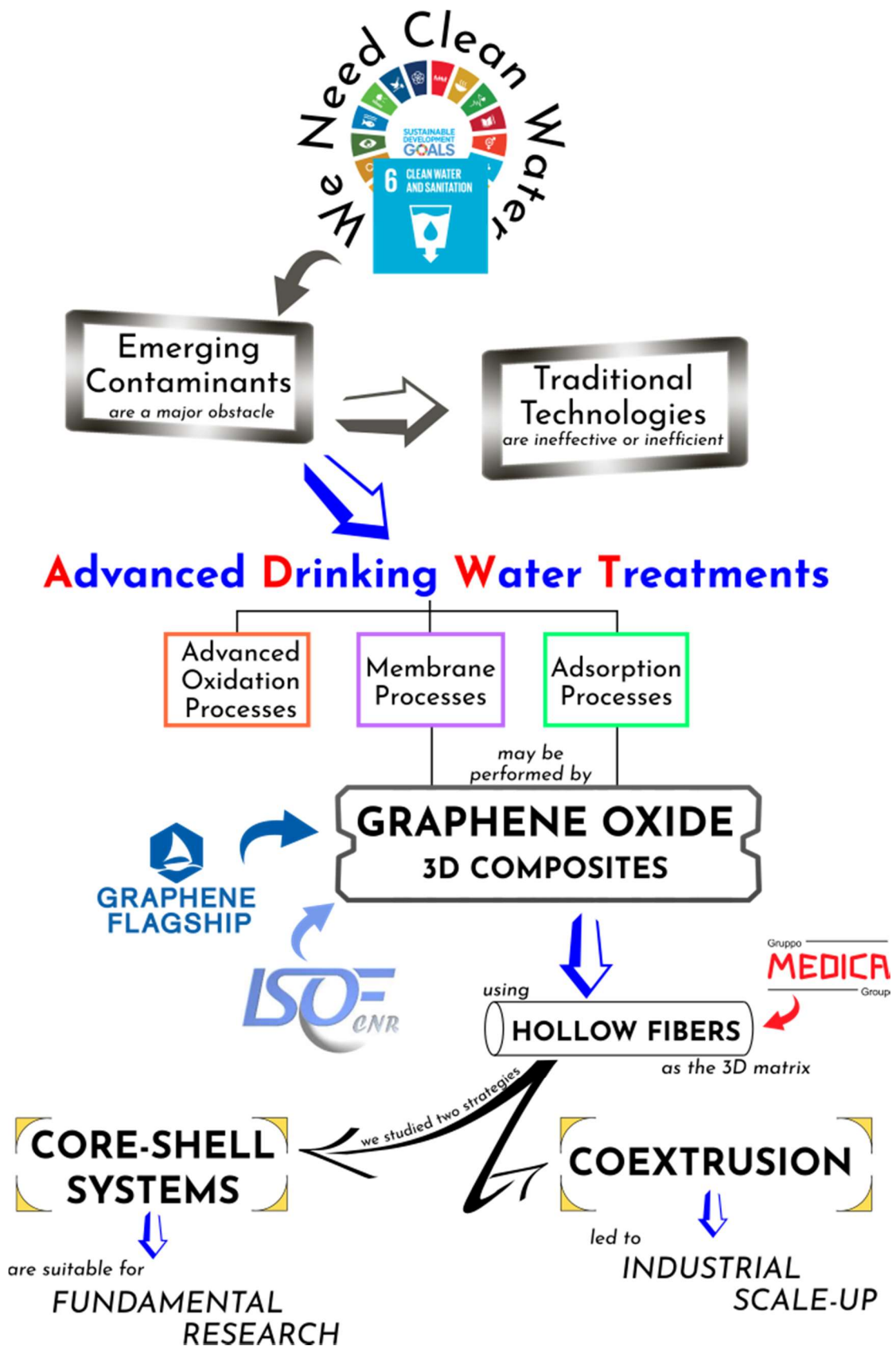


Figure 6 Graphical abstract.

Bibliography

1. Herbert, F. P., *Dune*. Philadelphia, 1965, Chilton Books.
2. <https://unstats.un.org/sdgs/report/2021/goal-06/>.
3. <https://unstats.un.org/sdgs/report/2022/>.
4. <https://unesdoc.unesco.org/ark:/48223/pf0000247553>.
5. <https://eur-lex.europa.eu/legal-content/IT/TXT/?uri=CELEX%3A32020L2184>.
6. <https://eur-lex.europa.eu/legal-content/IT/ALL/?uri=celex%3A31998L0083>.
7. Rosenfeld, P. F.; Feng, L., *Risks of hazardous wastes*. William Andrew: 2011.
8. Petrie, B.; Barden, R.; Kasprzyk-Hordern, B., A review on emerging contaminants in wastewaters and the environment: Current knowledge, understudied areas and recommendations for future monitoring. *Water Res.* **2015**, *72*, 3-27.
9. Teodosiu, C.; Gilca, A.-F.; Barjoveanu, G.; Fiore, S., Emerging pollutants removal through advanced drinking water treatment: A review on processes and environmental performances assessment. *Journal of Cleaner Production* **2018**, *197*, 1210-1221.
10. Tröger, R.; Ren, H.; Yin, D.; Postigo, C.; Nguyen, P. D.; Baduel, C.; Golovko, O.; Been, F.; Joerss, H.; Boleda, M. R.; Polesello, S.; Roncoroni, M.; Taniyasu, S.; Menger, F.; Ahrens, L.; Yin Lai, F.; Wiberg, K., What's in the water? – Target and suspect screening of contaminants of emerging concern in raw water and drinking water from Europe and Asia. *Water Res.* **2021**, *198*, 117099.
11. Murray, K. E.; Thomas, S. M.; Bodour, A. A., Prioritizing research for trace pollutants and emerging contaminants in the freshwater environment. *Environ. Pollut.* **2010**, *158* (12), 3462-3471.
12. Hughes, S. R.; Kay, P.; Brown, L. E., Global Synthesis and Critical Evaluation of Pharmaceutical Data Sets Collected from River Systems. *Environ. Sci. Technol.* **2013**, *47* (2), 661-677.
13. Sorlini, S.; Collivignarelli, M.; Carnevale Miino, M., Technologies for the control of emerging contaminants in drinking water treatment plants. *Environmental engineering and management journal* **2019**, *18*, 2203-2216.
14. Ternes, T. A.; Meisenheimer, M.; McDowell, D.; Sacher, F.; Brauch, H.-J.; Haist-Gulde, B.; Preuss, G.; Wilme, U.; Zulei-Seibert, N., Removal of Pharmaceuticals during Drinking Water Treatment. *Environ. Sci. Technol.* **2002**, *36* (17), 3855-3863.
15. Söregård, M.; Campos-Pereira, H.; Ullberg, M.; Lai, F. Y.; Golovko, O.; Ahrens, L., Mass loads, source apportionment, and risk estimation of organic micropollutants from hospital and municipal wastewater in recipient catchments. *Chemosphere* **2019**, *234*, 931-941.
16. Stackelberg, P. E.; Gibs, J.; Furlong, E. T.; Meyer, M. T.; Zaugg, S. D.; Lippincott, R. L., Efficiency of conventional drinking-water-treatment processes in removal of pharmaceuticals and other organic compounds. *Sci. Total Environ.* **2007**, *377* (2), 255-272.
17. Margot, J.; Kienle, C.; Magnet, A.; Weil, M.; Rossi, L.; de Alencastro, L. F.; Abegglen, C.; Thonney, D.; Chèvre, N.; Schärer, M.; Barry, D. A., Treatment of micropollutants in municipal wastewater: Ozone or powdered activated carbon? *Sci. Total Environ.* **2013**, *461-462*, 480-498.
18. Al Aukidy, M.; Verlicchi, P.; Jelic, A.; Petrovic, M.; Barcelò, D., Monitoring release of pharmaceutical compounds: Occurrence and environmental risk assessment of two WWTP effluents and their receiving bodies in the Po Valley, Italy. *Sci. Total Environ.* **2012**, *438*, 15-25.
19. Verlicchi, P.; Al Aukidy, M.; Zambello, E., Occurrence of pharmaceutical compounds in urban wastewater: Removal, mass load and environmental risk after a secondary treatment—A review. *Sci. Total Environ.* **2012**, *429*, 123-155.
20. Antonopoulou, M.; Evgenidou, E.; Lambropoulou, D.; Konstantinou, I., A review on advanced oxidation processes for the removal of taste and odor compounds from aqueous media. *Water Res.* **2014**, *53*, 215-234.
21. Wang, X.; Mao, Y.; Tang, S.; Yang, H.; Xie, Y. F., Disinfection byproducts in drinking water and regulatory compliance: A critical review. *Frontiers of Environmental Science & Engineering* **2015**, *9* (1), 3-15.

22. Gupta, V. K.; Ali, I., Chapter 5 - Water Treatment by Membrane Filtration Techniques. In *Environmental Water*, Gupta, V. K.; Ali, I., Eds. Elsevier: 2013; pp 135-154.
23. Arribas, P.; Khayet, M.; García-Payo, M. C.; Gil, L., 8 - Novel and emerging membranes for water treatment by hydrostatic pressure and vapor pressure gradient membrane processes. In *Advances in Membrane Technologies for Water Treatment*, Basile, A.; Cassano, A.; Rastogi, N. K., Eds. Woodhead Publishing: Oxford, 2015; pp 239-285.
24. Rodriguez-Narvaez, O. M.; Peralta-Hernandez, J. M.; Goonetilleke, A.; Bandala, E. R., Treatment technologies for emerging contaminants in water: A review. *Chem. Eng. J.* **2017**, *323*, 361-380.
25. Thines, R. K.; Mubarak, N. M.; Nizamuddin, S.; Sahu, J. N.; Abdullah, E. C.; Ganesan, P., Application potential of carbon nanomaterials in water and wastewater treatment: A review. *J. Taiwan Inst. Chem. Eng.* **2017**, *72*, 116-133.
26. Westerhoff, P.; Alvarez, P.; Li, Q.; Gardea-Torresdey, J.; Zimmerman, J., Overcoming implementation barriers for nanotechnology in drinking water treatment. *Environ. Sci.: Nano* **2016**, *3* (6), 1241-1253.
27. Haider, A. J.; Jameel, Z. N.; Al-Hussaini, I. H. M., Review on: Titanium Dioxide Applications. *Energy Procedia* **2019**, *157*, 17-29.
28. Akharam, M. O.; Fagbayigbo, B. O.; Perea, O.; Oputu, O. U.; Olorunfemi, D. I.; Fatoki, O. S.; Opeolu, B. O., Beta-FeOOH nanoparticles: a promising nano-based material for water treatment and remediation. *J. Nanopart. Res.* **2021**, *23* (1), 8.
29. Sun, Y.; Li, Y., Potential environmental applications of MXenes: A critical review. *Chemosphere* **2021**, *271*, 129578.
30. Emam, H. E.; Abdelhameed, R. M.; Ahmed, H. B., Adsorptive Performance of MOFs and MOF Containing Composites for Clean Energy and Safe Environment. *J. Environ. Chem. Eng* **2020**, *8* (5), 104386.
31. Chen, X.; McDonald, A. R., Functionalization of Two-Dimensional Transition-Metal Dichalcogenides. *Adv. Mater.* **2016**, *28* (27), 5738-5746.
32. Hu, Z.; Wu, Z.; Han, C.; He, J.; Ni, Z.; Chen, W., Two-dimensional transition metal dichalcogenides: interface and defect engineering. *ChSRv* **2018**, *47* (9), 3100-3128.
33. Xiao, J.; Long, M.; Zhang, X.; Ouyang, J.; Xu, H.; Gao, Y., Theoretical predictions on the electronic structure and charge carrier mobility in 2D Phosphorus sheets. *Sci. Rep.* **2015**, *5* (1), 9961.
34. Li, Y.; Wang, R.; Guo, Z.; Xiao, Z.; Wang, H.; Luo, X.; Zhang, H., Emerging two-dimensional noncarbon nanomaterials for flexible lithium-ion batteries: opportunities and challenges. *Journal of Materials Chemistry A* **2019**, *7* (44), 25227-25246.
35. Aslam, M. K.; Xu, M., A Mini-Review: MXene composites for sodium/potassium-ion batteries. *Nanoscale* **2020**, *12* (30), 15993-16007.
36. Wang, Y.; Chen, Y.; Lacey, S. D.; Xu, L.; Xie, H.; Li, T.; Danner, V. A.; Hu, L., Reduced graphene oxide film with record-high conductivity and mobility. *Mater. Today* **2018**, *21* (2), 186-192.
37. Dillon, A. D.; Ghidui, M. J.; Krick, A. L.; Griggs, J.; May, S. J.; Gogotsi, Y.; Barsoum, M. W.; Fafarman, A. T., Highly Conductive Optical Quality Solution-Processed Films of 2D Titanium Carbide. *Adv. Funct. Mater.* **2016**, *26* (23), 4162-4168.
38. Cheng, L.; Wang, X.; Gong, F.; Liu, T.; Liu, Z., 2D Nanomaterials for Cancer Theranostic Applications. *Adv. Mater.* **2020**, *32* (13), 1902333.
39. Khan, K.; Tareen, A. K.; Aslam, M.; Wang, R.; Zhang, Y.; Mahmood, A.; Ouyang, Z.; Zhang, H.; Guo, Z., Recent developments in emerging two-dimensional materials and their applications. *Journal of Materials Chemistry C* **2020**, *8* (2), 387-440.
40. Jiang, H.; Zheng, L.; Liu, Z.; Wang, X., Two-dimensional materials: From mechanical properties to flexible mechanical sensors. *InfoMat* **2020**, *2* (6), 1077-1094.
41. Carey, M.; Barsoum, M. W., MXene polymer nanocomposites: a review. *Materials Today Advances* **2021**, *9*, 100120.
42. Feynman, R. P.; Leighton, R., *Surely you are Joking, Mr. Feynman!* 1985, W. W. Norton.

43. Thostenson, E. T.; Ren, Z.; Chou, T.-W., Advances in the science and technology of carbon nanotubes and their composites: a review. *Compos. Sci. Technol.* **2001**, *61* (13), 1899-1912.
44. Bhakta, P.; Barthunia, B., Fullerene and its applications: A review. *Journal of Indian Academy of Oral Medicine and Radiology* **2020**, *32*, 159.
45. Geim, A. K., Graphene: Status and Prospects. *Sci* **2009**, *324* (5934), 1530-1534.
46. Allen, M. J.; Tung, V. C.; Kaner, R. B., Honeycomb Carbon: A Review of Graphene. *Chem. Rev.* **2010**, *110* (1), 132-145.
47. Dreyer, D. R.; Ruoff, R. S.; Bielawski, C. W., From Conception to Realization: An Historical Account of Graphene and Some Perspectives for Its Future. *Angew. Chem. Int. Ed.* **2010**, *49* (49), 9336-9344.
48. Bianco, A.; Cheng, H.-M.; Enoki, T.; Gogotsi, Y.; Hurt, R. H.; Koratkar, N.; Kyotani, T.; Monthieux, M.; Park, C. R.; Tascon, J. M. D.; Zhang, J., All in the graphene family – A recommended nomenclature for two-dimensional carbon materials. *Carbon* **2013**, *65*, 1-6.
49. <https://www.nobelprize.org/prizes/physics/2010/summary/>.
50. Farjadian, F.; Abbaspour, S.; Sadatlu, M. A. A.; Mirkiani, S.; Ghasemi, A.; Hoseini-Ghahfarokhi, M.; Mozaffari, N.; Karimi, M.; Hamblin, M. R., Recent Developments in Graphene and Graphene Oxide: Properties, Synthesis, and Modifications: A Review. *ChemistrySelect* **2020**, *5* (33), 10200-10219.
51. Papageorgiou, D. G.; Kinloch, I. A.; Young, R. J., Mechanical properties of graphene and graphene-based nanocomposites. *PrMS* **2017**, *90*, 75-127.
52. Moharana, S.; Kar, S. K.; Mishra, M. K.; Mahaling, R. N., Synthesis and Properties of Graphene and Graphene Oxide-Based Polymer Composites. In *Surface Engineering of Graphene*, Sahoo, S.; Tiwari, S. K.; Nayak, G. C., Eds. Springer International Publishing: Cham, 2019; pp 175-201.
53. Wei, W.; Qu, X., Extraordinary Physical Properties of Functionalized Graphene. *Small* **2012**, *8* (14), 2138-2151.
54. Lee, C. H.; Chen, S. C.; Su, W. S.; Chen, R. B.; Lin, M. F., Tuning the electronic properties of monolayer graphene by the periodic aligned graphene nanoribbons. *SynMe* **2011**, *161* (5), 489-495.
55. Bilisik, K.; Akter, M., Graphene nanocomposites: A review on processes, properties, and applications. *J. Ind. Text.* **2021**, *51* (3_suppl), 3718S-3766S.
56. Sahoo, S.; Tiwari, S. K.; Nayak, G. C., *Surface Engeneering of Graphene*. 2019.
57. Berktaş, I.; Ghafar, A.; Fontana, P.; Caputcu, A.; Menciloglu, Y.; Okan Burcu, S. Facile Synthesis of Graphene from Waste Tire Silica Hybrid Additives
Optimization Study for the Fabrication of Thermally Enhanced Cement *Molecules* [Online], 2020.
58. Liu, L.; Qing, M.; Wang, Y.; Chen, S., Defects in Graphene: Generation, Healing, and Their Effects on the Properties of Graphene: A Review. *Journal of Materials Science & Technology* **2015**, *31* (6), 599-606.
59. Khaliha, S.; Marforio, T. D.; Kovtun, A.; Mantovani, S.; Bianchi, A.; Luisa Navacchia, M.; Zambianchi, M.; Bocchi, L.; Boulanger, N.; Iakunkov, A.; Calvaresi, M.; Talyzin, A. V.; Palermo, V.; Melucci, M., Defective graphene nanosheets for drinking water purification: Adsorption mechanism, performance, and recovery. *FlatChem* **2021**, *29*, 100283.
60. Chronopoulos, D. D.; Bakandritsos, A.; Pykal, M.; Zbořil, R.; Otyepka, M., Chemistry, properties, and applications of fluorographene. *Applied Materials Today* **2017**, *9*, 60-70.
61. Feng, L.; Zhang, W. X., The structure and magnetism of graphone. *AIP Advances* **2012**, *2* (4), 042138.
62. Vartanian, A., Correcting and perfecting graphyne. *Nature Reviews Materials* **2022**, *7* (6), 427-427.
63. Gao, X.; Liu, H.; Wang, D.; Zhang, J., Graphdiyne: synthesis, properties, and applications. *ChSRv* **2019**, *48* (3), 908-936.
64. Geim, A. K.; Novoselov, K. S., The rise of graphene. *Nature Materials* **2007**, *6* (3), 183-191.
65. Guo, S.; Garaj, S.; Bianco, A.; Ménard-Moyon, C., Controlling covalent chemistry on graphene oxide. *Nature Reviews Physics* **2022**, *4* (4), 247-262.

66. Mantovani, S.; Khaliha, S.; Favaretto, L.; Bettini, C.; Bianchi, A.; Kovtun, A.; Zambianchi, M.; Gazzano, M.; Casentini, B.; Palermo, V.; Melucci, M., Scalable synthesis and purification of functionalized graphene nanosheets for water remediation. *ChCom* **2021**, *57* (31), 3765-3768.
67. Melucci, M.; Treossi, E.; Ortolani, L.; Giambastiani, G.; Morandi, V.; Klar, P.; Casiraghi, C.; Samorì, P.; Palermo, V., Facile covalent functionalization of graphene oxide using microwaves: bottom-up development of functional graphitic materials. *J. Mater. Chem.* **2010**, *20* (41), 9052-9060.
68. Favaretto, L.; An, J.; Sambo, M.; De Nisi, A.; Bettini, C.; Melucci, M.; Kovtun, A.; Liscio, A.; Palermo, V.; Bottoni, A.; Zerbetto, F.; Calvaresi, M.; Bandini, M., Graphene Oxide Promotes Site-Selective Allylic Alkylation of Thiophenes with Alcohols. *Org. Lett.* **2018**, *20* (12), 3705-3709.
69. Dreyer, D. R.; Todd, A. D.; Bielawski, C. W., Harnessing the chemistry of graphene oxide. *ChSRv* **2014**, *43* (15), 5288-5301.
70. Uozumi, Y.; Sugiyama, Y., C-H Allylation of Thiophenes on Graphene Oxide. *Synfacts* **2018**, *14* (09), 0991.
71. Thakur, K.; Kandasubramanian, B., Graphene and Graphene Oxide-Based Composites for Removal of Organic Pollutants: A Review. *Journal of Chemical & Engineering Data* **2019**, *64* (3), 833-867.
72. Su, C.; Loh, K. P., Carbocatalysts: Graphene Oxide and Its Derivatives. *Acc. Chem. Res.* **2013**, *46* (10), 2275-2285.
73. Ersan, G.; Apul, O. G.; Perreault, F.; Karanfil, T., Adsorption of organic contaminants by graphene nanosheets: A review. *Water Res.* **2017**, *126*, 385-398.
74. IUPAC, Compendium of Chemical Terminology, 2nd ed. (the "Gold Book"). Oxford, UK, 1997.
75. Akbari, M.; Shariaty-Niassar, M.; Matsuura, T.; Ismail, A. F., Janus graphene oxide nanosheet: A promising additive for enhancement of polymeric membranes performance prepared via phase inversion. *J. Colloid Interface Sci.* **2018**, *527*, 10-24.
76. Ali, I.; Alharbi, O. M. L.; Tkachev, A.; Galunin, E.; Burakov, A.; Grachev, V. A., Water treatment by new-generation graphene materials: hope for bright future. *Environmental Science and Pollution Research* **2018**, *25* (8), 7315-7329.
77. Cheng, C.; Liu, Z.; Li, X.; Su, B.; Zhou, T.; Zhao, C., Graphene oxide interpenetrated polymeric composite hydrogels as highly effective adsorbents for water treatment. *RSC Advances* **2014**, *4* (80), 42346-42357.
78. Liu, Q.; Shi, J.; Sun, J.; Wang, T.; Zeng, L.; Jiang, G., Graphene and Graphene Oxide Sheets Supported on Silica as Versatile and High-Performance Adsorbents for Solid-Phase Extraction. *Angew. Chem. Int. Ed.* **2011**, *50* (26), 5913-5917.
79. Molla, A.; Li, Y.; Mandal, B.; Kang, S. G.; Hur, S. H.; Chung, J. S., Selective adsorption of organic dyes on graphene oxide: Theoretical and experimental analysis. *ApSS* **2019**, *464*, 170-177.
80. Peng, B.; Chen, L.; Que, C.; Yang, K.; Deng, F.; Deng, X.; Shi, G.; Xu, G.; Wu, M., Adsorption of Antibiotics on Graphene and Biochar in Aqueous Solutions Induced by π - π Interactions. *Sci. Rep.* **2016**, *6* (1), 31920.
81. Peng, W.; Li, H.; Liu, Y.; Song, S., A review on heavy metal ions adsorption from water by graphene oxide and its composites. *J. Mol. Liq.* **2017**, *230*, 496-504.
82. Fan, X.; Zhang, G.; Zhang, F., Multiple roles of graphene in heterogeneous catalysis. *ChSRv* **2015**, *44* (10), 3023-3035.
83. Adeleye, A. S.; Conway, J. R.; Garner, K.; Huang, Y.; Su, Y.; Keller, A. A., Engineered nanomaterials for water treatment and remediation: Costs, benefits, and applicability. *Chem. Eng. J.* **2016**, *286*, 640-662.
84. Baruah, S.; Najam Khan, M.; Dutta, J., Perspectives and applications of nanotechnology in water treatment. *Environmental Chemistry Letters* **2016**, *14* (1), 1-14.
85. Qu, X.; Alvarez, P. J. J.; Li, Q., Applications of nanotechnology in water and wastewater treatment. *Water Res.* **2013**, *47* (12), 3931-3946.

86. Lounsbury, A. W.; Yamani, J. S.; Johnston, C. P.; Larese-Casanova, P.; Zimmerman, J. B., The role of counter ions in nano-hematite synthesis: Implications for surface area and selenium adsorption capacity. *J. Hazard. Mater.* **2016**, *310*, 117-124.
87. Guex, L. G.; Sacchi, B.; Peuvot, K. F.; Andersson, R. L.; Pourrahimi, A. M.; Ström, V.; Farris, S.; Olsson, R. T., Experimental review: chemical reduction of graphene oxide (GO) to reduced graphene oxide (rGO) by aqueous chemistry. *Nanoscale* **2017**, *9* (27), 9562-9571.
88. Döscher, H.; Schmaltz, T.; Neef, C.; Thielmann, A.; Reiss, T., Graphene Roadmap Briefs (No. 2): industrialization status and prospects 2020. *2D Materials* **2021**, *8* (2), 022005.
89. Wu, Y.; Wu, Y.; Kang, K.; Chen, Y.; Li, Y.; Chen, T.; Xu, Y., Characterization of CVD graphene permittivity and conductivity in micro-/millimeter wave frequency range. *AIP Advances* **2016**, *6* (9), 095014.
90. <https://www.globenewswire.com/en/news-release/2021/12/16/2353239/0/en/Global-Activated-Carbon-Market-Rising-Demand-for-Water-Purification-Drives-U-S-Trade-IndexBox.html>.
91. <https://investingnews.com/daily/tech-investing/nanoscience-investing/graphene-investing/graphene-cost/>.
92. Döscher, H.; Reiss, T., Graphene Roadmap Briefs (No. 1): innovation interfaces of the Graphene Flagship. *2D Materials* **2021**, *8* (2), 022004.
93. Zanjani, J. S. M.; Poudeh, L. H.; Ozunlu, B. G.; Yagci, Y. E.; Menciloglu, Y.; Saner Okan, B., Development of waste tire-derived graphene reinforced polypropylene nanocomposites with controlled polymer grade, crystallization and mechanical characteristics via melt-mixing. *Polym. Int.* **2020**, *69* (9), 771-779.
94. Qu, X.; Brame, J.; Li, Q.; Alvarez, P. J. J., Nanotechnology for a Safe and Sustainable Water Supply: Enabling Integrated Water Treatment and Reuse. *Acc. Chem. Res.* **2013**, *46* (3), 834-843.
95. Khaliha, S.; Bianchi, A.; Kovtun, A.; Tunioli, F.; Boschi, A.; Zambianchi, M.; Paci, D.; Bocchi, L.; Valsecchi, S.; Polesello, S.; Liscio, A.; Bergamini, M.; Brunetti, M.; Luisa Navacchia, M.; Palermo, V.; Melucci, M., Graphene oxide nanosheets for drinking water purification by tandem adsorption and microfiltration. *Sep. Purif. Technol.* **2022**, *300*, 121826.
96. Perreault, F.; Fonseca de Faria, A.; Elimelech, M., Environmental applications of graphene-based nanomaterials. *ChSRv* **2015**, *44* (16), 5861-5896.
97. Yousefi, N.; Lu, X.; Elimelech, M.; Tufenkji, N., Environmental performance of graphene-based 3D macrostructures. *Nat. Nanotechnol.* **2019**, *14* (2), 107-119.
98. <https://graphene-flagship.eu/innovation/spearheads/c3-sh01-graphil/>.
99. <https://graphene-flagship.eu/>.
100. Ferrari, A. C.; Bonaccorso, F.; Fal'ko, V.; Novoselov, K. S.; Roche, S.; Bøggild, P.; Borini, S.; Koppens, F. H. L.; Palermo, V.; Pugno, N.; Garrido, J. A.; Sordan, R.; Bianco, A.; Ballerini, L.; Prato, M.; Lidorikis, E.; Kivioja, J.; Marinelli, C.; Ryhänen, T.; Morpurgo, A.; Coleman, J. N.; Nicolosi, V.; Colombo, L.; Fert, A.; Garcia-Hernandez, M.; Bachtold, A.; Schneider, G. F.; Guinea, F.; Dekker, C.; Barbone, M.; Sun, Z.; Galiotis, C.; Grigorenko, A. N.; Konstantatos, G.; Kis, A.; Katsnelson, M.; Vandersypen, L.; Loiseau, A.; Morandi, V.; Neumaier, D.; Treossi, E.; Pellegrini, V.; Polini, M.; Tredicucci, A.; Williams, G. M.; Hee Hong, B.; Ahn, J.-H.; Min Kim, J.; Zirath, H.; van Wees, B. J.; van der Zant, H.; Occhipinti, L.; Di Matteo, A.; Kinloch, I. A.; Seyller, T.; Quesnel, E.; Feng, X.; Teo, K.; Rupesinghe, N.; Hakonen, P.; Neil, S. R. T.; Tannock, Q.; Löfwander, T.; Kinaret, J., Science and technology roadmap for graphene, related two-dimensional crystals, and hybrid systems. *Nanoscale* **2015**, *7* (11), 4598-4810.
101. <https://fet11.ercim.eu/about/fet-flagships>.
102. Posati, T.; Nocchetti, M.; Kovtun, A.; Donnadio, A.; Zambianchi, M.; Aluigi, A.; Capobianco, M. L.; Corticelli, F.; Palermo, V.; Ruani, G.; Zamboni, R.; Navacchia, M. L.; Melucci, M., Polydopamine Nanoparticle-Coated Polysulfone Porous Granules as Adsorbents for Water Remediation. *ACS Omega* **2019**, *4* (3), 4839-4847.
103. Zambianchi, M.; Aluigi, A.; Capobianco, M. L.; Corticelli, F.; Elmi, I.; Zampolli, S.; Stante, F.; Bocchi, L.; Belosi, F.; Navacchia, M. L.; Melucci, M., Polysulfone Hollow Porous Granules Prepared

from Wastes of Ultrafiltration Membranes as Sustainable Adsorbent for Water and Air Remediation. *Advanced Sustainable Systems* **2017**, 1 (7), 1700019.

104. Zambianchi, M.; Durso, M.; Liscio, A.; Treossi, E.; Bettini, C.; Capobianco, M. L.; Aluigi, A.; Kovtun, A.; Ruani, G.; Corticelli, F.; Brucale, M.; Palermo, V.; Navacchia, M. L.; Melucci, M., Graphene oxide doped polysulfone membrane adsorbers for the removal of organic contaminants from water. *Chem. Eng. J.* **2017**, 326, 130-140.

PART 2

CORE-SHELL SYSTEM

2.1 Double trouble, single solution: adsorptive membranes

In the article you are about to read, polyethersulfone hollow fibers (HF) are coated with GO in order to produce a composite material (HF-GO). Hollow fibers¹⁻³ are an established technology that find application in many fields, thanks to several worthwhile characteristics, *in primis* a significantly larger effective membrane area per unit of volume than flat membranes. Briefly, HF are flexible, porous tubes with an internal diameter in the range 10^2 - 10^3 μm . The dimension of the pores that populate the walls of the fibers, their pore size distribution, and their shape depend on the polymer and the procedure used to create them. Medica s.p.a.⁴ is one of the few Italian HF producers. They produce HF with two different polymers: polysulfone^{5,6} (PSU) and polyethersulfone⁷⁻⁹ (PES). These HF possess cut-offs of 5 nm and 150 nm, respectively, which makes them suitable to perform ultrafiltration (UF) and microfiltration (MF), respectively again.

This kind of membrane is highly effective in retaining particles over their cut-off ($R^2 > 9.9$), but is utterly ineffective in removing small molecules from water. On the other hand, GO is an excellent adsorber of small molecules but is unsuitable for the production of HF. Their combination in a composite gives what is called an *adsorptive membrane*,¹⁰⁻¹³ meaning a membrane capable filtering particles and adsorb molecules simultaneously. Adsorption and filtration are normally performed in water purification during two distinct steps, both in POU/POE systems and in water purification plants. Adsorptive membranes permit the

development of multivalent filters that unify adsorption and filtration in a single step, allowing simpler, cheaper, and less energy demanding purification systems.

2.2 Benefits of “core-shell” strategy

The choice of creating a core-shell system is bound to the desire of maximizing the exploitable surface of GO. Water is forced to pass through the filtering module in a dead end setup, compelling a transmembrane motion. When a GO suspension passes through the module, GO sheets (being larger than the pore size of the HF) stack onto the surface of PES, and are then fixated in the form of a solid coating through a thermal annealing. In this way, all of GO is exploitable for adsorption, in contraposition to the coextruded composite (PSUGO, which we will see in part 4), where a fraction of GO is submerged into the polymeric matrix and thus cannot be reached by water (and consequently is not exploitable for adsorption). The repetition of the loading/annealing cycle allows to tune the amount of GO loaded in each module and permits ultrahigh GO loadings.

This allows a total exploitation of GO, which is then comparable to the bulk use, but prevents the need of recovery: GO never leaves the filtering module (as demonstrated with UV-Vis analyses), effectively avoiding secondary contaminations. The system is therefore compatible with human use. In addition to that, we had the filtered water certified as potable by an accredited laboratory. It is also important to stress the fact that all of the experiments in this paper use tap water as the matrix, spiked with the analytes. The majority of data collected in this field are obtained from purified water spiked with analytes, which obnubilates the potential for real applications of those studies.

Another important aspect is that the kinetics of the composite is much better than that of bulk GO. HF-GO achieves significant removal of EC within a contact time (GO-pollutants) of ~ 10 s, while equilibrium conditions would require minutes or hours to be achieved (depending on the pollutant). We explained this performance to the arising of a synergistic effect. Water must cross the GO coating in order to leave the filtering module. In doing so, it forces the pollutants in between the GO sheets, creating the optimal conditions for their intercalation and adsorption. Both X-ray diffraction spectroscopy (XRD) and molecular dynamics (MD) simulations support this model, highlighting that the swelling (i.e. the increase of interlayer distance) of GO sheets corresponds perfectly to the thickness of the studied pollutant (ofloxacin, 0.14 nm).

2.3 An important limitation

The loss in water permeability represent the main drawback of the “core-shell” strategy. The higher the amount of GO loaded into the filtering module is, the harder it is for water to cross the GO coating. Unfortunately, this hinders significantly the potential for industrial application of this material in POU devices, considering that pipeline water is supplied at 3 bar, which translates roughly in 10 L/min. This means that it is necessary to choose the best compromise between GO loading and loss in water permeability. For the sake of this study (and the following one), the best ratio happened to be 5% GO w/w to the mass of the composite.

Despite this (yet) unresolved problem limits the industrial applications of HF-GO, it still represent an interesting 3D membrane to study, as we will see in part 3: ion transport. On the other hand, in part 4: coextrusion, we will see a different approach, where water permeability has priority over the exploitation of the surface, and all that this implies.

The poster I prepared for core-shell work was my first poster contribution as a PhD student. The covid-19 lockdown started when I was at the fourth month of the PhD, so the first conferences I attended were purely online, and so were my posters (you may find the link here ¹⁴). Online conferences were doubtlessly fundamental during the pandemic outbreak. They allowed numerous research groups to have their work slowed down instead of shut down, and the scientific community to remain in touch. So, as scientists, we must be grateful that this futuristic phenomenon happened. At some point, online conferences became incredibly articulated: parallel sessions, dedicated chatrooms, events, videos, even examples of gamification, with “victory points”-like systems to reward the most active participants. At that point, I asked myself if we were to go back to in-person conferences at all. If it possible to recreate an audience online, and save on travel costs, renting, catering, and so on, why bother meeting at all? Well, there is an important reason, indeed. Online conferences make up for just one of the two fundamental task of conferences, which is making information flow throughout the scientific community. The second task, which in my humble opinion is the most important, is networking, meaning the creation of significant connections between people. The scientific community works because is a *community*, even before being *scientific*. It is composed of people who exchange ideas, opinions, viewpoints, forge relationships, and argue, too. The most enthralling discussions between scientists do not happen from the speaker stand to the armchairs in the audience, with a microphone in the middle, but from a bench to a stool, with a coffee or beer in between (depending on latitude). Just like any other community, our one is as strong as it is united and cohesive. Personal relationships between scientists are as fundamental to scientific progress as the purely work-related ones. Online conferences permit the seconds, but not the firsts, due to the banal fact that drinking a coffee on your own is not the same experience as drinking it with others. I think that online conferences are a powerful and versatile tool for our community, but will not outdate in-person conferences.

Bibliography

1. Cheung, T. W.; Li, L., A review of hollow fibers in application-based learning: from textiles to medical. *Textile Research Journal* **2017**, *89* (3), 237-253.
2. Peng, N.; Widjojo, N.; Sukitpaneelit, P.; Teoh, M. M.; Lipscomb, G. G.; Chung, T.-S.; Lai, J.-Y., Evolution of polymeric hollow fibers as sustainable technologies: Past, present, and future. *Prog. Polym. Sci.* **2012**, *37* (10), 1401-1424.
3. Tian, Y.; Wang, Z.; Wang, L., Hollow fibers: from fabrication to applications. *ChCom* **2021**, *57* (73), 9166-9177.
4. www.medica.it.
5. Cabasso, I.; Klein, E.; Smith, J. K., Polysulfone hollow fibers. I. Spinning and properties. *J. Appl. Polym. Sci.* **1976**, *20* (9), 2377-2394.
6. Mamah, S. C.; Goh, P. S.; Ismail, A. F.; Suzaimi, N. D.; Yogarathinam, L. T.; Raji, Y. O.; El-badawy, T. H., Recent development in modification of polysulfone membrane for water treatment application. *J. Water Process Eng.* **2021**, *40*, 101835.
7. Chung, T. S.; Teoh, S. K.; Hu, X., Formation of ultrathin high-performance polyethersulfone hollow-fiber membranes. *J. Membr. Sci.* **1997**, *133* (2), 161-175.
8. Tsai, H. A.; Kuo, C. Y.; Lin, J. H.; Wang, D. M.; Deratani, A.; Pochat-Bohatier, C.; Lee, K. R.; Lai, J. Y., Morphology control of polysulfone hollow fiber membranes via water vapor induced phase separation. *J. Membr. Sci.* **2006**, *278* (1), 390-400.
9. Xu, Z.-L.; Alsahy Qusay, F., Polyethersulfone (PES) hollow fiber ultrafiltration membranes prepared by PES/non-solvent/NMP solution. *J. Membr. Sci.* **2004**, *233* (1), 101-111.
10. Hao, S.; Jia, Z.; Wen, J.; Li, S.; Peng, W.; Huang, R.; Xu, X., Progress in adsorptive membranes for separation – A review. *Sep. Purif. Technol.* **2021**, *255*, 117772.
11. Huang, Z.-Q.; Cheng, Z.-F., Recent advances in adsorptive membranes for removal of harmful cations. *J. Appl. Polym. Sci.* **2020**, *137* (13), 48579.
12. Qalyoubi, L.; Al-Othman, A.; Al-Asheh, S., Recent progress and challenges of adsorptive membranes for the removal of pollutants from wastewater. Part II: Environmental applications. *Case Stud. Chem. Environ. Eng.* **2021**, *3*, 100102.
13. Roper, D. K.; Lightfoot, E. N., Separation of biomolecules using adsorptive membranes. *J. Chromatogr.* **1995**, *702* (1), 3-26.
14. <https://2dmaterials-rsc.ipostersessions.com/default.aspx?s=1B-17-B5-3C-16-38-91-E5-37-BD-F4-95-A3-4C-D0-F7&guestview=true>.

Core-shell graphene oxide-polymer hollow fibers as water filters with enhanced performance and selectivity

Alessandro Kovtun,^{a,‡} Antonio Bianchi,^{a,‡} Massimo Zambianchi,^a Cristian Bettini,^a Franco Corticelli,^b
G. P. Ruani,^c Letizia Bocchi,^d Francesco Stante,^e Massimo Gazzano,^a Tainah Dorina Marforio,^f Matteo
Calvaresi,^f Matteo Minelli,^g Maria Luisa Navacchia,^a

Vincenzo Palermo,^{a,h*} Manuela Melucci^{a*}

* Corresponding authors

^a Consiglio Nazionale delle Ricerche-Institute of Organic Synthesis and Photoreactivity (CNR-ISOF),
via Piero Gobetti 101, 40129 Bologna, Italy

^b Consiglio Nazionale delle Ricerche-Institute for Microelectronics and Microsystems, (CNR-IMM),
via Piero Gobetti 101, 40129 Bologna, Italy ^c Consiglio Nazionale delle Ricerche-Institute of
Nanostructured Materials (CNR-ISMN), via Piero Gobetti 101, 40129 Bologna, Italy

^d Medica spa, via degli Artigiani 7, 41036 Medolla, MO, Italy

^e Stante Laboratories, Via del Chiù 68-70, Bologna, Italy

^f Alma Mater Studiorum – University of Bologna, Department of Chemistry ‘G. Ciamician’, via Selmi
2, 40129 Bologna, Italy

^g Alma Mater Studiorum – University of Bologna, Department of Civil, Chemical, Environmental and
Materials Engineering (DICAM), via Terracini, 28 40131 Bologna, Italy

^h Chalmers University of Technology, Industrial and Materials Science, Hörsalsvägen 7A, SE-412 96
Göteborg, Sweden

‡ These authors contributed equally to this work

DOI: <https://doi.org/10.1039/C9FD00117D>

Abstract

Extraction of proteins from blood biological fluids requires the removal of large aggregates or cells by membrane filtration. However, conventional filters, based on simple size exclusion, do not allow to remove small molecules such as antibiotics. Here, we demonstrate that a graphene oxide (GO) layer can be firmly immobilized either inside or outside polyethersulfone-polyvinylpyrrolidone hollow fibers (PES) modules and that the resulting core-shell structure inherits the microfiltration ability of PES and the adsorption selectivity of GO.

GO nanosheets were deposited on fiber surface by filtration of a GO suspension through a PES cartridge (cut-off 0.1-0.2 μm), then fixed on it by thermal annealing at 80°C, rendering them insoluble. The filtration cut-off, retention selectivity and efficiency of the resulting inner and outer modified hollow fibers (HF-GO) were tested by performing filtration on water spiked with bovin serum albumin (BSA, 66KDa, ≈ 15 nm sized), monodisperse polystyrene nanoparticles (52 nm and 303 nm sized), water contaminated with two quinolonic antibiotics (ciprofloxacin and ofloxacin) and rhodamine B (RhB). These tests showed that microfiltration capability of PES was retained by HF-GO, in addition the GO coating can capture the molecular contaminants while letting through BSA and smaller Polystyrene nanoparticles. Combined XRD, molecular modelling and adsorption experiments show the separation mechanism does not rely only on a physical size exclusion, but it involves intercalation of solute molecules between GO layers.

Introduction

The development of novel membrane materials for purification of fluids is of great interest for the fabrication of personalized biomedical treatments (i.e. selective apheresis, dialysis), specific chemicals separation (organic solute from organic matrixes), advanced water purification¹ and gas separation technologies.²

Polymeric membranes are currently exploited at industrial level for a variety of processes applications, spanning from blood filtration to food/drugs purification, drinking and waste-water purification.³

The market trend for polymeric membrane filtration modules is growing, and it is expected to further increase in the next few years due to the increasing demand of advanced healthcare treatments and also drinkable water. In general, polymeric membrane filtration modules may be classified into three types, namely plate and frame, spiral wound, and hollow fiber (HF) modules. Among them, hollow fiber modules are the most used as separation units in industry because of their unique characteristics of self-support, high membrane packing density, and high surface/volume ratio.⁴ Compared to planar membranes, the hollow-fiber configuration has a much larger membrane area per unit volume of membrane module. Surface to volume ratio is about 300-500 m²/m³ for plate and frame modules, 600-800 m²/m³ for spiral wound modules, and 6000-13000 m²/m³ for hollow fiber modules, this resulting in a higher productivity. Nowadays, hollow fibers configurations are widely used in basically all types of membranes separation, including gas separation, ultrafiltration, pervaporation, dialysis and supported liquid membrane extraction.

Filtration mechanism of these membranes mainly relies on size exclusion, and the pore-size ultimately defines the cut-off range. Microfiltration is widely used in water treatment as a disinfection step and plasma apheresis since colloidal particles, microorganisms and other particulate material of size larger than about 200 nm are removed. Ultrafiltration and nanofiltration membrane modules have higher cut-off, 1-10 nm and 100-200 nm, respectively, thus enabling the decontamination from viruses/endotoxines (ultrafiltration) and low molecular weight molecules (nanofiltration), but the throughput is much lower than what achievable for microfiltration.

Though, there is an urgent market and societal need to improve the removal of emerging concern contaminants (EOC) such as pesticides or pharmaceuticals, surfactants used in large quantities in civil industrial and farming activities, able to contaminate water sources or food liquids causing severe environmental and health problems.

Recently, membrane doping with nanomaterials has been reported as a promising strategy to tune the

selectivity and enhance the efficiency of polymeric membranes.⁵ Among nanomaterials, graphene oxide (GO) is particularly suitable for promoting selective recognition processes due to its intrinsic 2-D configuration, a high surface area and abundance of surface chemical groups. For instance, addition of small amount of GO in polysulfones based membranes obtained by phase inversion increased their hydrophilicity and antimicrobial activity, reduced the biofouling⁶, promoted arseniate rejection,⁷ and allowed for oil water separation.⁸ In general, graphene containing membranes are receiving increasing attention because they exhibit enhanced separation performance with enormous potential outcomes for ion sieving, desalination and water purification applications.⁹⁻¹²

Graphene oxide has also excellent adsorption properties toward EOC (including Pharmaceuticals and Personal Care Products)¹³⁻¹⁶ and metal ions even at very low concentration.¹⁷ This feature that have led to the development of 3D structures with removal efficiencies superior to that of other nanomaterial-based adsorbents included Granular Activated Carbon (GAC), the industrial standard, for some metal ions and organic compounds. Moreover, covalent chemical modification of the oxygen-based functionalities of GO allows to tune the adsorption selectivity of GO based structure.¹⁸ In this direction, enhanced adsorption of heavy metal ions and organic dyes in water and wastewater have been reported for EDTA¹⁹ sulphonated²⁰ and amino rich²¹ graphenes.

Aiming at the exploitation of both adsorption properties and membrane enhancing effects of GO to develop new multifunctional filters, we recently demonstrated the superior efficiency of GO doped polysulfone porous structures toward hydrophilic organic contaminants including dyes and drugs.²² We also described a simple method to fix GO on scraps of the production of polysulfone ultrafiltration membranes.²³ The process involves the partial removal under vacuum of water from a GO and PS suspension followed by thermal fixation.²⁴ This material showed enhanced removal capability (up to seven times) toward polar organic contaminants (e.g., ofloxacin and Rhodamine B) thanks to the high hydrophilicity of the GO layer exposed to the surface in contact with water. The coating process allows to fix GO on PS surface by means of supramolecular interactions, by exploiting spontaneous aggregation of GO sheets on PS and enable to cover up to 50% of the PS total surface area. The filter

could capture effectively EOC, but poor retention was obtained for larger chemical moieties with respect to hollow fibers based ultrafiltration cartridges.

Typically, polymers composites containing Graphene or GO are prepared by mixing or co-extrusion, then shaped in the final form. GO or graphene could in some cases be applied on the surface of simple shapes, such as powders²⁴ or flat sheets;²⁵ until now, it has instead never been possible to apply GO coatings on the surface of finite commercial devices such as filters.

We thus developed a completely different approach exploiting the filtration capability of commercial hollow fibers filter to achieve a uniform coating on a geometrically complex substrate. We could thus obtain GO coatings on polyethersulfone-polyvinylpyrrolidinone hollow fibers (HF) made of a commercial polymer, *Versatile PES*[®] (Fig. 1a-d), already assembled in a working filter cartridge. Then, we used these filters for purification of water solutions and showed the possibility to selectively remove small molecules (including two antibiotics of current environmental concern).

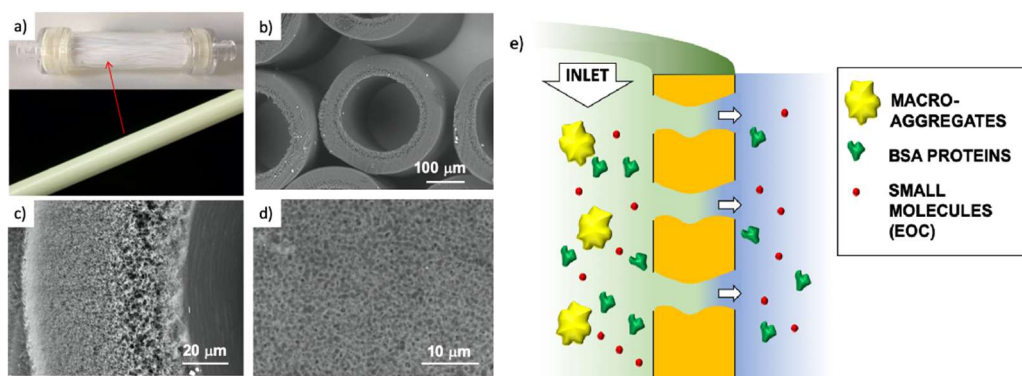


Figure 1. a) *Versatile PES*[®] hollow fiber filtration cartridge (lab. scale prototype 10 cm length) and single fiber, in the cartridge the edges of the fiber capillaries are sealed by an epoxy resin, b) fibers, c) cross-section, d) detail of the outer wall pores. E) Cartoon of the filtration through the cartridge (in-out).

Stable coating of the outer or inner walls of PES hollow fibers with a GO membrane and controlled membrane thickness was achieved by filtration of a GO suspension in dead-end configuration (Fig. 2), followed by thermal fixation by annealing in oven. Retained microfiltration capability was assessed for HF-GO by filtering a mixture containing:

1) nanoscopic objects of different size protein (Bovine Serum Albumin, BSA, $M_w=66\text{KDa}$) and polystyrene beads (52 nm and 303 nm sized);

2) molecular EOC contaminants. We choose as realistic test molecules ofloxacin, ciprofloxacin (two quinolonic antibiotics under monitoring by EU) and rhodamine B (a textile dye, Fig. S1_ESI).

2. Results and Discussion

2.1 GO immobilization and fixation

Graphene Oxide Powder < 35 mesh (purchased by Abalonyx, sheet lateral size about 1 μm , many primary single sheets declared) was suspended in milliQ water (2 mg/ml) and sonicated for 4 hours. Then, the GO solution was filtered through commercial HF filters (Versatile PES[®]). Each filter was composed of ca. 600 PES fibers, each fiber having a length of ca. ≈ 11 cm, an inner diameter of ≈ 280 -300 μm and an outer diameter of ≈ 360 -400 μm . Thanks to the approach used, we could choose to coat the inner surface of the HF (Fig. 2a) or the outer one (Fig. 2c), using two different dead-end filtration modalities. After filtration of 5 ml of solution containing about 10 mg of GO, the cartridges were kept in oven at 80°C overnight to give samples HF-GO1i samples, *i.e.* hollow fibers containing about 1% w/w of GO respect to PES membrane weight in the inner surface. Hereafter, we will name samples as HF-GO followed by the % of GO loading and a letter e/i, indicating if the coating is places on the outer or inner surface of the hollow fiber. Following this nomenclature, we repeated the filtration-fixation cycle to obtain samples HF-GO1e/i, HF-GO5e/i, HF-GO10e/i, varying thus the coating from about 1% to 5% and 10%, either on the inner or outer surface.

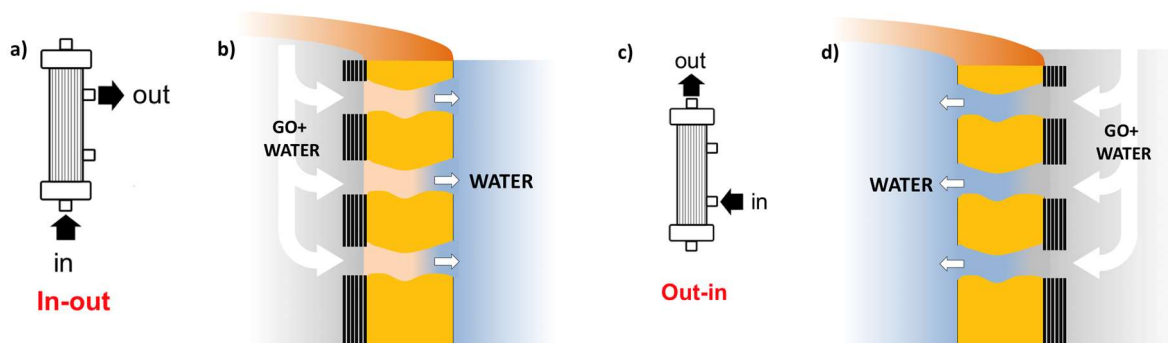


Figure 2. Sketch of the coating procedure. a) Filtration in-out to immobilize GO on the inner fiber wall and b) filtration out-in to immobilize GO on the outer fiber wall. Different GO % amount (1, 5, 10%) can be achieved by reiteration of the filtration/thermal fixation procedure. Partial fiber pores coverage and GO penetration are omitted for simplicity (see details in Fig.4 and Fig. S4, S5, ESI).

The HF-GO filters are shown in figure 3. In fibers coated outside, a dark color of the coating is clearly visible by increasing the amount of GO load from 1% to 10%. Fibers with inside GO coating showed no apparent change of colour (Fig. 3b), but a black coating could be observed in the inner wall by cutting the fibers (Fig. 3d).

The stability of the GO membrane coating was tested by flowing deionized water (1L) through the cartridges before and after the thermal fixation and by performing UV-vis absorption spectroscopy on the filtered water, comparing the results to what obtained with calibrated solutions of GO at known concentrations (Fig. S2, ESI). No evidence of GO nanosheets was found in the filtered water (detection limit 2-5 ppm, Fig. S2, ESI), confirming that the fixation process we already used on powders is effective on the hollow fibers as well.²⁴ We performed as well standard chemical potability tests (certified analysis on salts, metal ions, taste, total organic carbon) on tap water filtered through HF-GO5e/i cartridges confirming the potability of filtered water and the absence of any dangerous contaminant in accordance to current law limits (D. Lgs. 31/01 Agg. D.M. 14/06/2017, table S1, ESI).

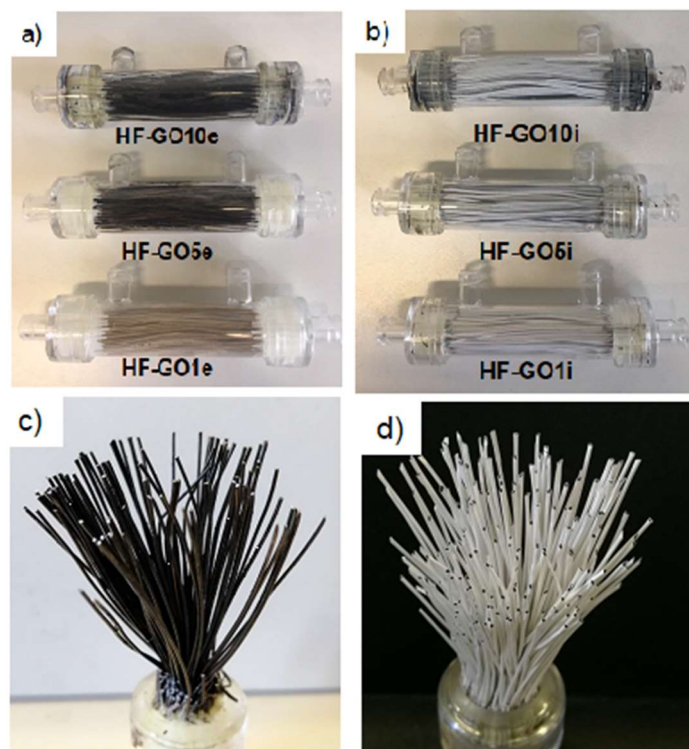


Figure 3. a) Cartridges of HF-GOe and b) HF-GOi at GO load 1, 5, 10% (w/w). Bundle of c) HF-GO5e and d) HF-GO5i.

2.2 Membrane characterization

Combined optical microscopy, SEM and Micro-Raman analyses were carried out to investigate the homogeneity of the coating, while XRD measurements were performed to estimate the periodic stacking in the GO coatings in HF-GO fibers and the number of GO layers. Optical microscopy on the HF-GO fibers (Fig. 4a and Fig. S3, ESI) showed a black coating on the whole fibers surface. GO coating was not uniform at the lowest GO load (1%) while uniform coating was found for all the other samples. Accordingly, SEM analysis on HF-GOe fibers (Fig. 4b,c) showed the presence of a GO layer covering the fiber surface. Fig. 4b,c show the case of HF-GO5e. Noteworthy, some open (uncoated) pores (about 1 μm size) were also observed (Fig. 4c and Fig. S4, ESI) this being highly beneficial, since it ensures that the membrane is not clogged due to the GO coating. Micro-Raman analysis performed on HF-GO1e and HF-GO10e (Fig. S5, ESI) showed a limited infiltration depth of GO within the fiber pore channels independently on the amount of GO used for coating. Indeed, in both outer modified HF, at 5 μm from the GO layer at the outer surface wall it was possible to detect the Raman peaks of GO that completely disappear in the bulk of the fiber section (at about 25 μm from the external wall, Fig. S5, ESI).

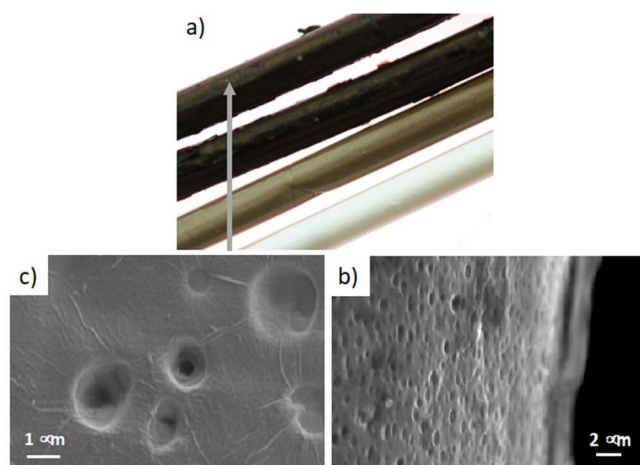


Figure 4. a) Fibers of PES and HF-GOe 1-5-10%, b) HF-GO5e, Representative SEM image of a GO coating on the outer fiber wall. c) detail of the coating of HF-GO10e fibers. SEM images of all samples at different magnification are reported in ESI (Fig. S4, ESI).

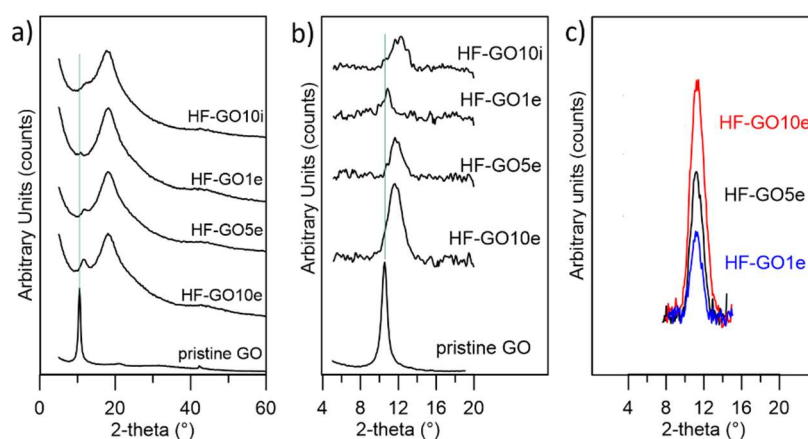


Figure 5. a) XRD patterns of HF-GO fibers and GO powder; b) and c) direct comparison of GO peaks. To allow a more direct comparison, in b) and c) the XRD signal due to background and polymer has been subtracted and in c) also a shift on 2-theta scale was applied.

Figures 5a show the XRD patterns of HF-GO fibers. The bell-shaped profiles centred at 18.1° (2-theta) were due to amorphous PES component. A signal due to the stacked GO nanosheets was observed at about 11.7° ($d=0.75$ nm), visible as a shoulder or peak depending on GO loading, and better evidenced after data treatment (Figure 5b). This distance is lightly smaller than what calculated for the pristine GO powder (10.5° , $d=0.84$ nm), and was ascribed to partial dehydration during the annealing treatment.²⁴ The thickness of the stacked crystalline domains was estimated from peak width using

Scherrer equation.²⁵ The stacked domains of GO had an average thickness of 6-8 layers on all fibers observed, indicating that even thicker coatings do not form a continuous, perfectly stacked layer (Figure 5c, Table S2, ESI). The coating is rather formed by a number of these crystalline nanometric sized regions assembled together in a compact structure of different thicknesses.

2.3 Filtration selectivity and efficiency

Water permeability test were firstly performed on HF-GO cartridges in the same dead-end configuration described in the experimental part. Each cartridge was filled with osmotic water, pressure value was measured at filter inlet, the amount of water micro filtered in 1 minute was weighted and the filtration coefficient (Kf) was calculated. As expected, permeability of PES decreased as long as the amount of GO loading increased. We observed the lowest Kf of $0.42 \pm 0.24 \text{ ml min}^{-1} \text{ mmHg}^{-1} \text{ m}^{-2}$ for the HF coated with 10% GO on the outside. Ideal Kf for filtering tests was instead obtained for inside coatings of 1% and 5% (figure 6).

Besides measuring permeability of water, we also measured (dry) air permeability, in order to distinguish the contribution water transport across swelled GO or polymer with respect to the transport in macroscopic pores.²⁶ The obtained air permeability measured confirmed the porous structure of the HF, revealing an incomplete coating of the PES HF at the lowest GO concentration, thus featuring several holes; for thicker coatings, a complete impermeable coating could not be detected as well, even though a significantly more compact structure was obtained, and the diffusing molecules have to proceed along a very tortuous path to cross coating, wiggling around GO layers (see ESI, Fig. S6 for more details).

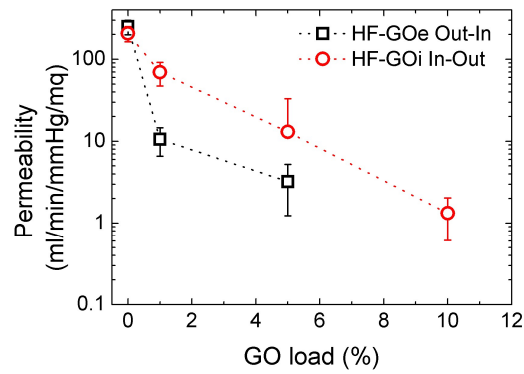


Figure 6. Water Permeability response for HF-GO e/i at different GO loads. Filtration was performed by flowing water first across the GO layer (i.e. in-out for HF-GOi and out-in in HF-GOe).

The cut-off of the of the PES hollow fibers pores used is in the range 0.1-0.2 μm , optimal for micro-filtration of biological samples, blocking colloids and microorganisms of size > 1.000 KDa (Fig. S7, S8 ESI). To establish the cut-off of HF-GO fibers filtration tests were performed on water spiked with BSA and polystyrene standard nanoparticles with size below and above the cut-off of PES cartridges (i.e. PS NPs, 52 nm and 303 nm sizes). BSA (about 15 nm, 66KDa) and PS 52 nm NPs are expected to cross a microfiltration membrane while PS NPs 303 nm sized are expected to be retained. Figure 7 shows that all filters blocked larger particles and let through smaller ones, as expected, and the retention of PS NPs 52 nm was basically equal to that of the bare HF modules (about 20%). This indicates that no clogging effect of GO occurred and that there were pores in the range 52-303 nm available for filtration.

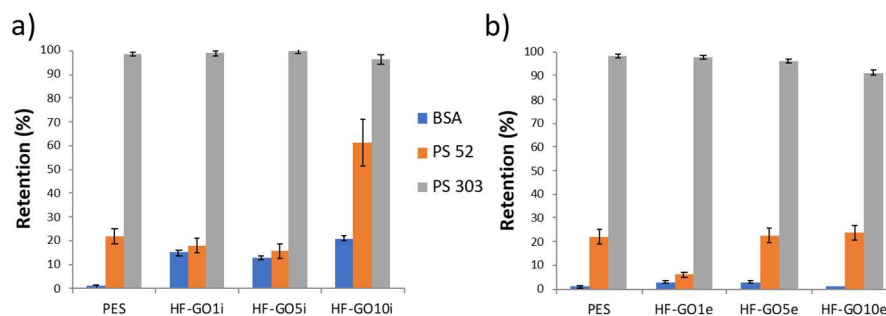


Figure 7. HF-GOi (a) and HF-GOe (b) retention efficiency of BSA, PS 52 and PS 303 from water solution. HF-GO behaves as commercial PES modules i.e. they retained large PS NPs.

A partial retention of BSA was observed in the HF-GO_i membranes (up to 15-20%), while no significant effect was detected from the cartridges with GO coatings on the external surface. This can hardly be attributed to a size exclusion mechanism, and effective nanofiltration operation was excluded, in view of the smaller size of BSA with respect to PS 52 nm NPs. Additional BSA and filtration experiments are reported in ESI (Fig. S6 and S8 respectively).

Once verified that the GO coating does not affect the size-dependent filtering performance of the filters, we measured their ability to retain, instead, small contaminant molecules (RhB, ofloxacin and ciprofloxacin, 5 mg/L in water), which cannot be blocked by the standard filters due to their nanometric size, much smaller than BSA protein.

We measured the removal efficiency of the filters for such molecular contaminants by fluxing through the filter 250 mL of solutions contaminated with each molecule (5 mg/L) at 15 mL/min, then analysing the filtered solution by HPLC/UV analysis (details in ESI).

Uncoated PES filters (GO load 0%) showed insignificant filtering effect for the standard contaminants inspected, as shown in Fig. 8 with removal efficiency <10% in all cases. Conversely, HF-GO fibers showed significant removal ability, up to about 80% in the best case (ciprofloxacin filtered by HF-GO_{10i}). Removal performance increased with GO loading, showing a monotonous increase for the outer-coated fibers (Fig. 8a), and saturation plateau for inner-coated ones (Fig. 8b). The best performances are reached with a lower amount of GO in inner-coated fibers, which showed a significant removal performance already at low GO loading i.e. removing 50% of ciprofloxacin vs. about 20% for inner-coated fibers at 1 % of GO loading. At the highest loadings (GO 10% w/w), the performances of the two filters (inner or outer coatings) are equivalent.

Therefore, the mechanism of capture of these substances does not rely on size exclusion, but it is rather given by adsorption onto GO layers surface, able to interact with such molecules. The larger is the GO amount on HF module, the larger is the EOC removal. Relevantly, the key aspect in the filtration step is the accessibility of the adsorbing sites in the GO layer, allowing thus these molecules to be

intercalated. The more open structure of inner coated filters, as indicated by both water and air permeability tests, and their larger porosity promote contaminants transport in the coating with a more effective contact with adsorbing sites.

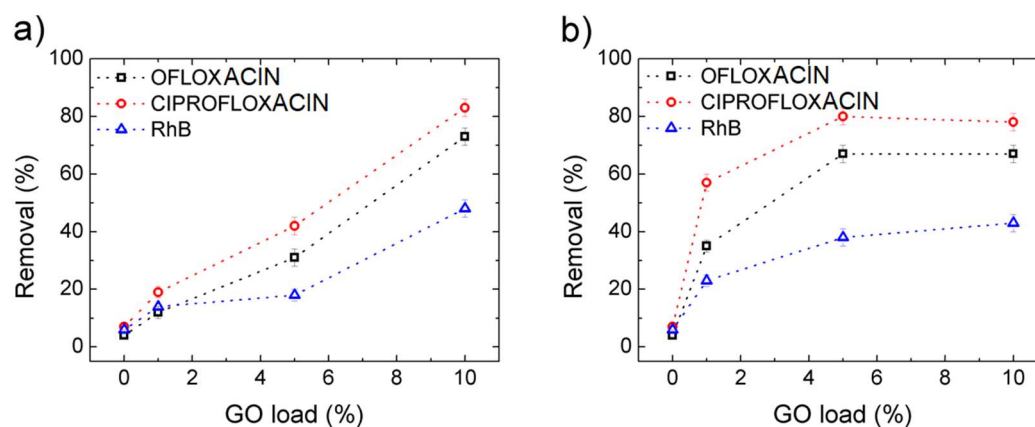


Figure 8. Removal efficiency for Oflox, ciprofloxacin and Rh B vs GO loading for a) HF-GOe and b) HF-GOi. The concentration (5 mg/L), flow (15 mL/min) and fluxed volume (250 mL) of the contaminants' solution was the same for all tests. Filtration was performed by flowing water firstly passing through the GO layer i.e. in-out for inner coated fibers and out-in for outer coated fibers.

Previous experiments confirmed that small quantities of GO can capture hundreds of mg of ofloxacin and RhB when the thermodynamic equilibrium is reached (isotherms), c.a. 590 mg/g for RhB and 360 mg/g for ofloxacin, but such experiments were always performed in static configuration, with a prolonged (24 h) contact time between GO and the contaminant solution. Kinetics studies of EOC removal showed how the equilibrium condition can be achieved with different times, 5-10 minutes for RhB²⁷ and 60-80 minutes for ofloxacin²⁸; such time scale is incompatible with continuous flow filtering, which is relevant for practical applications.

In our setup set-up, with a 15 mL/min flow and 2.5 mL volume of cartridge, the contact time is ≈ 10 seconds, thus indicating that the operative conditions of the filters are very far from thermodynamic equilibrium. However, we could achieve significant removal even if our contact time was one order of magnitude smaller than what reported in the above cited works. We attribute this remarkable performance to the synergic action of the fiber pores and the GO coating, with the solution being forced

to flow the GO coating (see scheme in Fig. 2), thus in the ideal condition to be captured and intercalate in the GO layers, as described in previous work.²⁴

After demonstrating the improved performance of the HF-GO filters compared to standard PES, we calculated also the filter longevity, i.e. the ability to filter significant amounts of solution before having to be replaced. The concentration of EOC pollutants is usually in sub ppb range, thus we estimated our filter consumption using a contaminant concentration of 0.2 $\mu\text{g/L}$ for ciprofloxacin. Figure 9 shows the removal efficiency of the filters as a function of cumulative mass fluxed. This plot allows to estimate the amount of ciprofloxacin removed by a single cartridge and normalise the removed EOC mass on the mass of the active material (GO). We see that HF-GO5i can have a reasonable removal of about 90 % with 15 mg/g_{GO} of ciprofloxacin, 14 mg/g_{GO} of ofloxacin and 7 mg/g_{GO} of RhB, that are not the adsorbed amount at equilibrium at high concentration, but the effective amount of EOC adsorbed in operative filter. It is remarkable that such values are obtained with a quite short contact time (seconds), while the reference on water treatment plants are usually 10-20 minutes, with c.a. 20 $\mu\text{g/g}$ of ciprofloxacin removed by using the traditional Powdered Activate Carbons.²⁹ In turn, the filter HF-GO5i still has a removal efficiency c.a. 90% after flowing a total mass of 0.5 mg of contaminant, corresponding to c.a. 2500 L of realistic, contaminated solution with 0.2 ppb of ciprofloxacin, this proving the suitability of HF-GO filters for realistic commercial applications (see also table S7, ESI).

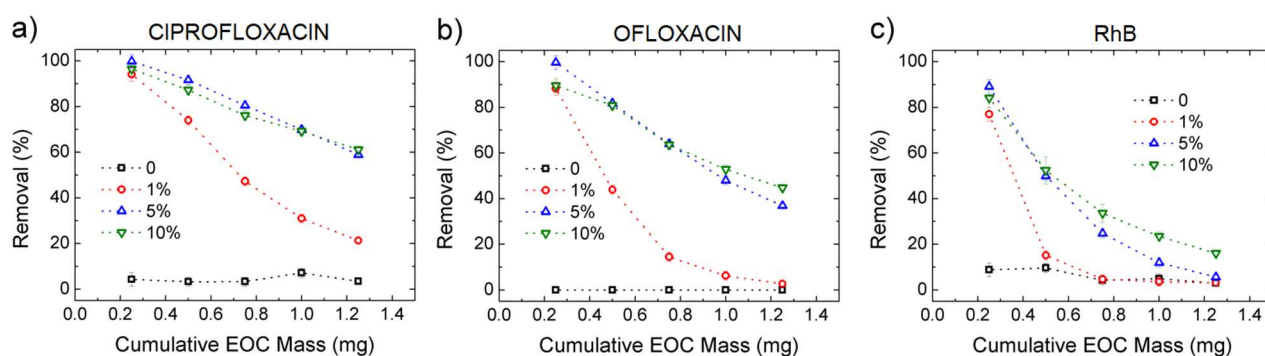


Figure 9. Removal efficiency for ciprofloxacin (a), ofloxacin (b) and RhB (c) for PES and increasing GO loading in HF-GO_i. The cumulative initial mass is obtained with fixed concentration (5 mg/L) and flow (15 mL/min). Details are reported in Fig. S10, S11, ESI.

Figure 9 compares the removal efficiency of the three different EOC studied for HF-GO1i and HF-GO1i filters. As expected, filters saturate rapidly with only a 1% GO loading, while the 5% and 10% loading gives the best performances, in particular for ciprofloxacin, while RhB gives the worst longevity performance in all cases.

2.4 Simultaneous filtration and adsorption test and working mechanism

Eventually, we performed filtration of a complex, realistic matrix of BSA and ofloxacin solution, to confirm the capability of HF-GO filters to work simultaneously as physical filter (cut-off depending on the pore size) and adsorbent (mediated by chemical interactions). The filtration tests were performed both on water (Fig. 10) and bovin plasma matrixes (Fig. S8, S12, ESI). As representative case study we show in Fig. 10 the removal of HF-GO-i filters that feature almost quantitative removal of ofloxacin ($\approx 90\%$) and negligible ($<1\%$) removal of BSA. Similar results were found in bovin plasma matrix containing BSA and other proteins with a total concentration of about 6-8 g/dL, with no significant reduction of BSA and TP amount occurring after filtration (Fig. S13, ESI).

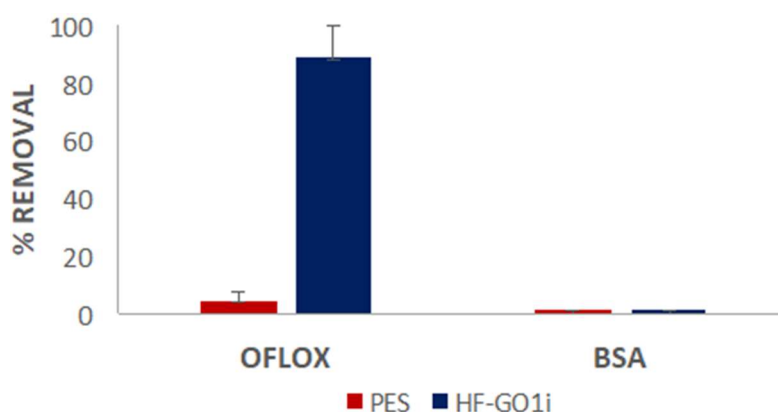


Figure 10. Filtration of tap water spiked with 50 mg/L of ofloxacin and 10g/L of BSA. Quantification by HPLC-UV analysis.

The mechanism of filtration was investigated by XRD analysis (Fig. 11a). We extracted the fibers from the filters after filtration of contaminated solutions, and estimated GO stacking using XRD, comparing them with pristine, not-used fibers. We observed a shift of the GO peak towards larger stacking distance after filtration of EOC (0.75 nm \rightarrow 0.89 nm), and a decrease in intensity, this suggesting that the removal mechanism is due to the strong affinity between the aromatic core of the EOC with the sp² structure of the GO layers that induces a partial swelling and exfoliation of the layers, as discussed in detail in a previous work.²⁴

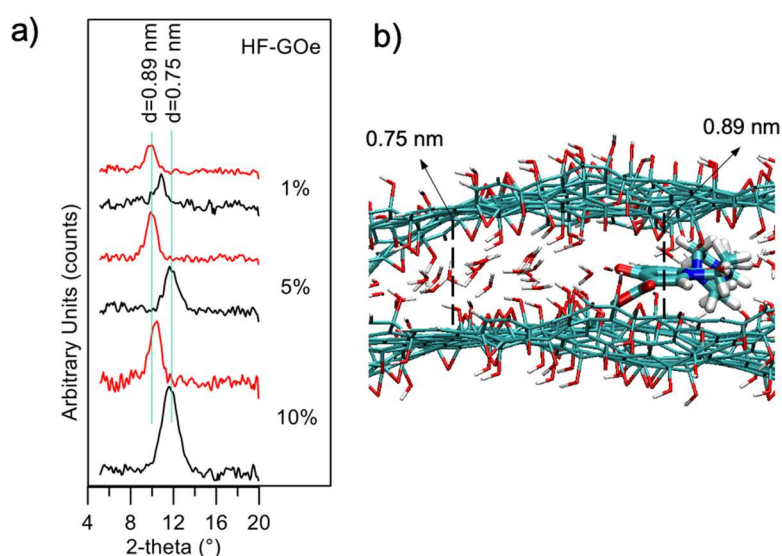


Figure 11. a) XRD patterns of HF-GOe fibers before (black) and after (red) filtration of organic microcontaminants. Two vertical lines as reference, are at angles corresponding to 0.89 nm and 0.75 nm respectively. b) Molecular structure of GO bilayers after ofloxacin intercalation.

Atomistic molecular mechanics simulations may reveal insights into the adsorption and packing of molecules, interacting with carbon nanomaterials.³⁰ Thus, molecular modelling simulation on GO-ofloxacin interactions were performed for a deeper understanding on the removal mechanism. First, simulations show that the spacing of 0,75 nm observed for GO (Fig. 11, black curves) can be explained by considering the uptake of a water monolayer in the interlayer space of GO.³¹ Indeed, GO preserves the layered structure of graphite, but in contrast to graphite, is hydrophilic, thus water molecules are hardly completely removed from GO layers. Consequently, spacings of the carbon layers in the range from 0.6 to 1.2 nm are observed in GO, depending on the water content of the samples.³²

This water layer is crucial to reach an equilibrium spacing between the GO layers because an attractive force between the two negative GO sheets is needed to overcome the electrostatic repulsive force between the GO layers. Intercalation of ofloxacin between GO layers (Fig. 11b) generates an increase from 0.75 to 0.89 nm in the spacing between the two GO layers. These values are in perfect agreement with observed XRD data (Fig. 11a, red profiles).

In fact, considering that i) the size of a water molecule is ~ 0.25 nm and the size of ofloxacin is ~ 0.4 nm, ii) during the intercalation process, the GO is locally dehydrated, an increase of ~ 0.15 nm is expected upon intercalation, as observed experimentally by XRD measurements and by molecular modelling simulations.

Collectively, the multitarget filtration experiments show that the synergic action of the PES membrane and GO coating porosity (micrometric and nanometric pores respectively) allows the removal from solution of large biological objects and small molecules at the same time. Differently to simple mixtures or bi-layered GO-polymer composites previously described,²² the approach here described allows to position the nano-adsorbant component (*i.e.* the GO) exactly on the surface more exposed to the solution, in particular in proximity of the nanopores. The results obtained show that this geometry allows to obtain significant removal of EOC even with short contact time and for low GO loadings, in particular when the GO is placed in the inner surface of the fibers, where contact time with the contaminated solution is maximal (see scheme in Fig. 12).

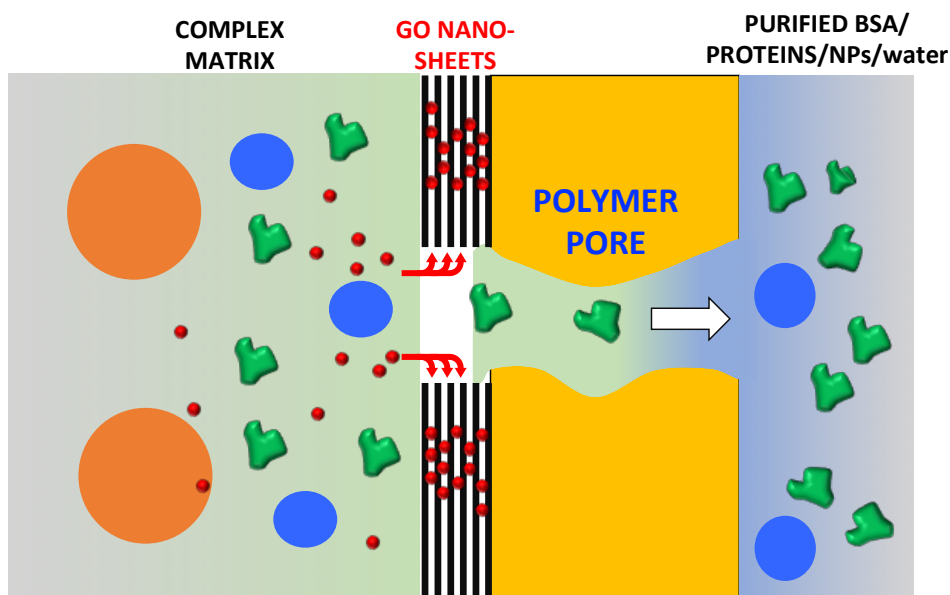


Figure 12. Simplified working mechanism of HF-GO allowing simultaneous filtration of BSA through PES and GO promoted adsorption of ofloxacin, ciprofloxacin and Rh B. GO layer does not cover all the pores this allowing EOC molecules to intercalate and to nano-objects to pass through the core shell HF.

3. Conclusions

In conclusions, GO coating was achieved by a simple and mild procedure on already commercially available microfiltration PES hollow fiber modules. While un-modified filters could stop large objects and let BSA pass through, only HF-GO hollow fiber filters were able to selectively capture three target EOC of environmental relevance. Air permeation tests revealed that diffusing molecules are forced to travel around the GO sheets, along tortuous paths depending on the in-plane distance between two near GO sheets and the intrinsic aspect ratio of the 2-D materials, this is of course not useful for filtration of large molecules like BSA, having a size 20 nm, but could be useful for selective filtration of smaller molecules. Accordingly, combined XRD analysis on virgin and used membranes and molecular modelling simulations revealed intercalation of organic molecules through the GO layers as mechanism of adsorption. This work demonstrates that HF-GO modules can be useful for removing antibiotics from water and plasma matrices while letting pass through proteins and nanoobjects through the HF pores, thus paving the way toward selective separation processes for biomedical and water treatment applications.

Acknowledgments

The research leading to these results has received funding from the European Union's Horizon 2020 research and innovation programme under GrapheneCore2 785219 – Graphene Flagship, POR-FERS 2014-2020 DGR 986/2018 MEDFIL (B54I19000030005) and Italian-PRIN 2017 NANO-CARBO-CAT (B54I19002770001).

MM thank Dr. F. Belosi (CNR-ISAC) for useful discussion.

Bibliography

1. a) S. Schulze, D. Zahn, R. Montes, R. Rodil, J. B. Quintana, T. P. Knepper, T. Reemtsma and U. Berger *Water Research* **2019**, *153*, 80-90, b) Recast of the EU drinking water directive: https://ec.europa.eu/info/law/better-regulation/initiatives/com-2017-753_en, c) F. Mao, Y. He and K. Yew-Hoong Gin, *Environ. Sci.: Water Res. Technol.*, **2019**, *5*, 209-223.
2. a) K. Zahri, K. C. Wong, P. S. Goh and A. F. Ismail *RSC Adv.*, 2016, *6*, 89130- 89139, b) F. David, F. Sanders, P. Zachary, P. Smith, R. Guo, M. Lloyd, C. Robeson, E. J. McGrath, D. R. Paul and B. D. Freeman, *Polymer*, **2013**, *54*, 4729-4761.
3. D. Sholl and R. P-Lively *Nature* **2016**, *532*, 435-437.
4. D. Li, R. Wang and T.-S. Chung, *Separation and Purification Technology* **2004**, *40*, 15–30.
5. a) P. Westerhoff, P. Alvarez, Q. Li, J. Gardea-Torresdey, J. Zimmermand *Environ. Sci.: Nano*, **2016**, *3*, 1241–1253, b) C. Santhosh, V. Velmurugan, G. Jacob, S. K. Jeong, A. N. Grace and Amit Bhatnagar *Chemical Engineering Journal*, **2016**, *306*, 1116–1137, c) X. Zhu, K. Yangab, B. Chen *Environ. Sci.: Nano*, **2017**, *4*, 2267–2285, d) D. Miller, D. R. Dreyer, C. W. Bielawski, D. R. Paul and B. D. Freeman *Angew. Chem. Inter. Ed.*, **2016**, *56*, 17, 4662-4711.
6. J. Alam, A. K. Shukla, M. Alhoshan, L. Arockiasamy Dass, R. Muthumareeswaran, A. Khan and F. A. A. Ali, *Adv. Polym. Technol.* **2018**, 1–12.
7. R. Rezaee, S. Nasser, A. Hossein Mahvi, R. Nabizadeh, S. A. Mousavi, A. Rashidi, A. Jafari and S. Nazmara *J. Environ. Health Science & Engineering*, **2015**, 13-61.
8. J.A. Prince, S. Bhuvana, V. Anbharasi, N. Ayyanar, K.V.K. Boodhoo and G. Singh *Water Research* **2016**, *103*, 311-318.
9. X. Zhu, K. Yangab and B. Chen *Environ. Sci.: Nano*, **2017**, *4*, 2267–2285.
10. M. Miculescu, V. Kumar Thakur, F. Miculescu and S. I. Voicu *Polym. Adv. Technol.* **2016**, *27*, 844–859.
11. X. Wang, Y. Zhao, E. Tian, J. Li and Y. Ren *Adv. Mater. Interfaces* **2018**, *5*, 1701427.
12. R. R. Nair, H. A. Wu, P. N. Jayaram, I. V. Grigorieva, A. K. Geim, *Science*, **2012**, *335*, 442.
13. N. Yousefi, X. Lu, M. Elimelech and N. Tufenkji *Nature Nanotechn.* **2019**, *14*, 107-119.
14. F. Perreault, A. Fonseca de Faria and M. Elimelech *Chem. Soc. Rev.*, **2015**, *44*, 5861—5896.
15. T. A. Tabish, F. A. Memon, D. E. Gomez, D. W. Horsell and S. Zhang *Scientific Reports* **2018**, *8*:1817 | DOI: 10.1038/s41598-018-19978-8
16. L. Jiang, Y. Liu, S. Liu, G. Zeng, X. Hu, X. Hu, Z. Guo, X. Tan, L. Wang and Z. Wu *Environ. Sci. Technol.* **2017**, *51*, 6352–6359.
17. G. Ersan, O. G. Apul, F. Perreault and T. Karanfil *Water Research* **2017**, *126*, 385-398.

18. a) D. Pakulski, W. Czepa, S. Witomska, A. Aliprandi, P. Pawlu´ V. Patroniak, A. Ciesielski and P. Samori' *J. Mater. Chem. A*, **2018**, *6*, 9384–9390, b) W. Gao, M. Majumder, L. B. Alemany, T. N. Narayanan, M. A. Ibarra, B. K. Pradhan and P. M. Ajayan *ACS Appl. Mater. Interfaces* **2011**, *3*, 1821–1826, c) M. Durso, A. I. Borrachero-Conejo, C. Bettini, E. Treossi, A. Scida`, E. Saracino, M. Gazzano, M. Christian, V. Morandi, G. Tuci, G. Giambastiani, de L. Ottaviano, F. Perrozzi, V. Benfenati, M. Melucci and V. Palermo *J. Mater. Chem. B*, **2018**, *6*, 5335–5342.
19. J. Clemonne, J. Madarang, H. Y. K, J. Zhu, H. Feng, M. Gorrng, M.L. Kasner, and S. Hou *ACS Appl. Mater. Interfaces* **2012**, *4*, 1186–1193.
20. M.-P. Wei, H. Chai, Y.-L. Cao and D.-Z Jia *Journal of Colloid and Interface Science* **2018**, *524*, 297–305.
21. C.-Z. Zhang, Y. Yuan and Z. Guo, *Separation Science and technology*, **2018**, *53*, 1666, 1677.
22. M. Zambianchi, M. Durso, A. Liscio, E. Treossi, C. Bettini, M. L. Capobianco, A. Aluigi, A. Kovtun, G. Ruani, F. Corticelli, M. Brucale, V. Palermo, M. L. Navacchia and M. Melucci, *Chem. Eng. J.*, **2017**, *326*, 130–140.
23. M. Zambianchi, A. Aluigi, M. L. Capobianco, F. Corticelli, I. Elmi, S. Zampolli, F. Stante, L. Bocchi, F. Belosi, M. L. Navacchia and M. Melucci, *Adv. Sustainable Syst.*, **2017**, *1*, 1700019.
24. A. Kovtun, M. Zambianchi, C. Bettini, A. Liscio, M. Gazzano, F. Corticelli, E. Treossi, M. L. Navacchia, V. Palermo and M. Melucci, *Nanoscale* **2019**, DOI 10.1039/C9NR06897J.
25. A. Liscio, K. Kouroupis-Agalou, A. Kovtun, E. Gebremedhn, M. El Garah, W. Rekab, E. Orgiu, L. Giorgini, P. Samori', D. Beljonne, V. Palermo, *Chem. Plus Chem.* **2017**, *82*, 358 – 367
26. J.I. Langford and A.J.C. Wilson Scherrer, *J. Appl. Cryst.* **1978**, *11*, 102-113.
27. J. Abraham, K. S. Vasu, Christopher D. Williams, K. Gopinadhan, Y. Su, C. T. Cherian, J. Dix, E. Prestat, S. J. Haigh, I. V. Grigorieva, P. Carbone, A. K. Geim and R. R. Nair, *Nat. Nanotechn.* **2017**, *12*, 546-550.
28. a) A. Molla, Y. Li, B. Mandal, S. G. Kang, S. H. Hur and J. S. Chung *App. Surf. Sci.* **2019**, *464*, 170-177, P. Bradder, S. King, L. S. Wang and S. Liu *J. Chem. Eng.* **2011**, *56*, 138–141. b) Q. Konga, X. Hea, L. Shuc and M.-S. Miao, *Process Safety and Environmental Protection*, **2017**, *112*, 254–264.
29. R. Mailler, J. Gasperi, Y. Coquet, S. Deshayes, S. Zedek, C. Cren-Oliv, N. Cartiser, V. Eudes, A. Bressy, E. Caupos, R. Moilleron, G. Chebbo and V. Rocher, *Water Research*, **2015**, *72*, 315-330.
30. M. Calvaresi and F. Zerbetto, *J. Mater. Chem. A*, **2014**, *2*, 12123-12135.
31. a) S. Zheng, Q. Tu, J.J. Urban, S. Li and B. Mi, *ACS Nano* **2017**, *11*, 6440-6450.
32. A. Buchsteiner, A. Lerf and J. Pieper, *J. Phys. Chem. B* **2006**, *110*, 45, 22328-22338, b) A. V. Talyzin, T. Hausmaninger, S. Youa and T. Szabo *Nanoscale*, **2014**, *6*, 272–281.

PART 3

ION TRANSPORT

3.1 She sells GO sheets by the seashore: graphene and desalination

Seawater desalination, meaning the production of drinking water from seawater, is one of the main targets of the international research in the fight against water shortage. At this date, more than 75 million people rely on seawater desalination for the bestowal of drinking water, but this number is bound to grow. Desalination gives coastal communities access to a virtually unlimited reserve of water suitable for human use (i.e. drinking, agriculture, etc.) and allows the rehabilitation of brackish areas or areas where freshwater can no longer support local populations.¹

There are two main technologies to perform seawater desalination: thermal processes and membrane processes. Thermal processes rely on ultra-optimized distillations (such as multi-stage flash desalination, multiple-effect evaporation, and vapour compression distillation),¹⁻³ while membrane processes exploit high pressure to push water through a semipermeable membrane, which retains salts and molecules. Reverse osmosis (RO) is the most common membrane technology for desalination. In forward osmosis, water moves from the most diluted phase to the most concentrated phase, until equilibrium is reached; in RO high pressure (60-100 bar) is used to invert this trend and force water from the most concentrated phase (i.e. seawater) to the most diluted phase (i.e. purified water). Through this process, roughly half of the treated water becomes purified water and can be converted in drinking water, and half of it becomes a highly concentrated brine, containing all of the salt and pollutants of the original matrix (and must be disposed of). The energy required for RO is

directly proportional to the concentration of the matrix, because an osmotic pressure must be overcome. Despite the fact that water characteristics (i.e. salinity, temperature, contamination degree, etc.) influence the choice of the best desalination technology in each case, RO is the most economically suitable solution in the majority of cases.^{3,4}

The development of adsorptive membranes^{5,6} for seawater desalination would open a new panorama of solution to apply at this problem, but research in this sense is still far from the deployment prototypes with an easy industrial scale up. GRM are a great candidate for designing adsorptive membranes for desalination, but the theoretical knowledge of water and ion movement inside GRM membranes is still in its cradle. At this date, the discussion in the scientific community on this subject is very active.⁷⁻¹¹ One side holds the thesis that GO can perform nanofiltration-enabled ion sieving. The basic idea is that it is possible to keep the interlayer distance between the GO sheets at a stable value below the hydrated radius of sodium, thus preventing thoroughly sodium to pass the GO membrane. This would of course be a groundbreaking technology. The other side argues that this is possible with our current knowledge and technology. In any case, it is not totally clear what happens when ions enter a GO membrane.

An additional aspect to consider is that the pressure required by RO makes it an energy-hungry technology. Hydrodynamic force are not necessarily the only driving force to “push” water through a semipermeable membrane. Studies are deepening electric fields as valid alternatives.

3.2 HF-GO for ion transport

In the next article, the reader will find a study of the ion separation potential possessed by the core-shell system described in the previous part. GO can efficiently discriminate ions in water thanks to two fundamental features: hydrated radii and charge. The role that these two parameters play in the mass transport of each element is still unclear. Ions and molecules cannot pass through the single GO sheets, but must rather pass in between the single sheets, to find the exit. This implies that the motion to cross the totality of the GO membrane is extremely tortuous (please remember that a GO membrane is composed of tens or hundreds of layers).

The majority of the studies on this subject concerns planar membranes composed by pristine GO (in contraposition to adsorptive membranes) and relies on theoretical models to back their hypothesis, instead of sound physical-chemical analyses. In this study, my colleagues and I studied how the ionic concentration at the opposite sides of a GO-HF module varies with time. We obtained such insight through electrochemical impedance spectroscopy (EIS), ionic-coupled plasma (ICP) analyses, and atomic adsorption spectroscopy (AAS).

In this paper, we studied several cations. The application of an electric field (0.5-3 V) at the opposite side of a HF-GO module generates a concentration gradient, due to the amassing of ions at the electrodes, primarily provided by the bicarbonate buffer in water. This concentration gradient acts as the driving force of mass transport through the HF-GO module (i.e. the GO membrane). The most compelling results concern the difference that HF-GO shows in the selectivity toward the transport of sodium and calcium: sodium can traverse the core-shell membrane almost 100 times more than calcium. While it is alluring to explain this phenomenon with a purely steric explanation (Na^+ and Ca^{2+} hydrated radii are 4 Å and 6 Å

respectively), we find it more relatable to say that the oxygenated groups on the GO sheets coordinate Ca^{2+} , slowing down its transport or trapping it inside the membrane, while Na^+ unaffected by coordination. The role of coordination is highlighted by the fact that if the oxygenated groups are saturated with protons (thanks to a pre-treatment with diluted HCl), the mass transport of Ca^{2+} grows 1'000 times, while the transport of Na^+ is unaltered. Please note that ζ potential (which serve as an indicator of the surface charge of the GO sheets) does not change due to this pre-treatment. The effect of charge is evident also in the comparison between Na^+ and Pb^{2+} . These two ions have the same hydrated radius (4 Å), but different charge, but the transport of Pb^{2+} is about ten times the transport of Na^+ .

Despite the role of the charge that we have highlighted, hydrated radius has an undeniable role in mass transport too. The analysis of K^+ , Na^+ , Ca^{2+} , and Mg^{2+} show a precise logarithmic progression, independently from the charge.

The fact that GO holds back calcium but not sodium is bad news for the application of HF-GO to desalination, but is great news for its application in water sweeteners.

I inherited the “ion transport in GO membrane” subject from a person who worked in ISOF before me. We could say that she “passed me the baton” of this research line. Either because at the time I had just started working in a lab, or because my communicational skills were not as refined as they are now, this transition did not happen smoothly. I failed in creating a constructive relationship with this person, and this led to a bad transmission of the necessary knowledge to continue this research with ease. It is common for long-term projects to be carried on by research fellows, master students, or PhD students, whom work on such projects for a limited amount of time and then leave. In such cases, a good transmission of the already-done work and acquired knowledge is fundamental to avoid repeating the same introductory work again and again, which is a waste of time and resources. This “passing of the baton” is not trivial, though. It requires for the leaving person to know how to transmit their knowledge effectively, for the receiving person to be a good learner, and for both of them to be willing to do it. Unfortunately, this aspect is often underestimated, or neglected, while it benefits the job by a great extent if performed properly. In my case, if I will ever find myself again in such a situation, I will ensure to create the best interpersonal relationship possible, for the sake of both my personal life and working activity.

Bibliography

1. Khawaji, A. D.; Kutubkhanah, I. K.; Wie, J.-M., Advances in seawater desalination technologies. *Desalination* **2008**, *221* (1), 47-69.
2. Feria-Díaz, J. J.; López-Méndez, M. C.; Rodríguez-Miranda, J. P.; Sandoval-Herazo, L. C.; Correa-Mahecha, F. Commercial Thermal Technologies for Desalination of Water from Renewable Energies: A State of the Art Review *Processes* [Online], 2021.
3. Miller, J. E., Review of Water Resources and Desalination Technologies. **2003**.
4. Greenlee, L. F.; Lawler, D. F.; Freeman, B. D.; Marrot, B.; Moulin, P., Reverse osmosis desalination: Water sources, technology, and today's challenges. *Water Res.* **2009**, *43* (9), 2317-2348.
5. Qiu, B.; Gorgojo, P.; Fan, X., Adsorption desalination: Advances in porous adsorbents. *Chin. J. Chem. Eng.* **2022**, *42*, 151-169.
6. Sarai Atab, M.; Smallbone, A. J.; Roskilly, A. P., A hybrid reverse osmosis/adsorption desalination plant for irrigation and drinking water. *Desalination* **2018**, *444*, 44-52.
7. Abraham, J.; Vasu, K. S.; Williams, C. D.; Gopinadhan, K.; Su, Y.; Cherian, C. T.; Dix, J.; Prestat, E.; Haigh, S. J.; Grigorieva, I. V.; Carbone, P.; Geim, A. K.; Nair, R. R., Tunable sieving of ions using graphene oxide membranes. *Nat. Nanotechnol.* **2017**, *12* (6), 546-550.
8. Joshi, R. K.; Carbone, P.; Wang, F. C.; Kravets, V. G.; Su, Y.; Grigorieva, I. V.; Wu, H. A.; Geim, A. K.; Nair, R. R., Precise and Ultrafast Molecular Sieving Through Graphene Oxide Membranes. *Sci* **2014**, *343* (6172), 752-754.
9. Nair, R. R.; Wu, H. A.; Jayaram, P. N.; Grigorieva, I. V.; Geim, A. K., Unimpeded Permeation of Water Through Helium-Leak-Tight Graphene-Based Membranes. *Sci* **2012**, *335* (6067), 442-444.
10. Talyzin, A. V., Random interstratification in hydrated graphene oxide membranes and implications for seawater desalination. *Nat. Nanotechnol.* **2022**, *17* (2), 131-133.
11. Abraham, J.; Vasu, K. S.; Williams, C. D.; Gopinadhan, K.; Su, Y.; Cherian, C. T.; Dix, J.; Prestat, E.; Haigh, S. J.; Grigorieva, I. V.; Carbone, P.; Geim, A. K.; Nair, R., Reply to: Random interstratification in hydrated graphene oxide membranes and implications for seawater desalination. *Nat. Nanotechnol.* **2022**, *17* (2), 134-135.

Ion Migration Control *via* Electric Field Modulation in a Core-Shell 3D GO-Polymer Water Treatment Device

Antonio Bianchi,^{‡a} Lidia Lancellotti,^{‡a} Massimo Gazzano,^b Chiara Zanardi,^{a,c} Manuela Melucci,^a Vincenzo Palermo^a

^a Consiglio Nazionale delle Ricerche, Institute for Organic Synthesis and Photoreactivity (CNR-ISOF), via Piero Gobetti 101, 40129 Bologna (BO), Italy

^bAlma Mater Studiorum – University of Bologna, Department of Chemistry ‘G. Ciamician’, via Selmi 2, 40129 Bologna, Italy

^cUniversity of Venice ‘Ca’ Foscari’, Department of Molecular Sciences and Nanosystems, via Torino 155, 30170 Venice, Italy

‡ These authors contributed equally to this work

1. Introduction

Control over ion transport inside membranes is a matter of interest for many fields, such as healthcare, water purification and desalination of seawater.¹⁻⁵ In particular, separation among multi-valent (e.g. Ca^{2+} , Mg^{2+} , Pb^{2+} , Cr^{3+}) and mono-valent (e.g. Na^+ , K^+) metal ions is crucial in the purification and softening procedures. Indeed, the most common treatment that water undergoes is the suppression of Ca^{2+} coming from leaching of rocks, that should ideally occur without altering the amount of ions essential for the physiological conditions, namely Na^+ and K^+ . This holds also for the removal of some multi-valent metal ions present at trace levels and deriving from industrial processes,⁶⁻⁸ like Pb^{2+} , Cd^{2+} , and Cr^{3+} , which are dangerous and poisonous for humans, living organisms and the environment.⁹⁻¹² In addition, one of the most interesting applications for membranes capable of ion transport control would be desalination of water, to meet the increasing worldwide demand of drinking water. All these applications require a deep knowledge of the processes occurring during the transport of ions inside membranes, aiming at the production of membranes with high transport efficiency and selectivity toward target ions.

Membrane-based technologies have been proven to be very effective for sieving mono- and multivalent metal ions. Although the mechanisms of ion transport inside nanopores and nanochannels of membranes are often poorly defined, they are mainly based on electrostatic interaction and/or size exclusion.¹³ The latter phenomenon is possible thanks to the different diameter of hydrated ions of K^+ and Na^+ (3 and 4.5 Å, respectively), with respect to that of the multivalent metal ions previously cited, ranging from 6 to 7.¹⁴ Therefore, the presence of nanopores or nanochannels with diameters of approximately 8 Å in membranes is supposed to enable the sieving of mono- and of multivalent metal ions based on the steric effect. Several strategies have been developed to modulate the dimension of nanopores and nanochannels: interfacial polymerization,¹⁵ ion beam technologies^{16, 17} and the use of 2D materials arranged in well-ordered lamellar structures with defined interlayer spacing (d).¹⁸⁻²⁰ As an example, d stacking distance in graphene oxide (GO) nanosheets is larger than the hydrated radii of the ions of most common salts. d in GO can be modulated from 6.4 to 9.8 Å²¹ through chemical modification of the carbon-based nanofoils, as well as by changing the pH or the ionic strength of the surrounding solution.²² While water can exhibit low frictional flow in nanoporous membranes,²³ ions can be sieved by such membranes, where the sieving cut-off depends on their hydrated radii.²⁴⁻²⁷

Mass transport through nanochannels and nanopores is normally realized by an osmotic or hydrostatic pressure gradient, obtained with mechanical pumps. However, the use of a pump could cause irreversible swelling or even break the membrane. The application of an electric field is one of the most promising methods as an alternative route for the transport of ions inside these systems.²⁸⁻³⁴ It can be obtained with a simple and cheap electrochemical setup, which generates a flux of ions possessing the right charge, i.e. a flux of cations from the positive to the negative poled, and vice versa for anions. An advantage of this approach is the possibility to separate ions possessing opposite charges and to impart them a different

electrophoretic mobility according to the different effective charges. Despite these properties, examples of ion transport in membranes driven by an electric field are still uncommon.

GO is emerging in the latest years as one of the most promising materials to produce innovative membranes,^{35, 36} as GO nanosheets are easy to fabricate, mechanically robust and amenable to industrial-scale production. GO-based membranes find application in many fields, like filtration and separation, despite having some limitations, such as membrane swelling, and hard post-treatment recovery for environmental applications. In addition to that, most research work is performed on flat GO membranes with a surface of few mm² or cm², which is not sufficient to give realistic flows of water for environmental applications.

The synthesis of 3D graphene-based materials is a promising strategy to solve these issues. A vast array of 3D structures can be produced, such as sponges, aerogels, and foams.³⁷⁻⁴⁰ In particular, in one of our previous works, we described the synthesis of core-shell polyethersulfone-GO hollow fibers (HF-GO), which were proved to be effective as adsorptive membranes for organic molecules.⁴¹ Each filtering module contains a bundle of ~275 hollow fibers made of polyethersulfone. Each fiber is 4.5 cm long, has an internal diameter of 300 μm and an outer diameter of 400 μm, and features lateral pores on its surface with a cut-off of 150 nm. We demonstrated how it is possible to coat a uniform layer of GO the inner walls of the hollow fibres, generating a 3D structure of graphene nanosheets, with an overall filtering surface of 0.016 m²,⁴¹ which is significantly larger than the filtering surface typically achievable in lab using flat GO membranes (10⁻⁴ -10⁻³ m²).

Here, we studied the ion migration inside these HF-GO devices, achieved either by the presence of an electric field or by the occurrence of a hydrodynamic force. Na⁺ and Ca²⁺ were studied as a model system, since they constitute a mono- and multivalent cations and are two of the most strictly controlled ions for water quality. In this setup, the core-shell structure is set as a barrier between the source solution and the drain, so any ion or water molecule is

bound to cross the core-shell structure in order to leave the filtering module. A continuous GO layer is coated inside each fiber, i.e. on the side of the source solution, and each ion or molecule is forced to navigate in the 2D nanochannels formed by the stacked GO nanosheets. We could thus modulate the selectivity of the membrane by combining the hydrodynamic flow with a suitable electric field, thanks to the peculiar 2D structure of graphene nanosheets.

2. Experimental

2.1 Reagents and solutions

GO powder was purchased from LayerOne (<35 mesh, sheet lateral size about 1 μm , many primary single sheets declared) and suspended in ultrapure water (18 $\text{M}\Omega\cdot\text{cm}$ resistivity). Sodium chloride, calcium chloride and potassium chloride and the other chlorinated salts were purchased from Sigma Aldrich and were of pure grade. Solutions of these salts were prepared using ultrapure water.

2.2 Preparation of HF-GO modules

The structure of a typical HF-GO is represented in Fig. 1. HF with an internal coating of GO were obtained according to the method previously reported,⁴¹ by injecting a GO solution through commercial polyethersulfone (PES) modules (Plasmart 25, Medica s.p.a.). To this aim, GO powder was suspended in ultrapure water by 4 h of sonication, to achieve a homogeneous 2 mg/mL suspension. A certain amount of GO suspension was filtered through the PES modules, and then the module was kept in oven at 80°C for 12 h. Modules with three different amounts of GO were prepared, namely 1%, 2.5% or 5% GO w/w against PES, containing namely 10, 15 and 30 mg of GO per module, respectively. Modules containing 1% and 2.5% GO amount can be produced with a single filtration/heating sequence; while 5% modules need a second cycle, after cooling at room temperature, to obtain the final device.

1 L of 10^{-5} M aqueous KCl was used to wash each module in a dead-end configuration, which forces a transmembrane flow. The module was then stored, filled with the KCl solution. This treatment is meant to increase the ionic conductivity in measuring stage.

2.3 Ion migration across HF-GO modules

2.3.1 Migration induced by an electric field

Ion migration was induced by connecting the setup schematized in Fig. 1 to an Autolab PGSTAT12 potentiostat/galvanostat, from Metrohm-Ecochemie. Two Pt wire electrodes were set at the opposite sites of the module, inside tanks containing 2 mL of water solution each: tank 1 contained the electrolytic solution (0.1 M solution of either NaCl or CaCl₂), while tank 2 contained ultrapure water (resistivity >18 M Ω ·cm). The two tanks were set at the same height to avoid any artifact due to differences in pressure which could spontaneously move the liquid between the two tanks. A constant potential difference of -1.0 V was applied between the two electrodes for 120 min. The variation of the conductivity of solution in tank 2 was tested every 20 min by performing measurements by electrochemical impedance spectroscopy (EIS) with interdigitate gold electrodes acquired from Metrohm-DropSens, and connected to the FRA module of the Autolab PGSTAT12 (Metrohm-Ecochemie). Frequency scans were performed over the range 100–10 KHz with a signal amplitude of 50 mV. The DC bias was temporarily stopped during the test to avoid any interference. The impedance values were converted in conductivity values according to the methodology previously reported.⁴² Each experiment was performed three times..

2.3.3 Migration induced by hydrodynamic flow

In a different experiment, we forced a flow of 2.5 mL/min across the filter using a Perimax 12 peristaltic pump (Spetec). We collected 10 mL aliquotes from tank 2 at periodic intervals. Samples were analysed as reported in paragraph 2.4 to determine the ions concentration in the different aliquotes.

2.3.4 Migration induced by electric field coupled with hydrodynamic flow

A flow of 2.5 mL/min was applied to the module with a Perimax 12 peristaltic pump (Spetec) and 10 mL aliquotes were collected from tank 2. We applied potentials ranging from 0 to -3.0 V. The original electrodes setting (cathode in tank 1 and anode in tank 2) was exploited to couple the electric field and the hydrodynamic force with the same vector direction (concordant); while inverted setting (anode in tank 1 and cathode in tank 2) was exploited to couple field and force with vectors in opposite direction (discordant). Samples solution were analysed as reported in paragraph 2.4.

2.4 X-ray diffraction analyses

Planar membranes of GO were prepared with a procedure similar to the one used to prepare the HF-GO modules, to allow XRD measurements. Planar samples were prepared by vacuum filtration of a 2 mg/mL aqueous GO (obtained by 4 h sonication of GO in ultrapure water) on an alumina Whatman filter (pore size 0.2 μm). The dry membranes were accommodated on a PES substrate (to avoid the ripping of the GO membrane) and exposed to ion solutions and electric field in a tailor-made setup, with ion flow taking place perpendicularly to the GO membrane plane. Electric field and hydrodynamic flow were produced with a Perimax 12 peristaltic pump (Spetec) and a Autolab PGSTAT12 potentiostat/galvanostat, respectively. X-ray diffraction (XRD) patterns were scanned by means of PANalytical X'Pert Pro X-ray diffractometer, with nickel-filtered Cu K α radiation and fast X'Celerator detector. Data were collected at 40 mA, 40 kV, collecting 25 s at each 0.05° 2-theta. Each experiment was performed three times.

2.5 Absorption experiments in solution

30 mg of GO powder were added to 4 mL of a 10⁻⁵ M chlorinated salt solution (KCl or HCl). The system stirred for 2 h at room temperature. The liquid phase was then filtered to remove GO and was analyzed as reported in paragraph 2.6.

2.6 Determination of ionic concentration

The concentrations of cations (in the migration and adsorption experiments) were determined by atomic spectroscopy. The concentration of Na^+ and K^+ were determined by atomic absorption spectroscopy (AAS) using a Varian SpectrAA220FS equipped with a Varian SPS-S auto-sampler. An air-acetylene flame was used, and CsCl_2 was utilized as ionic suppressor. The samples were prepared in ultrapure water with Suprapur nitric acid. Standard solutions were prepared starting from a 1'000 ppm stock solutions. All solutions were stored in polythene bottles.

The quantification of Ca^{2+} , Mg^{2+} , and Pb^{2+} was performed by inductively coupled plasma optical emission spectrometry (ICP-OES), performed with a Perkin-Elmer Optima 4200 DV simultaneous spectrometer. The sample introduction system consisted of a pneumatic nebulizer coupled with a glass spray chamber. Four standard solutions for each cation were prepared from a 1'000 ppm standard solution of Ca^{2+} , Mg^{2+} , and Pb^{2+} (single element); the higher standard concentration used was 1 ppm. Solutions with known ion concentrations were used to prepare a calibration curve for the determination of the unknown samples concentration.

3. Results and Discussion

3.1 Ion migration induced with an electric field

Fig. 1 shows the setup used in the experiments. The commercial filtration modules have four inlets, two on the side and two on the tops. The side inlet connects tank 1 (source) to the inner sides of the hollow fibers (containing the GO coating), while the top outlet connects tank 2 (drain) to the outer part of the filter, i.e. the outer side of the fibers. The other two inlets are not used, and thus sealed. This setup permits only dead-end filtration; water or ion migration

from tank 1 to tank 2 can take place only through the micropores of the hollow fiber filters (cut-off 150 nm).

We tested Na^+ and Ca^{2+} as representatives of mono- and bivalent ions, due to their importance for several water treatments, such as softening and desalination.

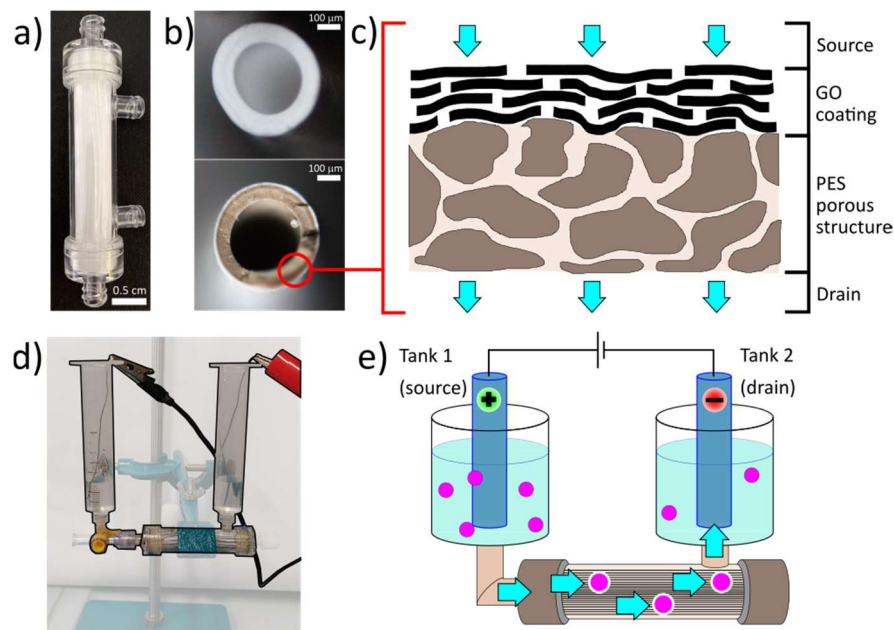


Figure 1 a) Microfiltration PES module; b) cross section of a pristine PES fiber (top) and a HF-GO 5% fiber (bottom); c) scheme of the internal coating of GO laying on the PES substrate; d) highlight of the experimental setup; e) scheme of the experimental setup.

Pristine polyethersulfone (PES, i.e. without the GO coating inside the hollow fibers) gives no barrier to ion migration, as expected. In absence of an electric field (Fig. 2), the system reaches equilibrium thanks to the diffusion induced by the concentration gradient. The application of an electric field generates a migration gradient, but equilibrium is quickly recovered as soon as the electric field is removed.

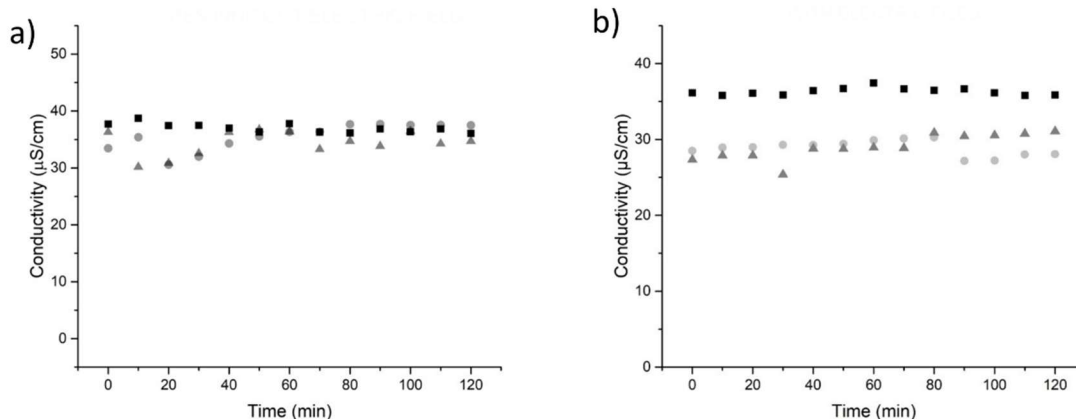


Figure 2 Conductivity over time past a pristine PES module a) without any electric field, and b) with a -1 V field on. Experiment performed three times.

The behaviour of pristine PES modules contrasts starkly with the one observed for the composite material HF-GO. Initially, Na^+ and Ca^{2+} levels in tank 2 after 2 h are negligible at AAS and ICP-OES analyses, meaning that the presence of GO prevents the diffusion of the ions. Fig. 3a shows the trend of conductivity in tank 2 for Na^+ migration when an electric field (-1 V) is applied to a HF-GO 5% module. We observed an increase of conductivity in tank 2 with time, which could be converted to concentration of ions using calibration curves. Conductivity grows over time and reaches a plateau level after 1 h. This suggests that any contribution given by HF-GO to ion migration can be attributed to the sole GO coating inside the fibers and none to the polymeric structure beneath it. In addition to that, we studied how the amount of GO in the composition of the material affects ion migration. We compared modules with different contents of GO: 1%, 2.5%, and 5% (meaning 10, 15 and 30 mg of GO, respectively). We estimated a coating thickness of 0.5 μm and 1.5 μm for 1% and 5%, respectively.⁴¹ Fig. 3b shows the effect of GO amount on ion migration. The amount of Na^+ ions transported (measured as mmol present in tank 2) grows with the increase of the amount of GO, while the Ca^{2+} quantity grows passing from 1% to 2.5% but decreases drastically passing from 2.5% to 5%. Quintano et al.⁴³ observed a similar behaviour during in-plane

movement of ions through a GO membrane induced by the application of an electric field. In that case, the migration happened along the GO membranes, with ions travelling millimetres in GO. They showed that ions could move across the GO membrane only when subjected to an electric field or a hydrodynamic force, and that monovalent ions (K^+ , Na^+ , Li^+) move more easily than bivalent ions (Ca^{2+} , Mg^{2+}) through the membrane. An explanation to this trend could be found in the different modality of movement that ions exploit to roam the GO membrane. Ions can adopt an in-plane movement or an out-of-plane movement, as depicted in Fig. 3c. Out-of-plane movement is slower because it requires the ions to find the nanochannels connecting each GO interlayer with the next one, while in-plane movement is almost a free roaming on the surface of the nanosheets.

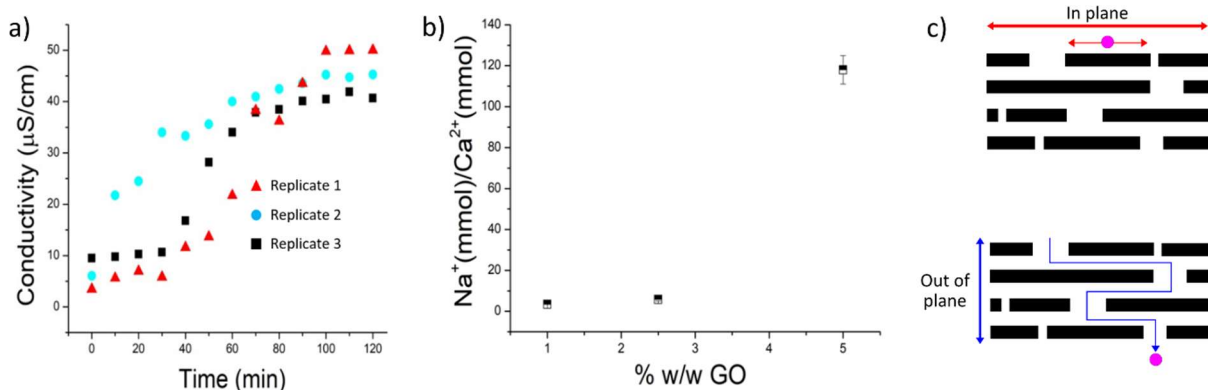


Figure 3 a) Conductivity over time past a HF-GO 5% for three different modules for Na^+ ; b) HF-GO ratio between the amount of Na^+ and Ca^{2+} collected in tank 2 after 2 h, according to GO loading. Experiment performed three times; c) in-plane (top) and out-of-plane (bottom) movements on and across a GO membrane.

The application of an electric field polarizes the electrode surface, and ions of opposite charge migrate in the diffused layer inducing the creation of an ionic gradient. The surface of GO is rich in oxygenated groups and aromatic areas (in contrast with typical polymer-based filters), the increase of the amount of GO deposited on the fibers force the ions to adopt an out-of-plane movement. Contrarily to Na^+ , Ca^{2+} can be coordinated by the oxygenated groups on the surface of GO. While the effect of the gradient is more prominent on Ca^{2+} than in Na^+ ,

thanks to its charge, the increasing number of oxygenated groups intensifies coordination of Ca^{2+} , thus lowering its mobility. Notably, HF-GO modules with lower amounts of GO (i.e. 1% and 2.5%) contain a lower number of interlayers, compared to 5%. At 1% and 2.5%, ions pass through the GO coating preferentially via in-plane movement, therefore Ca^{2+} has a smaller chance of being coordinated than in thicker membranes (i.e. 5%). Therefore, the amounts of Na^+ and Ca^{2+} at the end of the experiment are similar. On the other hand, with a 5% loading of GO, ions migration is mainly due to an out-of-plane movement. Consequently, Na^+ can easily cross the membrane, while Ca^{2+} is blocked inside the coating.

Our results agree with Quintano and Chen,^{43, 44} and confirm that the fundamental characteristics of the planar GO membranes are preserved when part of a complex 3D structure, more suitable for real applications.

In order to better understand the mechanism behind the selectivity of the module, other cations were studied. We investigate the migration of Li^+ , K^+ , Pb^{2+} , and Mg^{2+} . Fig. 4 shows the logarithmic correlation between the hydrated radii of the studied cations and the mass migrated through the module. The comparison between Pb^{2+} and Na^+ is noteworthy. They possess similar radii (4 Å) but the migration of Na^+ is tenfold the migration of Pb^{2+} . We attribute this difference to the fact that Pb^{2+} is highly subjected to coordination from the oxygenated groups on the surface of GO, due to its double positive charge.⁴⁵⁻⁴⁷ Na^+ , having only a single charge, has not an efficient interaction with the surface of GO.

Li^+ shows a different behaviour. Li^+ has the same hydrated radius of Ca^{2+} , but only one charge. This pair of cations is therefore similar to the pair Na/Ca, but the difference between their migrations is less relevant. This feature has already been noticed by Quintano et al.⁴³ This difference may be explained taking into consideration the specific interaction between Li and aromatic substrates. Li possess a partially occupied orbital at low energy ($2s^1$) which

may be stabilized by the π electrons provided by the aromatic domains of GO, thus allowing the intercalation of Li between the sheets of GO. It is likely that the potential we apply in our setup is not high enough to effectively remove Li^+ from the sheets, which is therefore prevented from traversing the module and remains trapped.⁴⁸⁻⁵² We preconditioned HF-GO modules with KCl (10^{-5} M) to increase the ionic conductivity, as described in section 2.2; but if we treated modules with HCl (10^{-5} M) instead of KCl, the amount of Ca^{2+} migrated in tank 2 is higher (Fig. 4), HCl can protonate oxygen groups and lead to a decrease in the coordination effect of these oxygenated groups against Ca^{2+} . The pH in tank 1 and tank 2 had the same value using either KCl or HCl in the module pretreatment, and the ζ potential did not varied significantly (GO: (-38.5 ± 2.6) mV; GO_{KCl} : (-41.0 ± 1.5) mV; GO_{HCl} : (-36.2 ± 2.1) mV). The same behavior was observed in absorption experiments. The concentration of Na^+ in solution remained almost the same after contact with the GO powder, and there was no noticeable difference between the solutions treated with KCl or HCl. However, in the presence of HCl, Ca^{2+} is less by the GO powder. This confirms the results obtained during the ionic migration in the module. The other cations (Li^+ , Pb^{2+} , and Mg^{2+}) are unaffected by the presence of HCl, because the adsorbed percentage does not change from HCl to KCl.

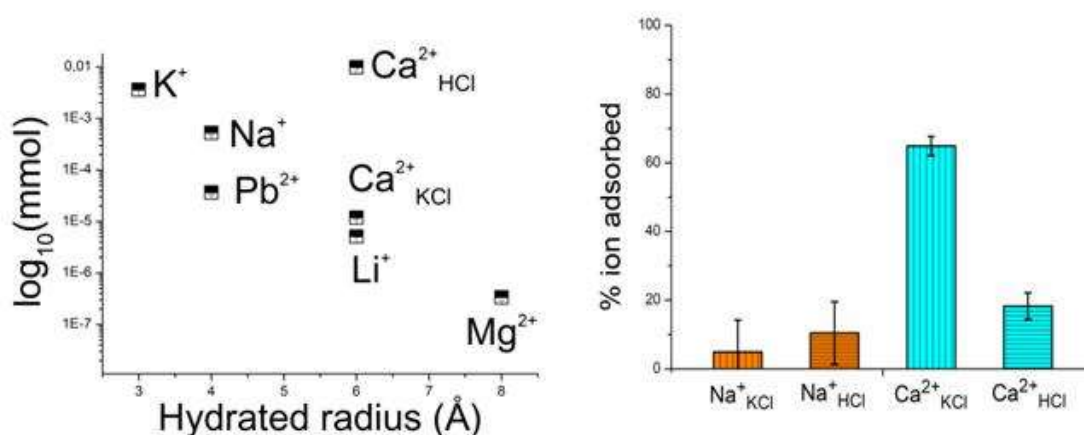


Figure 4 Correlation between the hydrated radii of the studied cations and the amount of molecules migrated through the module.

3.2 Ion migration induced by a hydrodynamic flow

This field-induced discrimination, which we have so far described in a static environment, can be applied to a dynamic environment, where a flow is the source of ion transport (Fig. 5). It is important to notice that this process is not comparable to reverse osmosis, which is designed to allow only the passage of water. In the HF-GO modules herein described, water, ions and some molecules could pass through the GO 3D structure. Pressure applied in reverse osmosis applications ranges between 15 bar and 80 bar, while in HF-GO modules, pressure is around 1.2 - 2 bar.

Fig. 5d shows the ion sieving efficiency of a HF-GO 5% module in presence of a flow of ultrapure water (2.5 mL/min). The module expresses a similar sieving behaviour when either a flow or an electric field are the sole sources for ion movement, meaning that also in this case the GO membrane can transport Na^+ better than Ca^{2+} (amount of ions transported in tank 2 after 2 h of filtration is 0.0247 ± 0.0013 mmol for Na^+ vs 0.0121 ± 0.0029 mmol for Ca^{2+} , respectively).

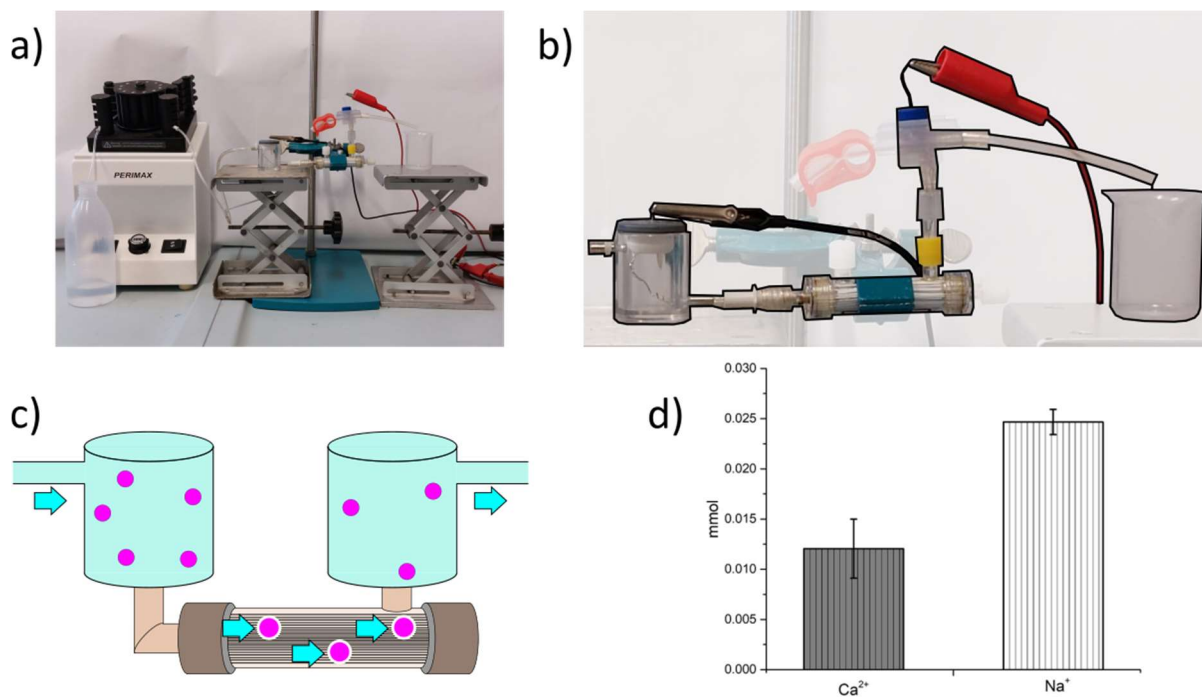


Figure 5 a) Picture of the hydrodynamic setup; b) detail of the setup; c) scheme of the migration induced by a sole flow of 2.5 mL/min, the feed contained the same molar quantity for Na⁺ and Ca²⁺, d) Ca²⁺ and Na⁺ in tank 2 after flow-induced migration (2.5 mL/min; 10 mL). Experiment performed three times.

We investigated this difference using XRD analysis. Due to the difficulties in analysing the GO coating in the HF-GO modules, planar GO membranes were produced and tested in the same conditions as the HF-GO modules, as described in section 2.3.5. Fig. 6a shows that the application of a flow brings no significant difference in the interlayer distance of GO nanosheets, thus the difference in sieving efficiency does not lay on a difference in swelling ratio. d of wet GO is (0.82 ± 0.02) nm, while d of GO exposed to Na⁺ is (0.830 ± 0.005) nm and for Ca²⁺ is (0.850 ± 0.004) nm.⁵³ Na⁺ shows a similar behaviour, giving no difference in the modification of interlayer distance due to electric field (d is (0.86 ± 0.01) nm) or flow (Fig. 6). On the other hand, Fig. 6 shows that Ca²⁺ brings a difference of 0.05 nm in the interlayer spacing when ion movement is induced with an electric field rather than a hydrodynamic flow: (0.90 ± 0.01) nm vs (0.850 ± 0.004) nm, respectively, as measured in three tests performed on three different filters.

The induction of ion movement with an electric field creates the best conditions to allow the coordination of Ca^{2+} by the surface oxygenated groups of GO. Na^+ is not subjected to the retentive effect of coordination, and so the application of an electric field does not influence its migration as much as that of Ca^{2+} . Therefore, the application of an electric field induces a higher discrimination between Na^+ and Ca^{2+} than the application of a hydrodynamic flow.

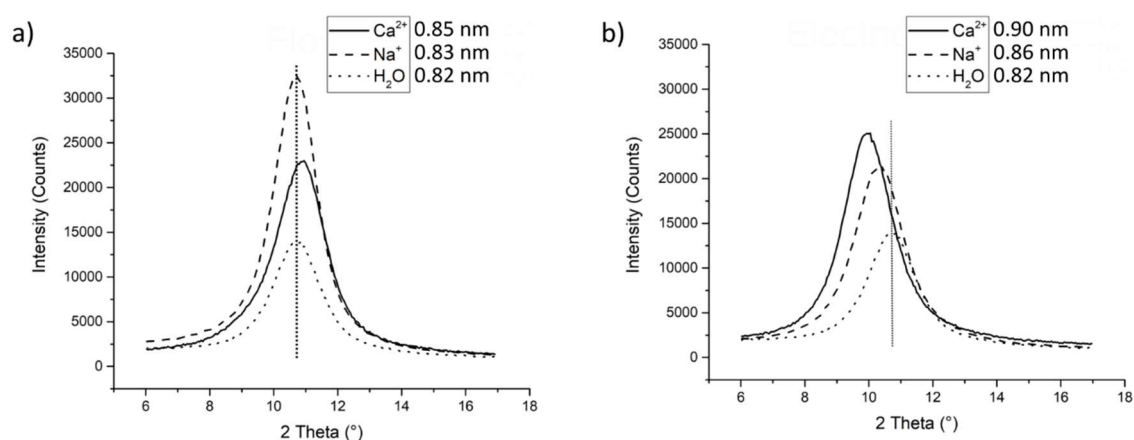


Figure 6 a) Interlayer of GO membranes where water and ions migration is due to a flow; b) interlayer of GO membranes where the ions migration is generated by an electric field. Experiment performed three times.

3.3 Modulation of ionic sieving with coupled electric field and hydrodynamic flow

It is possible to couple the application of an electric field and a hydrodynamic flow to modulate the ion discrimination of the HF-GO modules. Fig. 7a schematizes the coupling of electric field and hydrodynamic flow in the system. In this setup, field and force vectors point in the same direction (concordant); two different potential differences (-1 V, -3 V) were tested, while water flow remained constant (2.5 mL/min). The application of the electric field at -1 V enhances Ca^{2+} migration (Fig. 7b), which grows from 40% to 60%, while it does not alter Na^+ migration (Fig. 7c). Notably, the application of a higher voltage has the inverse

effect on Ca^{2+} migration, leading it from 40% to 35%, while leaving Na^+ migration unaltered again.

We attribute this evidence to a difference in ion movement. A -1 V electric field generates a gradient that helps the exit of Ca^{2+} ions from the module, making coordination less likely, and ultimately increasing the migration of Ca^{2+} across the HF-GO module. On the other hand, Na^+ is less subject to the effect of the gradient, because Na^+ is a monovalent ion and is not coordinated by GO. Therefore the electric field alters its migration less than that of Ca^{2+} . The amount of Na^+ found in tank 2 is not affected by the raising of voltage from -1 V to -3 V, while it has an evident impact on amount of Ca^{2+} measured in tank 2. In this latter case, a linear escalation would induce an amount of 60% respect to the feed solution, while it assesses approximately around 40%, which is the same amount collected in absence of electric field. Leong et al.⁵⁴ observed a similar phenomenon in planar GO membranes used for capacitive deionization. They explain that, in their case, when a low voltage is applied (0.8-1.2 V), the difference of valence between mono- and multivalent cations is less relevant than their difference in diffusion kinetics, so when mono- and multivalent cations are filtered together, the adsorption of monovalent cations prevails. At higher voltages (>1.2 V) however, the contribution of valence prevails over kinetics and adsorption of multivalent cations becomes favourite. As for our case, we suggest that a -3 V voltage increases the concentration of positive ions near the negative pole, hindering Ca^{2+} migration out of the HF-GO module.

The electric field can be applied in the opposite direction than the hydrodynamic flow (discordant), by simply inverting the bias, thus inverting the position of the cathode and the anode (Fig. 7d). Fig. 7e and 7f show the results obtained by the inversion of the electric field direction on Ca^{2+} and Na^+ migration, respectively. The migration of Ca^{2+} lowers from 40% to 35% at -1 V and to 30% at -3 V; while Na^+ migration remains in the same range despite the

change in voltage Na^+ migration does not depend on electric field variation, thus the migration gradient does not influence it. On the other hand, Ca^{2+} migration depends on gradient and on GO coordination. An electric field that is discordant to the hydrodynamic flow hinders Ca^{2+} migration, increasing their interaction with GO nanosheets and making coordination more likely, ultimately hindering their migration across the HF-GO module.

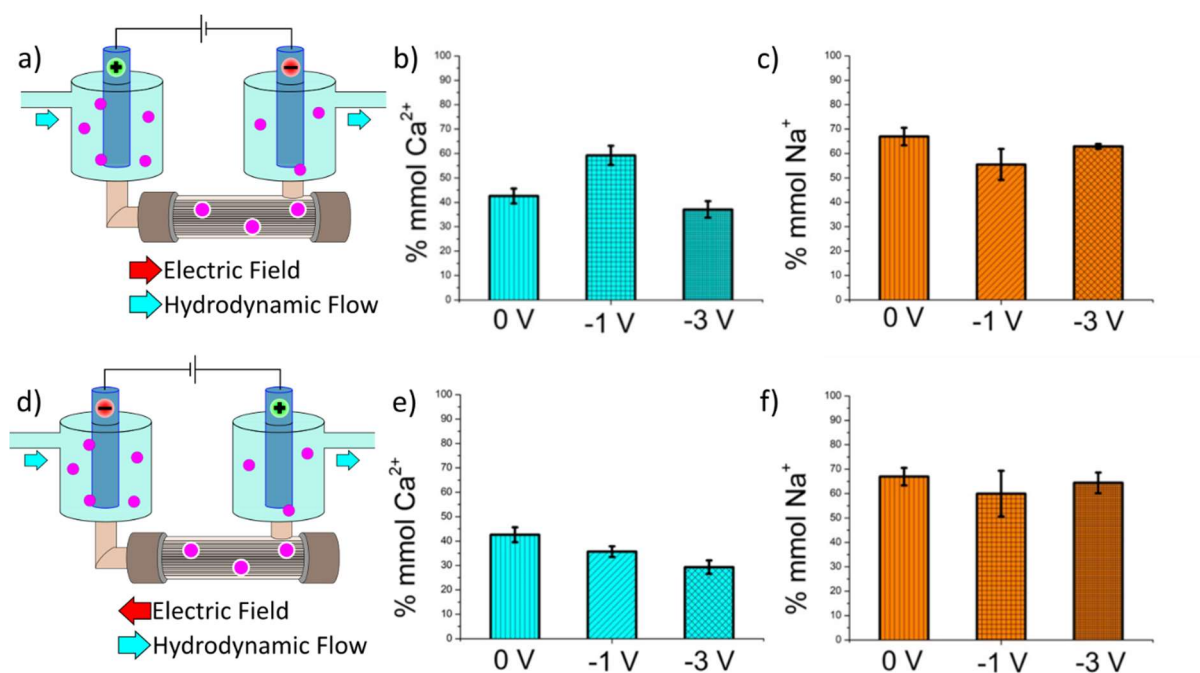


Figure 7 a) Scheme of the setup with concordant electric field and hydrodynamic flow; b) migration of Ca^{2+} in the ‘concordant’ setup with no potential applied, -1 V, and -3 V; c) migration of Na^+ in the same conditions, d) scheme of the setup with the electric field discordant to the hydrodynamic flow, e) migration of Ca^{2+} in the ‘discordant’ setup with no potential applied, -1 V, and -3 V; f) migration of Na^+ in the same conditions. Experiment performed three times.

Conclusions

We have studied the migration and sieving mechanism in water of Na^+ and Ca^{2+} inside core-shell polyethersulfone-graphene oxide hollow fibers. We demonstrated that filtering modules obtained with these hollow fibers retain the fundamental sieving characteristics of planar GO membranes, despite having a more complex, 3D structure. We studied two different sources

of ion migration, electric field and hydrodynamic flow, and observed their effects on the sieving efficiency of the module, confirming that the main driving force for the discrimination of mono- and multivalent cations is coordination by GO nanosheets. We then showed that it is possible to modulate such sieving capability by the coupling of the electric field with the hydrodynamic flow, enhancing or hindering ion migration, depending on the relative direction of the field (concordant or discordant with the flow, respectively).

The understanding of ion migration inside 3D graphene-based structures is at the core of the development of new technologies for the control of ionic content inside liquids, firsts of all water softening and desalination. Optimization and further studies are ongoing in our lab.

Bibliography

1. Dervin, S.; Dionysiou, D. D.; Pillai, S. C., 2D nanostructures for water purification: graphene and beyond. *Nanoscale* **2016**, *8* (33), 15115-15131.
2. Lin, Y.; Tian, Y.; Sun, H.; Hagio, T., Progress in modifications of 3D graphene-based adsorbents for environmental applications. *Chemosphere* **2021**, *270*, 129420.
3. Nicolai, A.; Sumpter, B. G.; Meunier, V., Tunable water desalination across graphene oxide framework membranes. *Physical Chemistry Chemical Physics* **2014**, *16* (18), 8646-8654.
4. Rizi, S. H.; Lohrasebi, A., Water distillation modeling by disjoint CNT-based channels under the influence of external electric fields. *Journal of Molecular Modeling* **2020**, *26* (9), 236.
5. Werber, J. R.; Osuji, C. O.; Elimelech, M., Materials for next-generation desalination and water purification membranes. *Nature Reviews Materials* **2016**, *1* (5), 16018.
6. Chong, W. C.; Choo, Y. L.; Koo, C. H.; Pang, Y. L.; Lai, S. O., Adsorptive membranes for heavy metal removal – A mini review. *AIP Conference Proceedings* **2019**, *2157* (1), 020005.
7. Peng, W.; Li, H.; Liu, Y.; Song, S., A review on heavy metal ions adsorption from water by graphene oxide and its composites. *J. Mol. Liq.* **2017**, *230*, 496-504.
8. Tröger, R.; Ren, H.; Yin, D.; Postigo, C.; Nguyen, P. D.; Baduel, C.; Golovko, O.; Been, F.; Joerss, H.; Boleda, M. R.; Polesello, S.; Roncoroni, M.; Taniyasu, S.; Menger, F.; Ahrens, L.; Yin Lai, F.; Wiberg, K., What's in the water? – Target and suspect screening of contaminants of emerging concern in raw water and drinking water from Europe and Asia. *Water Res.* **2021**, *198*, 117099.
9. Murray, K. E.; Thomas, S. M.; Bodour, A. A., Prioritizing research for trace pollutants and emerging contaminants in the freshwater environment. *Environ. Pollut.* **2010**, *158* (12), 3462-3471.
10. Petrie, B.; Barden, R.; Kasprzyk-Hordern, B., A review on emerging contaminants in wastewaters and the environment: Current knowledge, understudied areas and recommendations for future monitoring. *Water Res.* **2015**, *72*, 3-27.
11. Rathi, B. S.; Kumar, P. S.; Show, P.-L., A review on effective removal of emerging contaminants from aquatic systems: Current trends and scope for further research. *Journal of Hazardous Materials* **2021**, *409*, 124413.
12. Sorlini, S.; Collivignarelli, M. C.; Miino, M. C. J. E. E.; Journal, M., Technologies for the control of emerging contaminants in drinking water treatment plants. **2019**, *18*, 2203-2216.

13. Du, X.; Ma, X.; Zhang, P.; Zheng, J.; Wang, Z.; Gao, F.; Hao, X.; Liu, S.; Guan, G., A novel electric-field-accelerated ion-sieve membrane system coupling potential-oscillation for alkali metal ions separation. *Electrochimica Acta* **2017**, *258*, 718-726.
14. Kielland, J., Individual Activity Coefficients of Ions in Aqueous Solutions. *Journal of the American Chemical Society* **1937**, *59* (9), 1675-1678.
15. Zhang, F.; Fan, J.-b.; Wang, S., Interfacial Polymerization: From Chemistry to Functional Materials. *Angewandte Chemie International Edition* **2020**, *59* (49), 21840-21856.
16. Chennamsetty, R.; Escobar, I.; Xu, X., Characterization of commercial water treatment membranes modified via ion beam irradiation. *Desalination* **2006**, *188* (1), 203-212.
17. Kim, Y. S.; Hong, W.; Woo, H. J.; Choi, H. W.; Kim, G. D.; Lee, J. H.; Lee, S., Ion Beam Lithography Using Membrane Masks. *Japanese Journal of Applied Physics* **2002**, *41* (Part 1, No. 6B), 4141-4145.
18. Liu, G.; Jin, W.; Xu, N., Graphene-based membranes. *Chemical Society Reviews* **2015**, *44* (15), 5016-5030.
19. Yang, J.; Li, Z.; Wang, Z.; Yuan, S.; Li, Y.; Zhao, W.; Zhang, X., 2D Material Based Thin-Film Nanocomposite Membranes for Water Treatment. *Advanced Materials Technologies* **2021**, *6* (10), 2000862.
20. Sun, J.; Sadd, M.; Edenborg, P.; Grönbeck, H.; Thiesen, P. H.; Xia, Z.; Quintano, V.; Qiu, R.; Matic, A.; Palermo, V., Real-time imaging of Na⁺ reversible intercalation in “Janus” graphene stacks for battery applications. *Science Advances* *7* (22), eabf0812.
21. Abraham, J.; Vasu, K. S.; Williams, C. D.; Gopinadhan, K.; Su, Y.; Cherian, C. T.; Dix, J.; Prestat, E.; Haigh, S. J.; Grigorieva, I. V.; Carbone, P.; Geim, A. K.; Nair, R. R., Tunable sieving of ions using graphene oxide membranes. *Nat. Nanotechnol.* **2017**, *12* (6), 546-550.
22. Huang, H.; Mao, Y.; Ying, Y.; Liu, Y.; Sun, L.; Peng, X., Salt concentration, pH and pressure controlled separation of small molecules through lamellar graphene oxide membranes. *Chemical Communications* **2013**, *49* (53), 5963-5965.
23. Nair, R. R.; Wu, H. A.; Jayaram, P. N.; Grigorieva, I. V.; Geim, A. K., Unimpeded Permeation of Water Through Helium-Leak-Tight Graphene-Based Membranes. *Sci* **2012**, *335* (6067), 442-444.
24. Tansel, B.; Sager, J.; Rector, T.; Garland, J.; Strayer, R. F.; Levine, L.; Roberts, M.; Hummerick, M.; Bauer, J., Significance of hydrated radius and hydration shells on ionic permeability during nanofiltration in dead end and cross flow modes. *Separation and Purification Technology* **2006**, *51* (1), 40-47.
25. Zhang, X.; Li, F.; Zhang, P.; Zhu, C.; Zhao, X., The role of interlayers in enlarging the flux of GO membranes. *Nanotechnology* **2020**, *31* (50), 505708.
26. Joshi, R. K.; Carbone, P.; Wang, F. C.; Kravets, V. G.; Su, Y.; Grigorieva, I. V.; Wu, H. A.; Geim, A. K.; Nair, R. R., Precise and Ultrafast Molecular Sieving Through Graphene Oxide Membranes. *Sci* **2014**, *343* (6172), 752-754.
27. Yang, Q.; Su, Y.; Chi, C.; Cherian, C. T.; Huang, K.; Kravets, V. G.; Wang, F. C.; Zhang, J. C.; Pratt, A.; Grigorenko, A. N.; Guinea, F.; Geim, A. K.; Nair, R. R., Ultrathin graphene-based membrane with precise molecular sieving and ultrafast solvent permeation. *Nature Materials* **2017**, *16* (12), 1198-1202.
28. Cheng, C.; Jiang, G.; Simon, G. P.; Liu, J. Z.; Li, D., Low-voltage electrostatic modulation of ion diffusion through layered graphene-based nanoporous membranes. *Nature Nanotechnology* **2018**, *13* (8), 685-690.
29. Gong, X.; Li, J.; Lu, H.; Wan, R.; Li, J.; Hu, J.; Fang, H., A charge-driven molecular water pump. *Nature Nanotechnology* **2007**, *2* (11), 709-712.
30. Hassanvand, A.; Chen, G. Q.; Webley, P. A.; Kentish, S. E., A comparison of multicomponent electrosorption in capacitive deionization and membrane capacitive deionization. *Water Research* **2018**, *131*, 100-109.

31. Kou, J.; Yao, J.; Lu, H.; Zhang, B.; Li, A.; Sun, Z.; Zhang, J.; Fang, Y.; Wu, F.; Fan, J., Electromanipulating Water Flow in Nanochannels. *Angewandte Chemie International Edition* **2015**, *54* (8), 2351-2355.
32. Sun, P.; Zheng, F.; Wang, K.; Zhong, M.; Wu, D.; Zhu, H., Electro- and Magneto-Modulated Ion Transport through Graphene Oxide Membranes. *Scientific Reports* **2014**, *4* (1), 6798.
33. Sun, P.; Zhu, M.; Wang, K.; Zhong, M.; Wei, J.; Wu, D.; Xu, Z.; Zhu, H., Selective Ion Penetration of Graphene Oxide Membranes. *ACS Nano* **2013**, *7* (1), 428-437.
34. Zhou, K. G.; Vasu, K. S.; Cherian, C. T.; Neek-Amal, M.; Zhang, J. C.; Ghorbanfekr-Kalashami, H.; Huang, K.; Marshall, O. P.; Kravets, V. G.; Abraham, J.; Su, Y.; Grigorenko, A. N.; Pratt, A.; Geim, A. K.; Peeters, F. M.; Novoselov, K. S.; Nair, R. R., Electrically controlled water permeation through graphene oxide membranes. *Nature* **2018**, *559* (7713), 236-240.
35. Huang, H.; Ying, Y.; Peng, X., Graphene oxide nanosheet: an emerging star material for novel separation membranes. *Journal of Materials Chemistry A* **2014**, *2* (34), 13772-13782.
36. Huang, L.; Zhang, M.; Li, C.; Shi, G., Graphene-Based Membranes for Molecular Separation. *The Journal of Physical Chemistry Letters* **2015**, *6* (14), 2806-2815.
37. Mohd Firdaus, R.; Berrada, N.; Desforges, A.; Mohamed, A. R.; Vigolo, B., From 2D Graphene Nanosheets to 3D Graphene-based Macrostructures. *Chemistry – An Asian Journal* **2020**, *15* (19), 2902-2924.
38. Shen, Y.; Fang, Q.; Chen, B., Environmental Applications of Three-Dimensional Graphene-Based Macrostructures: Adsorption, Transformation, and Detection. *Environmental Science & Technology* **2015**, *49* (1), 67-84.
39. Sun, Z.; Fang, S.; Hu, Y. H., 3D Graphene Materials: From Understanding to Design and Synthesis Control. *Chemical Reviews* **2020**, *120* (18), 10336-10453.
40. Yousefi, N.; Lu, X.; Elimelech, M.; Tufenkji, N., Environmental performance of graphene-based 3D macrostructures. *Nat. Nanotechnol.* **2019**, *14* (2), 107-119.
41. Kovtun, A.; Bianchi, A.; Zambianchi, M.; Bettini, C.; Corticelli, F.; Ruani, G.; Bocchi, L.; Stante, F.; Gazzano, M.; Marforio, T. D.; Calvaresi, M.; Minelli, M.; Navacchia, M. L.; Palermo, V.; Melucci, M., Core-shell graphene oxide-polymer hollow fibers as water filters with enhanced performance and selectivity. *Faraday Discuss.* **2021**, *227* (0), 274-290.
42. Brom-Verheijden, G. J. A. M.; Goedbloed, M. H.; Zevenbergen, M. A. G., A Microfabricated 4-Electrode Conductivity Sensor with Enhanced Range. *Proceedings* **2018**, *2* (13).
43. Quintano, V.; Kovtun, A.; Biscarini, F.; Liscio, F.; Liscio, A.; Palermo, V., Long-range selective transport of anions and cations in graphene oxide membranes, causing selective crystallization on the macroscale. *Nanoscale Advances* **2021**, *3* (2), 353-358.
44. Chen, L.; Shi, G.; Shen, J.; Peng, B.; Zhang, B.; Wang, Y.; Bian, F.; Wang, J.; Li, D.; Qian, Z.; Xu, G.; Liu, G.; Zeng, J.; Zhang, L.; Yang, Y.; Zhou, G.; Wu, M.; Jin, W.; Li, J.; Fang, H., Ion sieving in graphene oxide membranes via cationic control of interlayer spacing. *Nature* **2017**, *550* (7676), 380-383.
45. Khaligh, G. N.; Johan, R. M., Recent Advances in Water Treatment Using Graphene-based Materials. *Mini-Reviews in Organic Chemistry* **2020**, *17* (1), 74-90.
46. Chae, J.; Lim, T.; Cheng, H.; Hu, J.; Kim, S.; Jung, W., Graphene Oxide and Carbon Nanotubes-Based Polyvinylidene Fluoride Membrane for Highly Increased Water Treatment. *Nanomaterials* **2021**, *11* (10).
47. de Figueiredo Neves, T.; Kushima Assano, P.; Rodrigues Sabino, L.; Bardelin Nunes, W.; Prediger, P., Influence of Adsorbent/Adsorbate Interactions on the Removal of Cationic Surfactants from Water by Graphene Oxide. *Water, Air, & Soil Pollution* **2020**, *231* (6), 304.
48. Huang, P.; Xiong, T.; Zhou, S.; Yang, H.; Huang, Y.; Balogun, M. S. J. T.; Ding, Y., Advanced Tri-Layer Carbon Matrices with π - π Stacking Interaction for Binder-Free Lithium-Ion Storage. *ACS Applied Materials & Interfaces* **2021**, *13* (14), 16516-16527.
49. Matsumura, Y.; Wang, S.; Mondori, J., Interactions between disordered carbon and lithium in lithium ion rechargeable batteries. *Carbon* **1995**, *33* (10), 1457-1462.

50. Asahina, H.; Kurotaki, M.; Yonei, A.; Yamaguchi, S.; Mori, S., Real-time X-ray diffraction measurement of carbon structure during lithium-ion intercalation. *Journal of Power Sources* **1997**, *68* (2), 249-252.
51. Zaghbi, K.; Choquette, Y.; Guerfi, A.; Simoneau, M.; Bélanger, A.; Gauthier, M., Electrochemical intercalation of lithium into carbons using a solid polymer electrolyte. *Journal of Power Sources* **1997**, *68* (2), 368-371.
52. Márquez, A., Molecular dynamics studies of combined carbon/electrolyte/lithium-metal oxide interfaces. *Materials Chemistry and Physics* **2007**, *104* (1), 199-209.
53. Zheng, S.; Tu, Q.; Urban, J. J.; Li, S.; Mi, B., Swelling of Graphene Oxide Membranes in Aqueous Solution: Characterization of Interlayer Spacing and Insight into Water Transport Mechanisms. *ACS Nano* **2017**, *11* (6), 6440-6450.
54. Leong, Z. Y.; Han, Z.; Wang, G.; Li, D.-S.; Yang, S. A.; Yang, H. Y., Electric field modulated ion-sieving effects of graphene oxide membranes. *Journal of Materials Chemistry A* **2021**, *9* (1), 244-253.

PART 4

COEXTRUSION

4.1 The “coextrusion” strategy

Let's return to the strategy behind the development of the composite materials. In part 2: core-shell system, we have already seen that such strategy aims at maximizing the exploitable surface area of GO in the composite material. The main limit of this strategy for industrial application (as it is) is the loss of water permeability that a coating covering the pores of the HF implies. Despite this composite is appropriate for other uses, the target of the project that hosted this thesis is to develop a material suitable for commercialization. This led the research toward another strategy, which favours scale-up. This second strategy is the coextrusion of GO with the polymer. The industrial production of HF has two crucial steps: extrusion and phase inversion.

Extrusion is the mechanical process of pushing a malleable material through a die (a shaped hole) in order to impose to it the desired shape. This is a common technique in the production of a vast array of products, such as plastic pipes, metal bars, or glassware.¹⁻³

Phase inversion is too a common practise in HF production. It requires the application of a physical phenomenon (cooling down, exposure to an anti-solvent, evaporation) to force the transition from a phase to another. Usually, this transition is from a liquid phase to a solid phase. The choice of the type and conditions of the phase inversion depend primarily on the material under treatment.

Briefly, the HF exploited for this thesis are produced in this way: polymeric granules (PSU or PES) are dissolved in an organic solvent and converted in a viscous paste. This paste is then extruded into the HF, and its 3D shape is fixed *via* subsequent washings in water, which act as an anti-solvent to the polymer.

If GO is dispersed inside the paste, it is possible to extrude it together with the polymer (what I have so far called coextrusion). This leads to the encapsulation of GO into the structure of the HF. The composite obtained implementing GO in PSU (which is called PSUGO in the following article) possess the same three-dimensional structure of the pristine HF and the same ultrafiltration efficiency, but acts also as support for GO, which is the active component for adsorption of pollutants.

All those who have worked with this type of procedure know that the main issue is to make sure that the active component is exposed and not totally encapsulated inside the matrix, where it would not enter in contact with the pollutants. In this case, the chemistry of GO comes to our aid. GO is hydrophilic so, while the polymer solidifies during the phase inversion in water, it puts itself in the interface between the polymer and the bulk of water. The result is that the majority of GO gets exposed on the surface of the pores, and is actually available for water purification.⁴ The percentage of GO “lost” in the matrix is therefore significantly lower than what would get lost without this phenomenon.

4.2 New materials for new challenges

As anticipated in the introduction, one of the main characteristics of emerging contaminants is that water treatment plants are inefficient or ineffective in removing them from water. In the following article, we tested the coextruded composite material on three different classes of emerging contaminants: aromatic molecules, heavy metals, and perfluoroalkyl substances (PFAS).

It is unlikely that nanotechnologies will oust granular activated carbon (GAC) from the position of adsorber *par excellence* in the near future, due to its availability and low cost, but volume is not enough to overcome the limits of GAC in terms of selectivity. The aim of graphene-based adsorbers (and other nanomaterials) is not to substitute GAC, but to complement its applications, to face the problems that GAC cannot solve alone.

One example of such pollutants are heavy metals. As we know, GO surface is populated with oxygenated groups, which can coordinate cations. This allows the adsorption of those heavy metals that remain cationic in water, such as chromium, copper, and lead. The composite material PSUGO is at least ten times more active than both GAC and pristine PSU in the removal of these cations, making it an excellent alternative for their treatment (especially for lead, which may be still present in old pipelines).^{5,6}

An interesting thematic is the covalent modification of GO aimed at the tuning of its selectivity. This subject would deserve a thesis *per se*, but I will quote one of the works I took part in. In this paper,⁷ we grafted a polyethylenimine on the surface on GO and created core-shell filters with it. This procedure had the effect of inverting the ζ potential of GO, from negative to positive, and changing the selectivity toward heavy metal adsorption. Pristine GO is ineffective in adsorbing arsenic, because in water it exists in form of arsenate (AsO_4^{3-}), while the GO modified with the polyethylenimine is very effective in this task. This kind of specific modification permits the development for *ad hoc* remediation or high-selectivity sensors.

The same thing applies to PFAS.⁸⁻¹² More than four thousand substances compose this family of highly persistent, bioaccumulative, and toxic compounds. They are carboxylic or sulfonic acids, with poly- or perfluorinated alkyl chains of variable length. They saw extensive use in the end of the XX century as surfactants and resistant surfaces (oil-, water-, fireproof), such as non-stick cookware (Teflon®) and technical tissues (GORE-TEX®, Scotchgard™).¹³ Their persistency in the environment earned them the title of “forever chemicals”. In the article you are about to read, we tested 14 different PFAS with variable chain length and polar head, comparing GAC, PSU, and PSUGO. The composite material showed a better selectivity toward PFAS than both PSU and GAC in the majority of cases, especially in the mid-length range (6-8 alkyl carbon atoms). The total removal efficiency of PSUGO is one order of magnitude higher than that of GAC on the sum of the 14 PFAS.

Another important aspect of this paper concerns the detection of GO. When we produced the paper in part 2: core-shell system,¹⁴ there was not an high-efficiency technique for the detection of GO in water, so much so we exploited UV-Vis analyses to assess its absence within a limit of detection of 2.5 ppm. For this paper, we collaborated with a group from another Spearhead project of the Graphene Flagship, called *SafeGraph*,¹⁵ to test an innovative surface-enhanced Raman spectroscopy (SERS) technique they developed. We had our filters tested with such technique and this demonstrated that they do not release GO during use, within a limit of detection of 0.1 ppb. This value is up to date the state of the art for the detection of GO in water. I would like to stress the fact that all of the measurements in this paper were performed using tap water as the matrix, which gives real efficiency data. The majority of the data obtained in this field are produced spiking purified water.

Italy hosts the third worst case of environmental PFAS pollution in the world, in terms of the polluted area, in a triangle formed by Padua, Verona, and Vicenza. A big social movement arose from the population of this area, which ended having an effect on the new Drinking Water Directive 2020/2184. If the reader is interested in the social impact of PFAS, I suggest starting from the group *Mamme no PFAS*^{16, 17} (i.e. mothers against PFAS), whom fight to heal their homeland from these horrid pollutants. Another access point to this subject is the movie *Dark Waters*,¹⁸ a thrilling movie acting as a sort of documentary, which narrates a similar situation in the USA.

4.3 Strategy and industry

The core aim of the coextrusion strategy is to avoid as much as possible the loss of water permeability that the implementation of GO can impose to HF. This is in contrast with the core-shell strategy; where the aim is to maximize the exploitable surface area of GO. The coextrusion strategy happened to be more suitable for industrial applications than the core-shell one, because in real systems applications not hindering the water flow has priority over maximizing efficiency. There is also another aspect to consider. The starting point of the core-shell system is an already finished filtering

module, which makes it extremely handy to test new composites in the laboratory. This means that the production of the composite require more steps than the production of the pristine HF, which implies higher costs, production times, and machines. The coextrusion uses the same machines and procedure than the pristine HF, so a company does not have to adapt its facility to implement the production of the new material, saving money, time, and trouble. The result is that the coextrusion strategy is more attractive to the industrial world. In Q4 2022, Medica s.p.a. started a 200'000 km/year production of the composite, officialising this material as a TRL 9 product.

Bibliography

1. Smolders, C. A.; Reuvers, A. J.; Boom, R. M.; Wienk, I. M., Microstructures in phase-inversion membranes. Part 1. Formation of macrovoids. *J. Membr. Sci.* **1992**, *73* (2), 259-275.
2. Strathmann, H.; Kock, K., The formation mechanism of phase inversion membranes. *Desalination* **1977**, *21* (3), 241-255.
3. Yeo, L. Y.; Matar, O. K.; Perez de Ortiz, E. S.; Hewitt, G. F., PHASE INVERSION AND ASSOCIATED PHENOMENA. **2000**, *12* (1), 66.
4. Zambianchi, M.; Durso, M.; Liscio, A.; Treossi, E.; Bettini, C.; Capobianco, M. L.; Aluigi, A.; Kovtun, A.; Ruani, G.; Corticelli, F.; Brucale, M.; Palermo, V.; Navacchia, M. L.; Melucci, M., Graphene oxide doped polysulfone membrane adsorbers for the removal of organic contaminants from water. *Chem. Eng. J.* **2017**, *326*, 130-140.
5. Ahmad, S. Z. N.; Wan Salleh, W. N.; Ismail, A. F.; Yusof, N.; Mohd Yusop, M. Z.; Aziz, F., Adsorptive removal of heavy metal ions using graphene-based nanomaterials: Toxicity, roles of functional groups and mechanisms. *Chemosphere* **2020**, *248*, 126008.
6. Peng, W.; Li, H.; Liu, Y.; Song, S., A review on heavy metal ions adsorption from water by graphene oxide and its composites. *J. Mol. Liq.* **2017**, *230*, 496-504.
7. Mantovani, S.; Khaliha, S.; Favaretto, L.; Bettini, C.; Bianchi, A.; Kovtun, A.; Zambianchi, M.; Gazzano, M.; Casentini, B.; Palermo, V.; Melucci, M., Scalable synthesis and purification of functionalized graphene nanosheets for water remediation. *ChCom* **2021**, *57* (31), 3765-3768.
8. Barker, D.; Fors, A.; Lindgren, E.; Olesund, A.; Schröder, E., Filter function of graphene oxide: Trapping perfluorinated molecules. *J. Chem. Phys.* **2020**, *152* (2), 024704.
9. Gagliano, E.; Sgroi, M.; Falciglia, P. P.; Vagliasindi, F. G. A.; Roccaro, P., Removal of poly- and perfluoroalkyl substances (PFAS) from water by adsorption: Role of PFAS chain length, effect of organic matter and challenges in adsorbent regeneration. *Water Res.* **2020**, *171*, 115381.
10. Jin, T.; Peydayesh, M.; Mezzenga, R., Membrane-based technologies for per- and poly-fluoroalkyl substances (PFASs) removal from water: Removal mechanisms, applications, challenges and perspectives. *Environ. Int.* **2021**, *157*, 106876.
11. McCleaf, P.; Englund, S.; Östlund, A.; Lindegren, K.; Wiberg, K.; Ahrens, L., Removal efficiency of multiple poly- and perfluoroalkyl substances (PFASs) in drinking water using granular activated carbon (GAC) and anion exchange (AE) column tests. *Water Res.* **2017**, *120*, 77-87.

12. Wu, C.; Klemes, M. J.; Trang, B.; Dichtel, W. R.; Helbling, D. E., Exploring the factors that influence the adsorption of anionic PFAS on conventional and emerging adsorbents in aquatic matrices. *Water Res.* **2020**, *182*, 115950.
13. Glüge, J.; Scheringer, M.; Cousins, I. T.; DeWitt, J. C.; Goldenman, G.; Herzke, D.; Lohmann, R.; Ng, C. A.; Trier, X.; Wang, Z., An overview of the uses of per- and polyfluoroalkyl substances (PFAS). *Environmental Science: Processes & Impacts* **2020**, *22* (12), 2345-2373.
14. Kovtun, A.; Bianchi, A.; Zambianchi, M.; Bettini, C.; Corticelli, F.; Ruani, G.; Bocchi, L.; Stante, F.; Gazzano, M.; Marforio, T. D.; Calvaresi, M.; Minelli, M.; Navacchia, M. L.; Palermo, V.; Melucci, M., Core-shell graphene oxide-polymer hollow fibers as water filters with enhanced performance and selectivity. *Faraday Discuss.* **2021**, *227* (0), 274-290.
15. <https://graphene-flagship.eu/innovation/spearheads/c3-sh11-safegraph/>.
16. <https://www.mammenopfas.org/>.
17. <https://pfas.land/informazioni/>.
18. Haynes, T., Dark Waters. 2019, Participant LLC & Killer Films.

Graphene oxide-polysulfone hollow fibers membranes with synergic ultrafiltration and adsorption for enhanced drinking water treatment

Massimo Zambianchi,^{‡ a} Sara Khaliha,^{‡ a} Antonio Bianchi,^{‡ a} Francesca Tunioli,^a Alessandro Kovtun,^a Maria Luisa Navacchia,^a Anastasio Salatino,^b Zhenyuan Xia,^c Elena Briñas,^d Ester Vázquez,^{d, e} Davide Paci,^f Vincenzo Palermo,^a Letizia Bocchi,^f Barbara Casentini,^b Manuela Melucci^{a, *}

^a Consiglio Nazionale delle Ricerche, Institute for Organic Synthesis and Photoreactivity (CNR-ISOF), via Piero Gobetti 101, 40129 Bologna (BO), Italy

^b Consiglio Nazionale delle Ricerche, Institute for Water Research (CNR-IRSA), Via del Mulino, 20861, Roma (RM), Italy

^c Industrial and Materials Science, Chalmers University of Technology, 41258 Göteborg, Sweden

^d Regional Institute of Applied Scientific Research (IRICA), UCLM, 13071 Ciudad Real, Spain

^e Department of Organic Chemistry, Faculty of Science and Chemistry Technologies, University of Castilla-La Mancha (UCLM), 13071 Ciudad Real, Spain

^f Medica Spa, via degli Artigiani 7, 41036 Medolla (MO), Italy

[‡] These authors contributed equally to this work

DOI: <https://doi.org/10.1016/j.memsci.2022.120707>

Abstract

Polysulfone-graphene oxide hollow fiber membranes (PSU-GO HF) with simultaneous adsorption and ultrafiltration capabilities are herein described and proposed for enhanced and simplified Point-of-Use (POU) drinking water purification. The PSU-GO HF were prepared by phase inversion extrusion by a customized semi-industrial plant and their morphology, surface properties, and porosity were investigated by combined Scanning Electron Microscopy (SEM), contact angle and Raman confocal microscopy, in relation to different GO:PSU ratios (1-5% w/w GO vs PSU) and to the final adsorption-ultrafiltration properties. Filtration modules of PSU-GO HF of filtering surface (FS) in the range 0.015-0.28 m² showed same ultrafiltration capability of PSU-HF standard filters. Synergic adsorption properties were demonstrated by studying the adsorption maximum capacity of

ciprofloxacin antibiotic (CIPRO) vs GO ratio in dead end in-out configuration, the standard configuration used for PSU HF commercial modules. Loading of 3.5% GO vs PSU was selected as case study, representing the best compromise between performance and GO nanofiller amount. Heavy metals (Pb, Cu and Cr(III)) and polyfluoroalkyl substances (PFAS) removal capabilities from tap water were competitive and in some cases outperformed Granular Activated Carbon (GAC), the standard industrial sorbent. Ciprofloxacin removal from tap water was also under real operational conditions. Moreover, release of GO from working PSU-GO modules was excluded by Surface Enhanced Raman Spectroscopy (SERS) analysis of treated water having the state-of-the-art limit of quantification of 0.1 $\mu\text{g/L}$ for GO nanosheets.

1. Introduction

Polysulfone (PSU) porous membranes are well-known and used membranes for micro and ultrafiltration for hemodialysis and water disinfection purposes.¹⁻⁴ Their wide range of applications relies on the structure versatility of such membranes, with morphology and porosity that can be tuned by the choice of several parameters including processing solvent/ non solvent, coagulation temperature, casting solution composition and humidity.⁵⁻⁷ In recent years, aiming at membranes with enhanced mechanical properties, biofouling resistance and multifunctionality, doping of PSU membranes (mainly flat membranes) with nanomaterials have been widely investigated.⁸

Carbon-based nanomaterials such as carbon nanotubes (CNT), nanofibers and graphene-reinforced membranes have been fabricated by phase inversion processes adapted to integrate such nanomaterials.⁹ It has been shown that doping of PSU with carbon nanotubes of different structure (single, multiwalled) and functionalization (i.e. amine, azide, carboxylic groups) increases water permeability (up to $\sim 600 \text{ Lm}^{-2}\text{h}^{-1}$)¹⁰, improves tensile strength and modulus, increases materials crystallinity and thermostability¹¹ and enhanced rejection of NaCl solution.¹² With the advent of graphene 2D materials, having higher processability and lower costs than CNT, graphene doped

membranes have been also realized ^{13 14} and have shown improved thermal and mechanical properties, ^{15 16} ion exchange capability ¹⁷ and arsenate rejection capability (just to mention few) ¹⁸, than non-doped analogues.

Adsorption properties were observed for these membranes. ^{19, 20} For instance Badrinezhad et al. demonstrated methylene blue adsorption from water with removal efficiency of about 80% by 0.75% doped PSU membranes ²¹ and desorption of about 40% which was lower than observed in graphene free membranes. Some of us, reported the fabrication of PSU-GO adsorptive membranes with 5% in weight of GO content and demonstrated the ability of this membranes to adsorb selected emerging contaminants (EC) in mixture in tap water with significant enhancement of removal of hydrophilic molecules including ofloxacin, carbamazepine and diclofenac. ²²

On this line, here we report the fabrication of PSU hollow fiber (PSU-HF) membranes through an ad hoc developed industrial pilot plants (Medica s.p.a., production capacity 200'000 km/yr) doped with GO at different loadings (PSU-GO HF). We investigated the structural, filtration and adsorption properties of modules realized by the newly developed HF aimed at their exploitation for the fabrication of multifunctional modules for point-of-use (POU) drinking water treatment.

POU drinking water treatment systems are installed on the water supply lines ahead of water taps, and/or dispensers to provide on-site water purification. A wide range of POU technologies have emerged in recent years including adsorption membrane filtration and disinfection that are combined in a specific sequence to form a POU system. These systems are exploited to adjust water taste and odour and are expected to remove hazardous contaminants such as EC ²³⁻²⁸ not completely removed during drinking water treatment such as perfluoroalkyl chain substances (PFAS) ²⁹⁻³⁶.

Polysulfone hollow fiber (PSU-HF) membranes consist of hollow fibers with surface pores and macrovoids of porosity in the range 5-100 nm that have been recently introduced in the POU water purification market for water disinfection, i.e. removal of bacteria, viruses and endotoxins capability. PSU-HF modules are exploited as last treatment step after adsorption and/or ion exchange and/or reverse osmosis steps to remove pathogens. ^{37 38} Aiming at simplified and more efficient POU

systems,³⁹ here we propose adsorptive PSU-GO HF based modules for combined ultrafiltration and adsorption of different water pollutants, both organics and heavy metals. Previous studies on PSU-HF doped with carbon nanoparticles and prepared by phase inversion (from DMF to water) showed adsorptive capability toward benzene, phenol and toluene from aqueous solution⁴⁰ with adsorption capacity (Q_{max}) of the membranes increasing with carbon nanoparticle concentration in the range 50-60 mg/g. Zahri et al.⁴¹ reported PSU-graphene oxide hollow fiber membranes prepared by phase inversion from a mixture DMAC, THF and EtOH to water and demonstrated gas separation properties with CO₂/N₂ and CO₂/CH₄ selectivity enhancement by 158% and 74% respectively with respect to neat PSU membranes. More recently, Sainath et al further enhance the CO₂/CH₄ gas separation performance of PSU-GO HF by zeolitic imidazolate nanoparticles inclusion.⁴²

However, at the best of our knowledge no examples of PSU-GO HF for combined adsorption and ultrafiltration for the removal of pollutants in mixture in tap water have been reported. Here, we consider selected organic and heavy metal contaminants of concern recently revised in the drinking water directive EU 2020/2184,⁴³ including perfluoroalkyl substances (PFAS)²⁹⁻³⁴ Pb and Cr^{44,45} and studied their adsorptive removal by the newly developed PSU-GO HF modules. Moreover, to evaluate safe use of the proposed filters for drinking water filtration, we tested the release of GO nanosheets from such modules through Surface Enhanced Raman Spectroscopy (SERS) method, allowing state of the art limit of quantification of GO in water down to 0.1 ppb.

2. Experimental Part

2.1 Materials

GO powder was purchased from Abalonyx (AS, Norway) and used without further purification (graphene oxide dry powder <35 mesh, product code 1.8, XPS: O/C ratio 0.39 ± 0.01 , C $70.1 \pm 0.9\%$, O $27.2 \pm 0.9\%$, N $0.2 \pm 0.1\%$, S $1.0 \pm 0.1\%$, Si $0.8 \pm 0.1\%$, Cl $0.7 \pm 0.1\%$, Mn below 0.1%). Standard PSU HF (Medisulfone®) and PSU Ultrafiltration modules were provided by Medica s.p.a.

Hollow fibers spinning is described in detail in ESI.

2.2 Porosity

PSU HF and PSU-GO 3.5% HF have been analyzed for pore size and pore distribution through liquid-liquid-displacement-porometer (LLDP), Poroliq TM1000 (Porometer, Germany-Belgium). PSU HF porosity were measured after spinning without glycerinization, since glycerin impairs the porometer measurement. PSU-GO 3.5% HF were analysed after mild glycerinization, extensive water washing and air-drying at room temperature, to remove any glycerin residual. Fibers to be analyzed by LLDP were prepared by horizontally placing one or more hollow fibers into the holder and sealing with a bicomponent glue the fibers' edges; measurement occurred in out-in modality.

2.3 Module assembling

Lab-scale modules of standard PSU Medisulfone[®] and PSU-GO HF were prepared. Filtering surface (FS) of the modules was 0.025 m² (standard PSU HF) or 0.015 m² (PSU-GO HF) and they were assembled into a cartridge of 5 ml dead volume.

For characterization at tap POU, modules with U-shaped fibers were prepared with FS 0.28 m²; U-shaped modules can be directly connected to the tap, working with tap water pressure (3 bar; mean flow rate 5 L/min).

2.4 Ciprofloxacin adsorption experiments

The adsorption capacity of PSU-GO HF containing different GO loadings (Fig. 1) was tested under dynamic conditions by filtering tap water spiked with ciprofloxacin. In a typical experiment, 5 mg/L CIPRO tap water solution was filtered in dead end in-out transmembrane modality on PSU-GO HF module at a constant flow of 5 mL/min. Fractions each 200 mL were collected and analysed by UV-Vis analysis (Agilent Cary 3500) to determine CIPRO concentration. The filtration experiments were carried out until the removal was below 2%. The experiments were repeated in triple by using new modules for each repetition.

2.5 Cut-off determination by dextrans filtration

Fluorescent dextrans at different molecular weight (MW) were used as tracers for cut-off determination. Fluorescein isothiocyanate dextran 4 kDa, 10 kDa, 20 kDa, 40 kDa, 70 kDa were

purchased from Merck. A solution of each tracer in *N*-propyl-gallate was prepared at a concentration of 5 mg/mL. Lab-scale modules of PSU and PSU-GO 3.5% HF were tested, (three modules for each tracer). The modules were pre-rinsed with water and the tracer solution was filtrated in dead end in-out modality at constant pressure. The filtrate was collected in sequential fraction of 500 μ L volume each. A total of 12-14 fractions were collected for each module. Samples were analyzed by a fluorometer (Fluoroskan, ThermoFisher Scientific) at the excitation wavelength of 484 nm and emission wavelength of 538 nm. Experiments were repeated in triple by using each time a new module.

2.6 PFAS removal experiments and analysis

Tap water spiked with a mixture of fourteen PFAS C₃-C₁₃ was prepared and filtered (dead end, in-out) at 5 mL/min using a Cole-Parmer Masterflex® peristaltic pump on the selected PSU HF, PSU-GO 3.5% HF and GAC modules, previously washed with 2 L of MilliQ water. GAC was tested for comparison. The concentration of each contaminant was 0.5 μ g/L in a total volume of 1 L. The concentration of PFAS in filtered water was analyzed by UPLC-MS/MS (Waters Acquity, UPLC BEH C18 analytical column, details in ESI).

2.7 Heavy metals removal experiments and analysis

Mineral water spiked with a mix of heavy metals and metalloids (Pb, Cu, Cd, Ni, Cr(III), As(V), V and U) at a final concentration of 100 μ g/L each was prepared starting from individual 1 g/L stock solutions (ICP-MS standards, VWR). Spiked mineral water was filtered on selected modules (PSU HF, PSU-GO 3.5% HF and GAC), previously washed with 1 L of MilliQ water. Flow was set at 5 mL/min and 3 L of water were treated, then flow was incremented to 40 mL/min and two more liters treated for a preliminary evaluation of performance under different flow conditions of the selected modules. Samples were collected every 200 mL. Each fraction was immediately acidified with 1% HNO₃ Suprapur (Sigma-Aldrich) and solutions were analyzed by ICP-OES (Model 5800, Agilent). At the end of the filtration experiment, the mobility of adsorbed contaminants was tested by passing three fractions of 50 mL MilliQ water at 20 mL/min in-out mode, and two more fractions of 50 mL

in reverse out-in flow. Concentration was measured as described above and percentage of release respect to total adsorbed was calculated. Module filling material weight was 0.2, 0.26 and 1.5 g for PSU HF, PSU-GO 3.5% HF and GAC, respectively. All tests were carried out in duplicate and reported as mean value with standard deviation.

2.8 Potability of filtered water

Chemical and biological parameters included in the Italian D. Lgs 31/01 (implementation of 98/83/EU Directive) were tested in tap water before and after in-out filtration through PSU-GO 5% module with U-shaped fibers of FS 0.28 m² at 5 L/min, total volume 100 L.

2.9 GO release tests by SERS

PSU HF and PSU-GO 3.5% HF modules were washed with 2 L of hot MilliQ water (80 °C) in dead end in-out configuration at 50 mL/min using a Cole-Parmer Masterflex® peristaltic pump, to remove glycerin. After that, 1 L of tap water was filtered in-out modality at a flow of 250 mL/min in PSU HF, sampling every 250 mL. Thereafter, 500 mL, collected from the previous fractions, were recirculated for 2 h at 250 mL/min. The flow used was significantly higher than the maximum one that the module is supposed to ensure to guarantee porosity and filtration capacity (i.e. max flow 50 mL/min). This flow may cause mechanical stress of the hollow fibers, with possible release of GO from the fibers. Same procedure was performed on PSU-GO HF. Samples were analyzed using surface-enhanced Raman spectroscopy (SERS), following a previously described protocol.⁴⁶ Analytical features of the method for the determination of GO nanosheets in water are described in ESI (Table S7, Fig. S13-S16, ESI). The calibration curve shown in the inset of Fig. 10 was built using the intensity of the D peak, as analytical signal, for the concentration range 0.1-10 µg/L. The practical limit of quantification (P-LOQ), which is defined as the minimum level at which GO can be measured in water samples with accuracy higher of 80% and relative standard deviation (RSD) lower than 10%, was 0.1 ppb.

Additionally, to confirm that our methodology can detect GO release from the PSU-GO fibers, previously used PSU HF modules and both used and new PSU-GO HF modules were opened with a

hacksaw (ESI, Fig. S14). Fibers extracted from the modules were cut and dried in a desiccator for 72 h. Subsequently, a known weight of fibers was added to 20 mL of deionized water and overstressed through sonication for 30 minutes in an ultrasonic bath. Three different weights of fibers were tested using three SERS substrates for each weight (ESI, Table S8).

3. Results and Discussion

3.1 PSU-GO HF modules fabrication and characterization

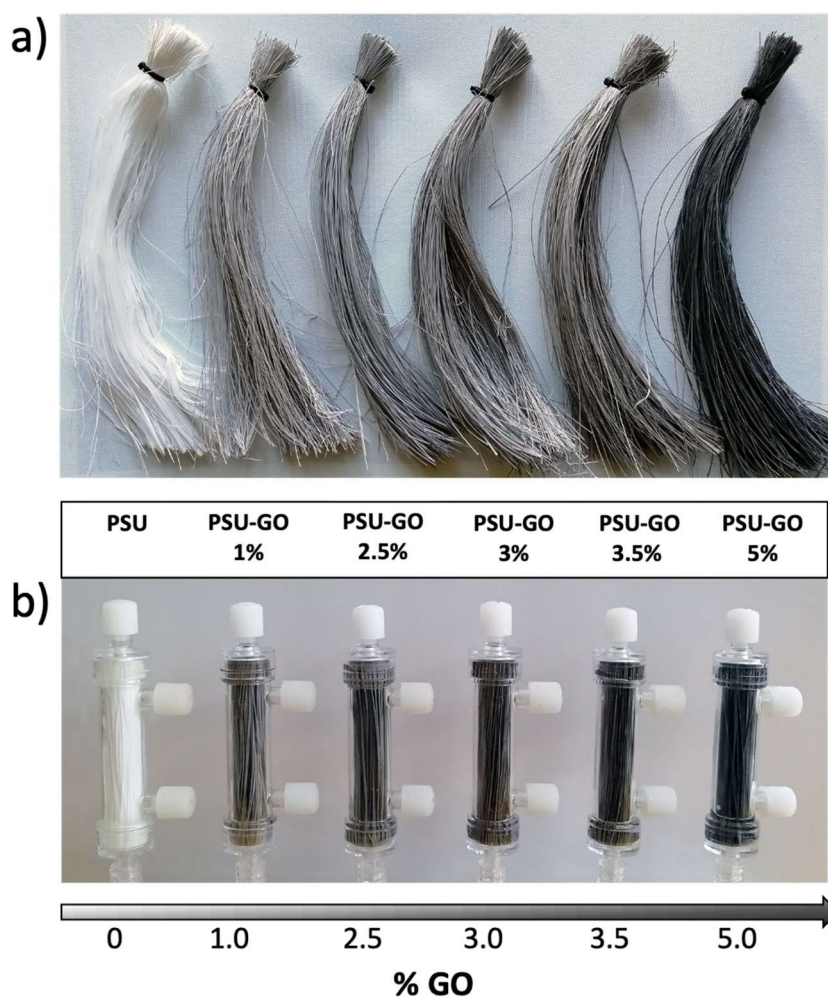


Figure 1 a) PSU HF and b) filtration modules, with different amounts of GO (w/w). From left to right: pristine PSU; PSU-GO 1%; PSU-GO 2.5%; PSU-GO 3%; PSU-GO 3.5%; PSU-GO 5%. Details of fibers spinning, and modules fabrication are described in ESI (Fig. S1). Cartridge size are 6.5 cm length, 1.5 cm diameter, 4.5 ml dead volume.

Hollow fibers of PSU-GO at 1%, 2.5%, 3%, 3.5% and 5% w/w (GO:PSU) were obtained by phase inversion procedure (from NMP to water) through a pilot spinning line, according to the protocol

described in ESI. The membranes were then assembled in prototype modules of filtering surface 0.015 m^2 that were then used for the following performance tests. The maximum flow rate acceptable for these cartridges was about 100 mL/min . Membranes and corresponding modules are shown in Fig. 1.

The pore average size of PSU-GO HF was analyzed by porosimeter and resulted being 13 nm , i.e. higher than that determined for standard PSU HF (6 nm , Table S1, ESI), this being likely due to the slightly different extrusion conditions exploited for PSU-GO spinning.

The cross-section SEM images of PSU HF and PSU-GO HF at 1%, 3.5% and 5% loading are shown in Fig. 2 and Fig. S2 ESI. PSU-GO HF show the typical hollow fiber structure, with extended finger-like pores and a thin sponge-like layer beneath it. An average wall thickness of $ca. 45 \pm 5 \mu\text{m}$ and inner diameter of $ca. 220 \pm 20 \mu\text{m}$ was observed for all the samples together with a slight increase in the micro-void size is observed on increasing GO loading. Some large GO flakes can be seen exposed at the outer surface of the pores (Fig. 2f, representative SEM image of PSU-GO 1%) in accordance with the contact angle measurements (Fig. S3, ESI), showing a decrease from $(60.1 \pm 4.1)^\circ$ for PSU to $(53.1 \pm 2.1)^\circ$ for PSU-GO 3.5%, indicating a slight enhancement of the surface hydrophilicity.

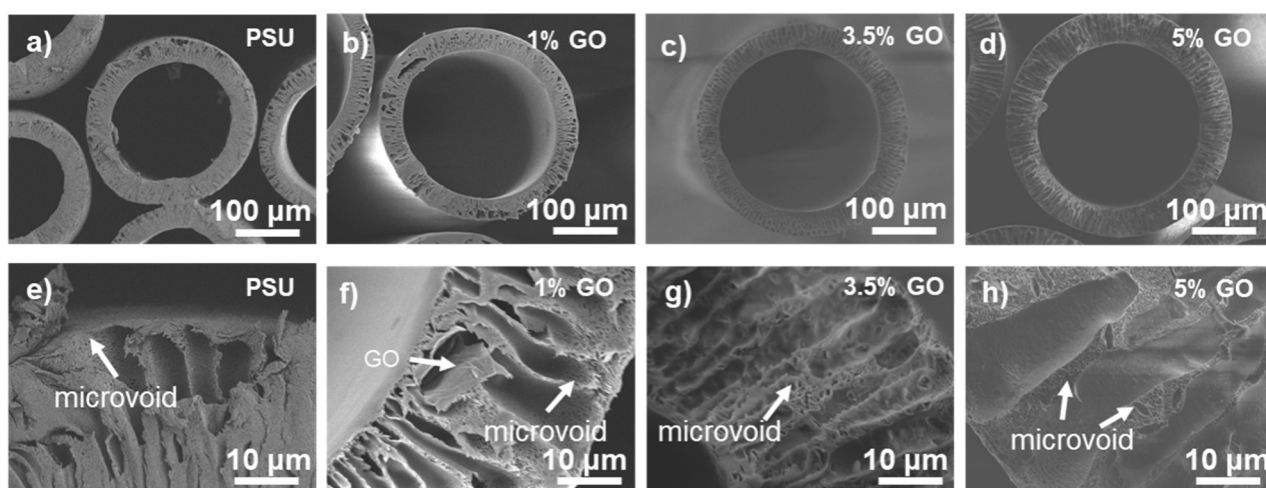


Figure 2 Low and high magnification SEM cross-section images of a,e) bare PSU, b,f) PSU-GO 1%, c,g) PSU-GO 3.5%, d,h) PSU-GO 5% HF.

Raman spectra of GO and PSU-GO HF are showed in Fig. 3. The spectrum of PSU showed main peaks located at around $790, 1146, 1584, 1605, \text{ and } 3068 \text{ cm}^{-1}$, correlated to the asymmetric C-S-C,

asymmetric C-O-C vibration, aromatic ring chain vibration, and C-H vibration, respectively. The broad peak at around 2900 cm^{-1} , can be ascribed to the PSU methyl bonds. The Raman spectrum of GO showed two characteristic peaks at 1350 and 1596 cm^{-1} (Fig. 3a), corresponding to the D band (defects or disorders) and G band (pristine sp^2 carbon atoms) of GO. No overlap between the D band from GO and other characteristic peaks of PSU were observed this allowing the identification of GO distribution on PSU-GO composites by Raman mapping.

Raman mapping and depth profiling techniques are shown in Fig. 3b and Fig. S4 (ESI). All tested PSU-GO samples, including 1%, 3.5% and 5% GO loading amount, showed GO almost homogeneous distribution inside the hollow fiber section. As expected, PSU-GO 5% revealed the highest D peak intensity (5×10^4 CCD cts). Meanwhile, GO flakes on PSU-GO 3.5% showed the best integration with the finger-like PSU matrix structure, according to the D peak distribution of GO from the relative z-stack imaging (Fig. 3b).

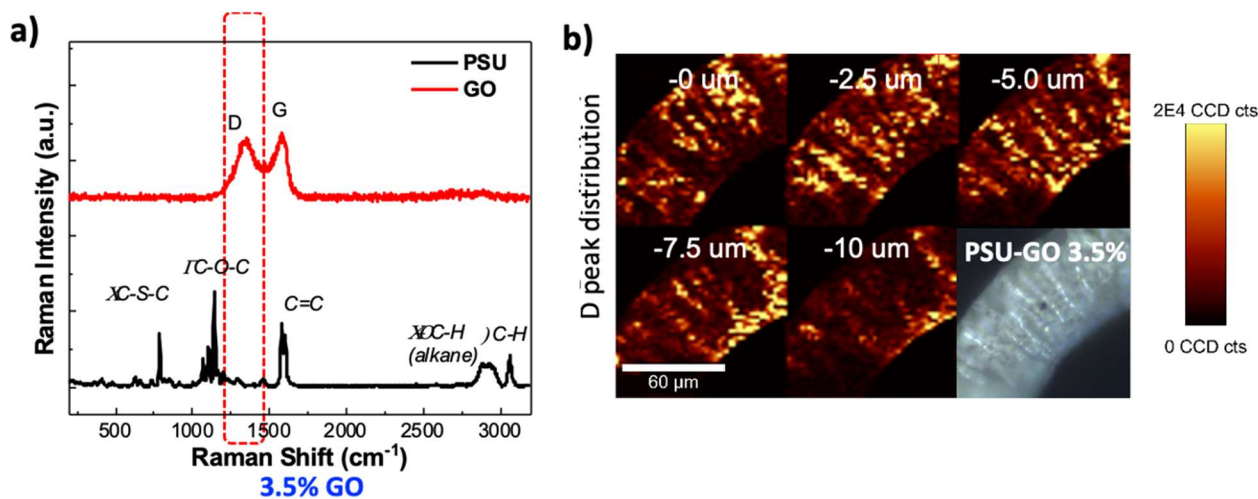


Figure 3 a) Raman spectra of GO and PSU; b) Z stack of Raman maps and the relative optical image of PSU-GO 3.5% HF, constructed by mapping the D-band region.

3.2 Tailoring of GO loading in PSU-GO HF

Ciprofloxacin (CIPRO), a fluoroquinolone antibiotic, is strongly adsorbed by GO⁴⁷ but it is not removed by PSU HF, thus we here exploited CIPRO removal from water to study its adsorption as a function of GO loading amount in order to optimize the hollow fibers composition. Tap water spiked with CIPRO was filtered through modules of PSU-GO HF in Fig. 4a, dead-end transmembrane modality (in-out), at low flow rate (5mL/min) until breakthrough was reached (about 3L filtered). CIPRO spike at 5 mg/L was chosen to enable fast detection by UV, the low flow rate was selected to reach the highest contact time allowed in flow experiments and establish the highest removal capacity of the modules. Three independent modules were used for each loading curve experiment. We estimated the maximum adsorption capacity (Q_{max}) as milligrams of CIPRO removed per gram of composite by the plateau of the loading curves (PSU-GO, Fig S5, ESI). As shown by Fig. 4b the performances were independent from the initial concentration of CIPRO in the range 0.5-5 mg/L. The overall trend of adsorption capacity Q_{max} on increasing GO doping amount is shown in Fig. 4c, with Q_{max} increasing from 0.25 mg/g to about 6 mg/g from PSU HF (0% GO) to PSU-GO 5% HF. No significant advantage was observed by increasing GO amount from 3.5% to 5%, this highlighting PSU-GO 3.5% as the best compromise between performance and costs, mainly affected by GO doping amount.

The maximum adsorption capacity of GO for CIPRO estimated by isotherm curve is about 250 mg/g of GO at the equilibrium time (24 h).⁴⁷ In our experimental conditions, the contact time at 5 mL/min is about 35 s, thus far from the equilibrium conditions, the maximum adsorption capacity expressed in mg removed/gr of total GO was 168 mg/g of GO (PSU-GO 3,5%), which is close to the value at the equilibrium (250 mg/g), this indicating that the flow rate does not significantly affect the total removal capacity of PSU-GO HF filters.

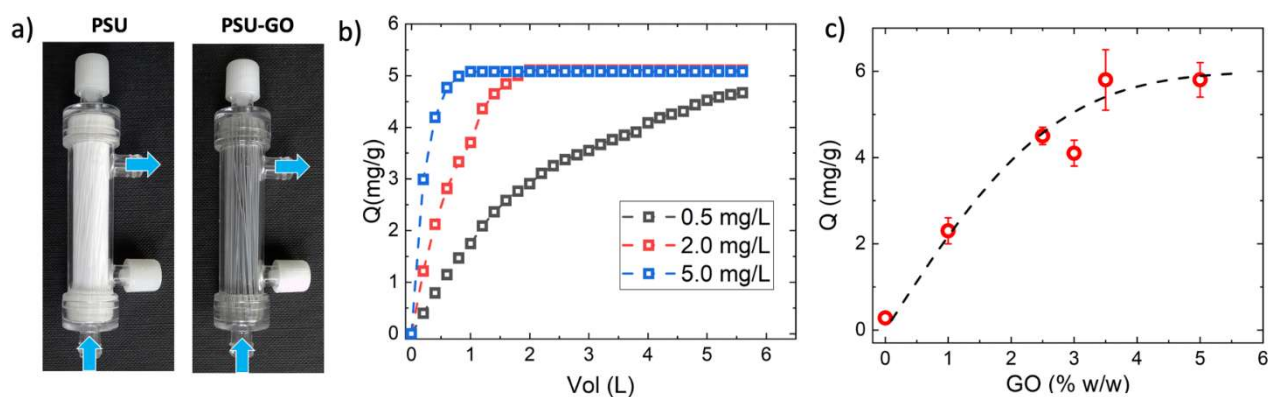


Figure 4 a) From left to right, modules of PSU HF, and PSU-GO 3.5% HF. The arrow indicates water in and out pathways (i.e. dead end transmembrane in-out modality for PSU HF and PSU-GO HF,). b) Adsorption capacity as a function of the initial CIPRO concentration on PSU-GO 3.5% HF. c) maximum adsorption capacity estimated by the loading curves (ESI), C_{IN} . CIPRO 5 mg/L, treated volume 3 L, flow rate 5 mL/min.

3.3 Molecular Weight Cut-Off (MWCO) and ultrafiltration of PSU-GO HF

The MWCO of PSU-GO 3.5% HF, taken as reference, was determined by fluorescent dextrane filtration experiments. Fluorescein isothiocyanate (FITC) dextrans of different MW were filtered over PSU and PSU-GO HF in dead end in-out modality. The MWCO of HF is conventionally defined as the MW of the molecule with 90% retention. Fig. 5a shows the trend of retention vs FITC-Dextrane MW and a MWCO of 15 kDa, and 62 kDa are estimated for PSU and PSU-GO 3.5% HF, respectively, in line with the porometer determination (Table S1, ESI). Nevertheless, permeability of PSU and PSU-GO HF (UF coefficient) were almost comparable. Indeed, ultrafiltration coefficients estimated by flowing pure water through the filters and measuring pressure and ultrafiltration rate, were similar, i.e. 7.6 ± 1.0 (PSU) and 10.1 ± 1.7 (PSU-GO) (Fig. 5b and also Fig. S6, ESI).

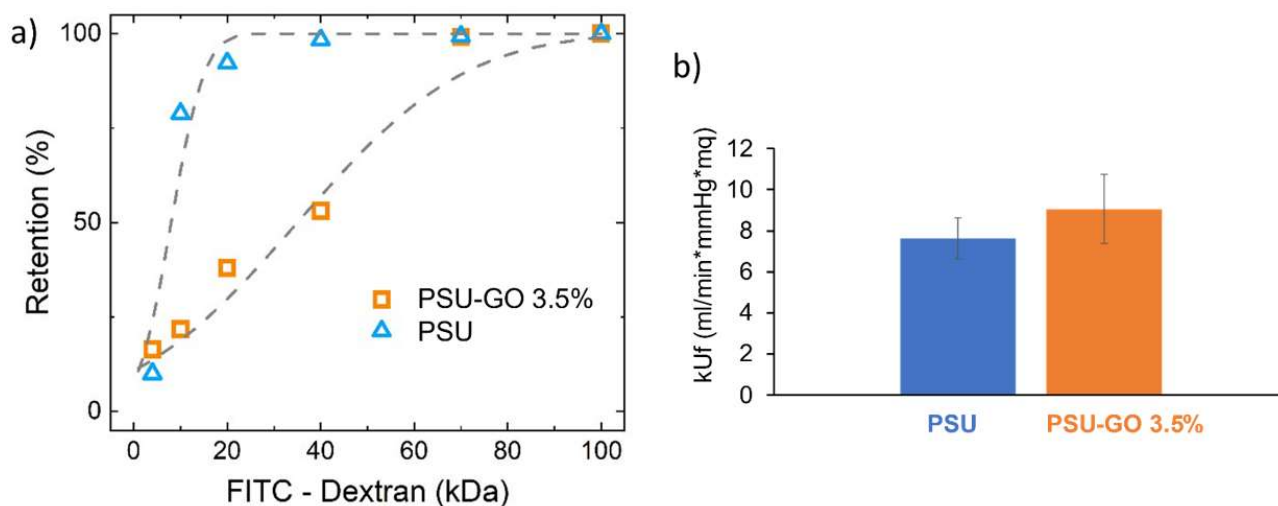


Figure 5 Ultrafiltration range flow rate of PSU and PSU-GO 3.5% HF. a) Retention of FITC-Dextran, b) Ultrafiltration coefficients of PSU and PSU-GO 3.5% HF. Flow rate is shown in Fig. 6, ESI.

3.4 Removal of PFAS and heavy metals

Tap water (pH 7, 1L) spiked with a mixture of fourteen PFAS (0.5 $\mu\text{g/L}$ each) of different molecular size (C_3 - C_{13} , Fig. 6) and end-substitution (sulphonates or carboxylates) was filtered through PSU, PSU-GO HF 3.5%, and GAC for comparison (details in ESI, Fig. S7). All modules showed higher removal toward long chain molecules (C_8 - C_{13}). PSU-GO showed higher removal for sulphonated PFAS respect to carboxylate analogues of same length (i.e. C_6 : 99% for PFHxS vs 79% for PFHpA, or C_4 : 35% for PFBS vs 4% for PFPeA). Fig. 6 shows the removal efficiencies normalized to the amount of adsorbing material in each module, expressed as mass of PFAS removed per gram of sorbent material. The adsorption capacity of PSU and PSU-GO HF was significantly higher than that of GAC for almost all PFAS. The total amount of PFAS removed by PSU-GO 3.5% was up to seven times more efficient than GAC.

According to previous studies⁴⁸⁻⁵¹, the two most important factors driving PFAS adsorption are hydrophobic interactions and electrostatic interactions. Fig. 6c shows the trend of PFAS removal with *n*-octanol/water partition coefficient ($\log K_{\text{OW}}$) for PSU and PSU-GO 3.5% HF. It can be seen how $\log K_{\text{OW}}$ grows linearly with PFAS molecular weight (Fig. S8, ESI).

It can be observed that PFAS with $\log K_{OW}$ in the range 4.5-6.5 are better removed by PSU-GO HF than PSU HF, and that the same removal is observed for $\log K_{OW}$ higher than 6.5. This effect emerges despite the higher hydrophilicity of PSU-GO with respect to PSU, as shown also by contact angle measurements (Fig. S3, ESI). The slightly higher hydrophilicity of PSU-GO seems particularly beneficial to the adsorption of short chain PFAS, ($4 < \log K_{OW} < 5$). Fig. 6c shows that in the $\log K_{OW}$ range 4.5-6.5, the higher is the hydrophilicity of the PFAS, the higher is the gap between the removal value for PSU and for PSU-GO HF. This evidence suggests that repulsive electrostatic interactions are less relevant than hydrophobic interactions. On the other hand, experiments at higher PFAS initial concentration (10 $\mu\text{g/L}$ rather than 0.5 $\mu\text{g/L}$; Fig. S9, ESI) show a significant drop in performance of PSU-GO HF. At higher concentration, it has been shown that PFAS can aggregate into micelles⁵², this would enhance the role of electrostatic rather than hydrophobic interactions as sorption driving forces. Overall, this evidence suggests a delicate interplay between hydrophobic and electrostatic interactions, which govern PFAS adsorption in this system. The overall proposed mechanism for PFAS adsorption in PSU-GO HF modules is summarized in Fig. 9.

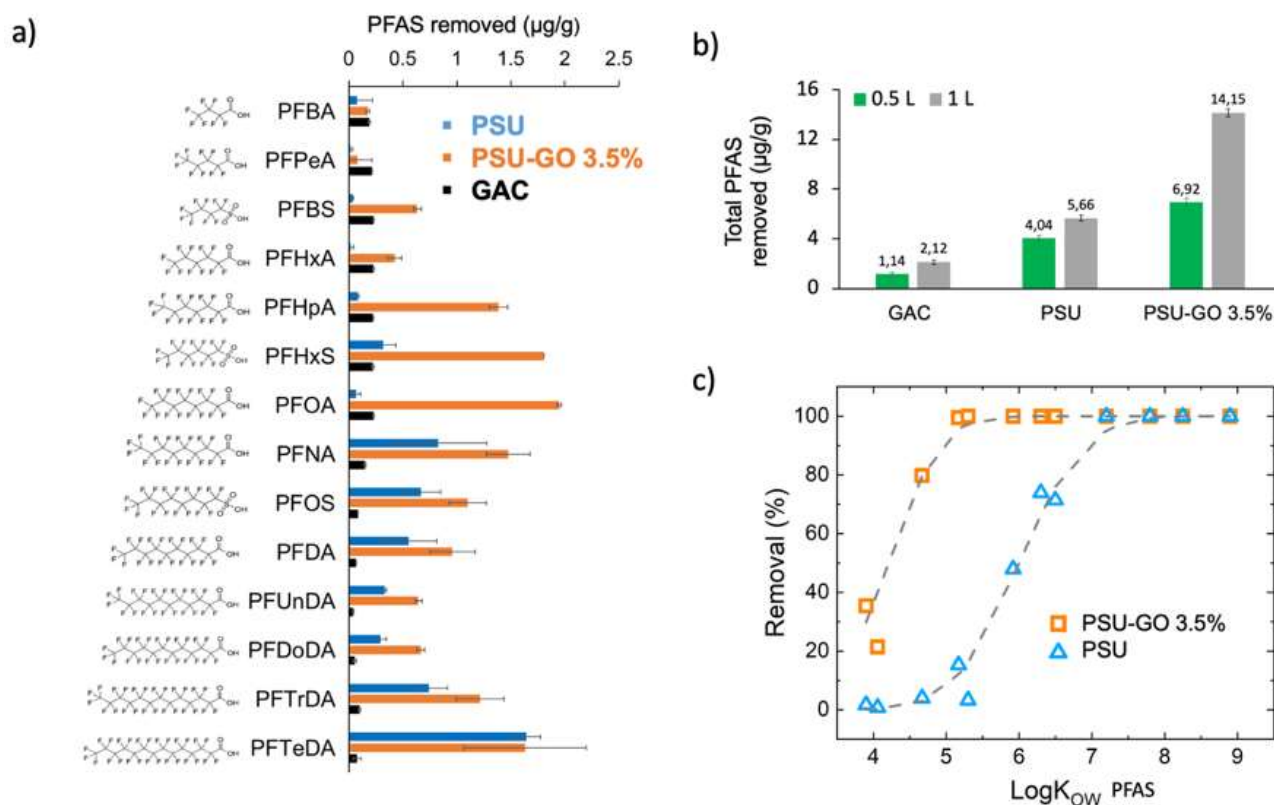


Figure 6 a) Removal of a mixture of fourteen PFAS in tap water, total volume=1 L, C_{IN} = 0.5 µg/L, flow rate= 5 mL/min in µg/g of PSU HF (blue, total mass of composite 260 mg), PSU-GO 3.5% HF (orange, total mass of composite 270 mg), and GAC (black, total mass 2.4 g). b) Total amount of PFAS removed µg/g after 0.5 L (green) and 1 L (grey) filtered. c) Removal of PFAS mixture in tap water vs the PFAS Log K_{OW} of PSU HF (blue) and PSU-GO 3.5% HF (orange).

The removal of heavy metals and metalloids mix (As(V), Cd, Cr(III), Cu, Ni, Pb, U, and V) at 100 µg/L in mineral water (pH 7.5, see ESI, Table S4) was also tested. After treating 3 L of contaminated water, different affinities of metals towards the proposed materials were highlighted. The adsorption capacity of PSU, PSU-GO 3.5% HF and GAC expressed as micrograms of contaminant removal normalized to gram of sorbent in the module, toward metal ions and metalloids is shown in Fig. 7. PSU-GO 3.5% HF outperform GAC in the removal of Cr(III), Cu and Pb.

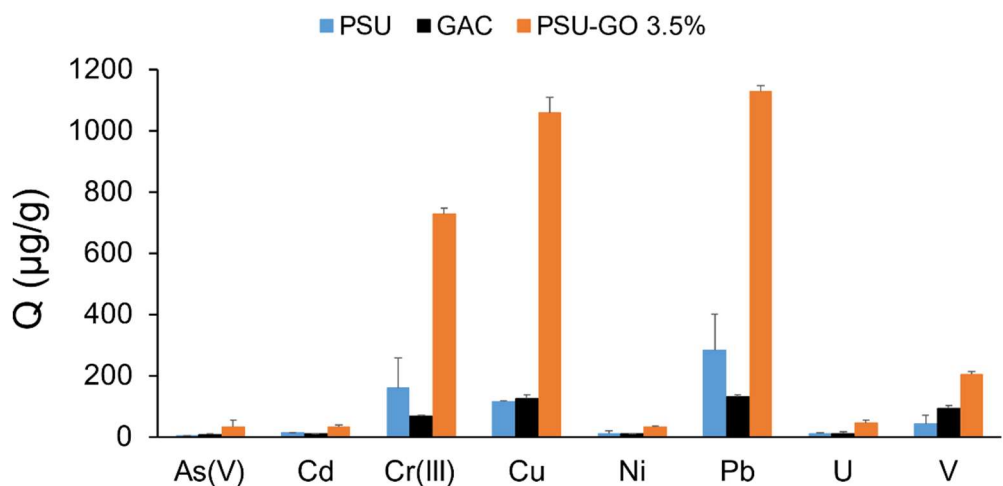


Figure 7 Adsorption capacity Q ($\mu\text{g/g}$) towards a mixture of different heavy metals and metalloids. Three different adsorption materials were compared: PSU HF (blue, left) and PSU-GO 3.5% HF (orange, right), and GAC granules (black, middle). Flow rate 5 mL/min and total filtered volume 3 L, $C_{IN} = 100 \mu\text{g/L}$ each.

The plotting of removal efficiency vs treated volume (Fig. 8) shows that removal of Pb and Cu follows a similar trend, with initial removal capacity close to 100% for PSU-GO 3.5% HF and final removal capacity of 50-60%. On the other hand, a constant removal of about 50% was observed for Cr(III). In the case of Pb and Cu, GAC removal capacity was about 10-20% lower for the first 2 L treated, then performance was similar to PSU-GO 3.5% HF while negligible adsorption on neat PSU HF was found for all the heavy metals and metalloids. The trend for remaining elements is reported in ESI (Fig. S10). Interestingly, as observed for ciprofloxacin removal, the observed PSU-GO HF performances were independent on the flow rate (changing flow from 5 mL/min to 40 mL/min) as instead observed in the case of GAC (Fig. S12, ESI) whose removal became lower than 20%. In addition, by increasing flow rate in GAC filter a release of contaminants was observed demonstrating a labile adsorption of a fraction of them, due only to entrapment in GAC small pore more than chemical bonding. This was not observed operating with PSU-GO HF filters. Mobility of trapped metals was tested and compared among selected materials (one module for each material). As expected, the weakest adsorption was observed for PSU HF, for which removal is likely to be governed just by pore trapping; while very low release was observed for Pb, Cu, and Cr(III) in both

GAC and PSU-GO 3.5% HF. The release of adsorbed metals was also tested, and details are reported in ESI (Fig. S13, Table S5).

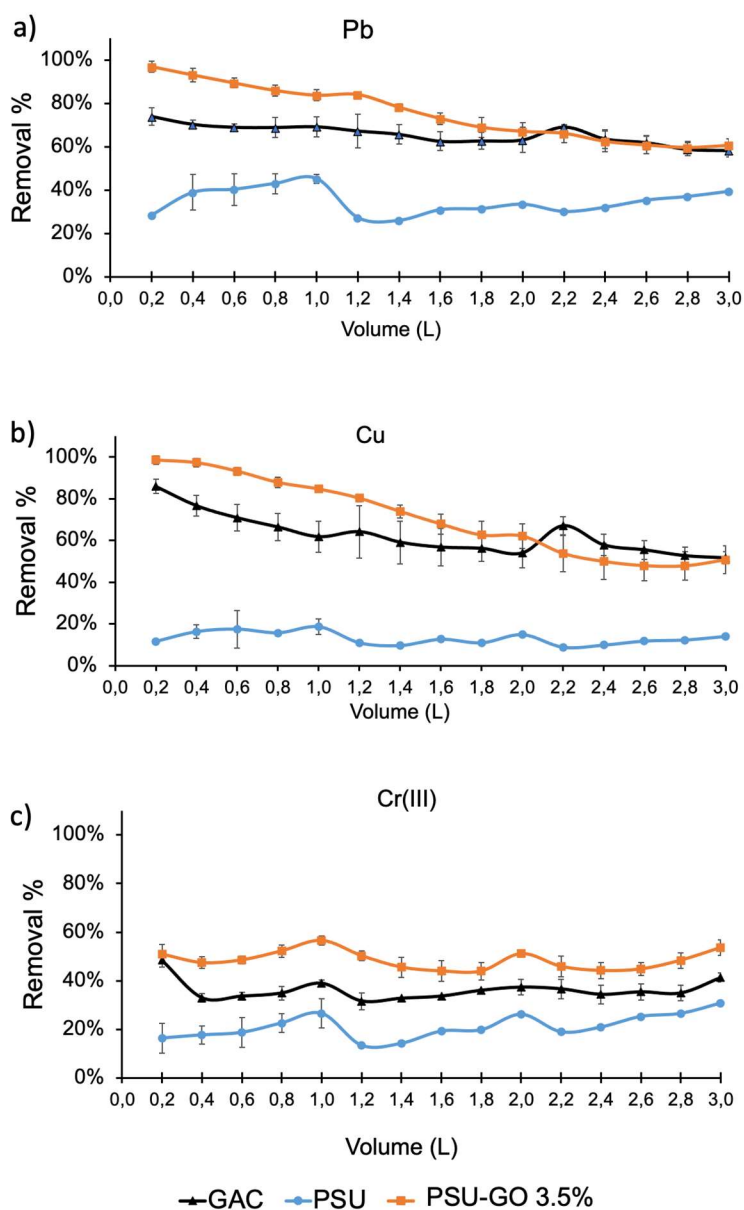


Figure 8 Removal efficiency as function of treated volume (L) of a) Pb^{2+} , b) Cu^{2+} , c) $\text{Cr}(\text{OH})_2^+/\text{Cr}(\text{OH})^{2+}$. Three different adsorption materials were compared. PSU HF (blue) and PSU-GO 3.5% HF (orange) and GAC (black) granules. Flow rate 5 mL/min and total filtered volume 3 L.

Different studies proved higher Cu and Pb adsorption, if compared to other heavy metals, onto negatively charged surfaces with exposed $-\text{OH}$ and $-\text{O}$ groups as in our case, i.e. adsorption on GO⁵³⁻⁵⁷. The adsorption passes through two different mechanisms: 1) exchange reaction onto permanent

negatively charged sites, that involves not hydrolyzed cations; and 2) surface complexation at variable charged hydroxyl edges, that follows selective adsorption, according to the tendency of different metals to hydrolyze⁵⁴.

Cu and Pb hydrolyze more readily than Ni and Cd, and hence are more likely to interact with a hydroxylated surface, while Ni and Cd do not compete effectively for variable surface charges, due to their lower tendency to form hydrolysis products. Consequently, Ni and Cd adsorption is more restricted to permanent charge sites, especially in a competitive environment, such as a mix of metals. Previous studies⁵⁷⁻⁶⁰ demonstrate that the overall metal affinities for goethite were generally found to follow the order $\text{Cr} > \text{Cu} > \text{Pb} > \text{Zn} > \text{Cd} > \text{Co} > \text{Ni} > \text{Mn} > \text{Ca} > \text{Mg}$, which was consistent with electronegativity or hydrated radii of the cations.

Overall, removal experiments on CIPRO, PFAS and metal ions suggest a removal mechanism based on the interplay of electrostatic interactions, hydrophobic interactions and π - π stacking between GO and the contaminants. Heavy metals are removed with higher performances than PFAS, likely thanks to the predominant surface complexation mechanisms favored also by positive electrostatic interaction with the negatively charged GO flakes. A schematic representation of adsorption mechanism for organics and heavy metals is depicted in Fig. 9.

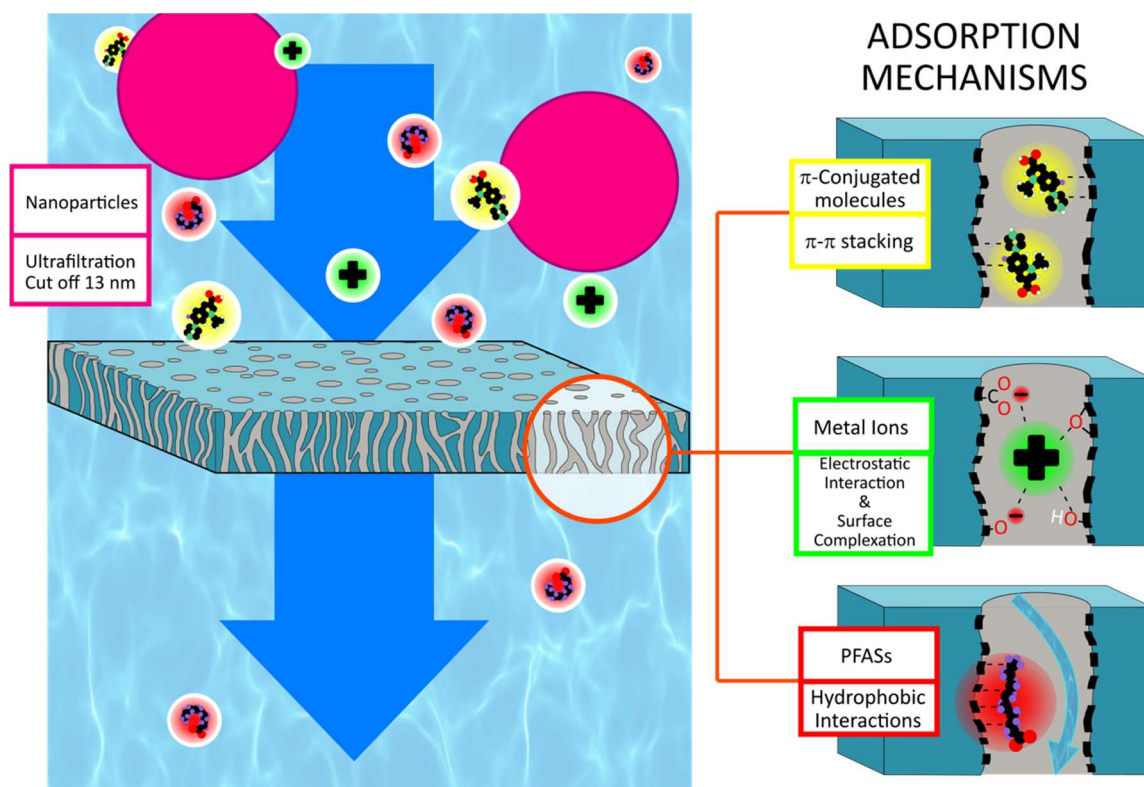


Figure 9 Sketch of the adsorption mechanisms of pollutants on PSU-GO: π -conjugated molecules are adsorbed through π - π stacking, metal ions through electrostatic interactions and surface complexation, and PFAS through hydrophobic interactions.

3.6 Water potability and GO release test by Surface-Enhanced Raman Spectroscopy (SERS)

Chemical and biological water potability was verified on tap water before and after filtration as listed in Table S6. In addition, to validate the safety of use of the PSU-GO HF modules, we studied possible release of GO nanosheets during water purification. To this aim, we exploited a method, recently developed by some of us,⁴⁶ able to detect and quantify GO in water samples at ultra-trace levels using surface-enhanced Raman spectroscopy (SERS). The methodology is based on the deposition of water GO dispersions on a SERS active substrate based on gold nanoparticles.

The optimized analytical protocol was applied to the detection and quantification of GO in tap water samples filtered through PSU HF and PSU-GO 3.5% HF modules. Water (1L) was filtered at a flow of 250 mL/min, i.e. 2.5-fold higher the maximum operating flow for PSU HF prototype cartridges in Fig. 1b.

No significant differences can be found between the spectra of water samples filtered using PSU and PSU-GO 3.5% HF modules (ESI, Fig. S15), indicating no GO release over the limit of detection ($0.11 \mu\text{g/L}$).

In order to further validate the measurements, one of the samples was fortified, i.e. GO was added to obtain a GO concentration of $0.1 \mu\text{g/L}$ and this new analyte was evaluated. Figure 10 shows the spectra of the filtered sample as it and after fortification (Fig. 10). Our methodology predicted a concentration of $0.11 \mu\text{g/L}$ (in agreement with the experimental spike), with a relative standard deviation (RSD) below 4, in accordance with previously RSD of the method.

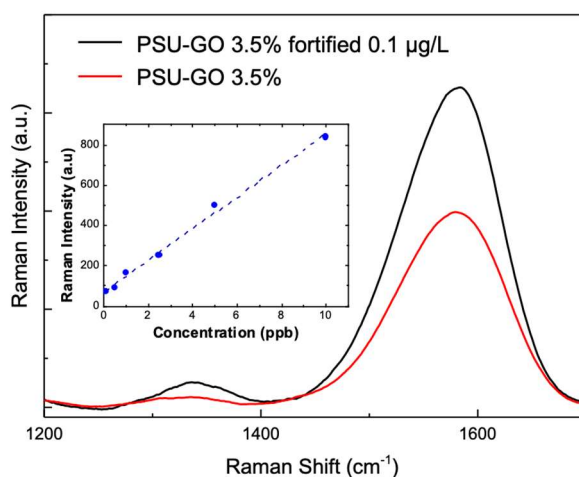


Figure 10 SERS spectra for PSU-GO 3.5% (red) and PSU-GO 3.5% fortified $0.1 \mu\text{g/L}$ (black). The inset shows the calibration curve.

Fig. S15 (ESI) shows the spectra of water samples prepared by sonication of different quantities of PSU-GO in water (Fig. S15a) as well as the comparison to the SERS spectra of water samples prepared from sonication of PSU HF as control sample (same amount, Fig. S15b). The sonication of PSU-GO fibers in water clearly causes the release of small quantities of GO and this release can be easily detected by our SERS protocol. Noteworthy, not significant differences between the results obtained with fibers extracted from new modules or modules already used for water filtration. Finally, considering a 3.5% of GO in PSU-GO HF, the calculated release of GO after 30 min of sonication,

was always lower than 0.2% (ESI, Table S8). To the best of our knowledge, this is the first case of study on release from PSU-graphene composite with a limit of quantification below the mg/L limit, typically achieved by UV-vis or TOC analyses.⁶¹

3.7 Preliminary real conditions POU test

For validation of PSU-GO 3.5% HF modules we performed a removal test in a pilot connected to the tap working with a reservoir allowing us to spike water before treatment with the PSU-GO modules. Module with U-shaped bundles (0.28 m² Fig. 11a, b) were produced since they are the standard POU module structure proposed by the producer (Medica s.p.a.). The amount of GO estimated in these modules was about 210 mg on a total HF weight of 6 g. For validation, tap water (100 L) was spiked with CIPRO (at 1 mg/L) and operated at about 2.5 bar (2 L/min). 5 L samples were collected and at each sampling the inlet solution was also collected and checked by HPLC-UV analysis. Figure 11 shows the overall set-up (a) the module structure (b) and U-shape membranes inside the module (c). An initial removal of about 65% was found which decrease to about 30% after 40 L (Fig. S17, ESI). Despite the observed removal decay, the total mass of removed CIPRO in 100 L normalized to the amount of GO in the module, was about 110 mg removed per g of GO, compared to the 168 mg/g GO obtained in lab scale prototypes tested at 5 mL/min (Fig. S5, ESI). The estimated contact time of real size U-shaped module at 2 L/min is 10 times lower than the one of lab scale prototypes tested at 5 mL/min, meaning that the removal of CIPRO by GO mediated adsorption is only partly affected by contact time (and/or flow rate).

It should be remarked that for this experiment we used a ppm spike of CIPRO which is far from the environmentally occurring concentration of CIPRO (ng- μ g/L). This preliminary study on real size devices suggested that for POU applications, GO distribution and availability seem to affect the adsorption capacity more than flow rate. The removal decay could be likely enhanced by improving the distribution of GO nanosheets within the composite and by reducing their aggregation which likely limits the exposed surface area and the overall adsorption.

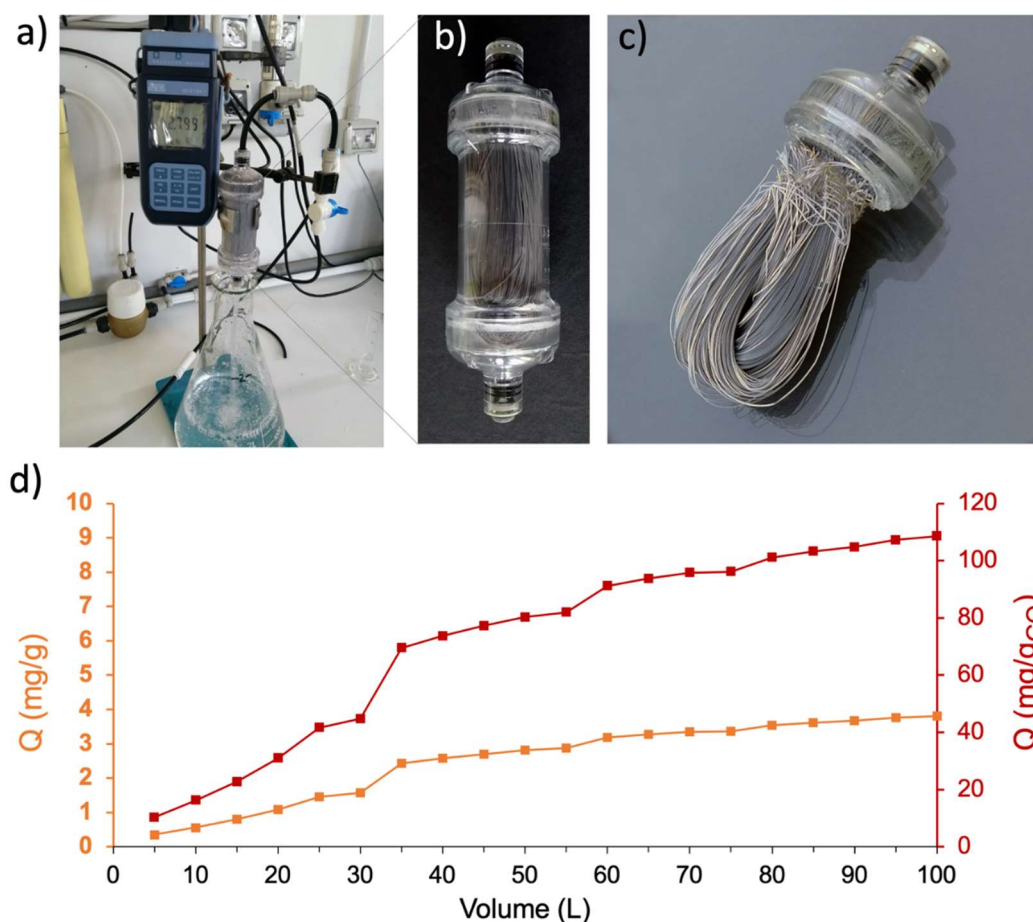


Figure 11 a) PSU-GO 3.5% cartridge (FS 0.28 m², U-shaped HF) connected at the tap (at 2.8 bar as shown by the manometer). Composite weight in each module about 6 g, with 210 mg of GO. b) Zoom of the cartridge and c) of the U shape assembled fibers. d) Removal trend of CIPRO (spike at 1 mg/L).

4. Conclusions

A new class of GO enhanced ultrafiltration modules produced with a semi-industrial pilot plant, has been herein described. We demonstrated that PSU-GO HF modules preserve ultrafiltration properties of commercial PSU HF modules, but also exhibited the adsorption properties typical of GO nanosheets. PSU-GO HF have been proved superior to both pristine PSU HF and GAC, the industrial standard adsorbent, in the removal of several classes of water contaminants. In particular, PSU-GO removal of ciprofloxacin antibiotic, Pb, Cu, and Cr(III); and perfluoroalkyl substances (PFAS, C4-C13) from real tap water matrix, were higher than that of GAC with a performance much less affected by the operational flow rate and negligible release at higher flow rate compared to for GAC. Higher selectivity for short chain PFAS with respect to GAC was observed. The importance of removing

PFAS with log K_{ow} higher than 5 was pointed out by the Stockholm Convention on Persistent Organic Pollutants,⁶² since that value is the threshold for bio-accumulation and bio-concentration. Preliminary tests on POU real scale filters for tap water purification at tap operational conditions (pressure-flow rate) demonstrated comparable performance of small prototype working at low flow rate (5mL/min) for CIPRO. Such capacity, as expected was lower than that of graphene nanosheets dispersion due to aggregation of GO sheets in the composite. The absence of GO secondary contamination in after-treatment water has been verified through SERS experiments with a limit of detection of 0.1 $\mu\text{g/L}$ and prove the safe use of these devices for water treatment. Some challenges are still to be tackled to exploit the full potential of this material, as compared to purely adsorption filters, to optimize the set-up to create more favorable kinetic conditions for the adsorption, to minimize the reaggregation of GO nanosheets to enhance their distribution and exposure of such sheets to the outer pore surface. Studies in these directions are currently in progress.

Acknowledgments

The authors gratefully acknowledge the support of this work by the project 881603- GrapheneCore3-H2020-SGA-FET- SH1 Graphil- GRAPHENE-FLAGSHIP and SH11 Saphegraph.

E. V. would like to thank the Spanish Ministerio de Ciencia e Innovación (project PID2020-113080RB-I00).

M.M. would like to thank Culligan® and MISTER Smart Innovation for the POU pilot installation at CNR.

Bibliography

1. Tweddle, T. A.; Kutowy, O.; Thayer, W. L.; Sourirajan, S., Polysulfone ultrafiltration membranes. *Ind. Eng. Chem. Prod. Res. Dev.* **1983**, *22* (2), 320-326.
2. Sewerin, T.; Elshof, M. G.; Matencio, S.; Boerrigter, M.; Yu, J.; de Groot, J., Advances and Applications of Hollow Fiber Nanofiltration Membranes: A Review. *Membranes* **2021**, *11* (11), 890.
3. Mondal, M.; De, S., Treatment of textile plant effluent by hollow fiber nanofiltration membrane and multi-component steady state modeling. *Chem. Eng. J.* **2016**, *285*, 304-318.
4. Ahmad, A. L.; Sarif, M.; Ismail, S., Development of an integrally skinned ultrafiltration membrane for wastewater treatment: effect of different formulations of PSf/NMP/PVP on flux and rejection. *Desalination* **2005**, *179* (1), 257-263.
5. Gao, J.; Wang, K. Y.; Chung, T.-S., Design of nanofiltration (NF) hollow fiber membranes made from functionalized bore fluids containing polyethyleneimine (PEI) for heavy metal removal. *J. Membr. Sci.* **2020**, *603*, 118022.
6. Abdelrasoul, A.; Doan, H.; Lohi, A.; Cheng, C.-H., Morphology Control of Polysulfone Membranes in Filtration Processes: a Critical Review. *ChemBioEng Rev* **2015**, *2* (1), 22-43.
7. Zhu, W.-P.; Sun, S.-P.; Gao, J.; Fu, F.-J.; Chung, T.-S., Dual-layer polybenzimidazole/polyethersulfone (PBI/PES) nanofiltration (NF) hollow fiber membranes for heavy metals removal from wastewater. *J. Membr. Sci.* **2014**, *456*, 117-127.
8. Otitoju, T. A.; Ahmad, A. L.; Ooi, B. S., Recent advances in hydrophilic modification and performance of polyethersulfone (PES) membrane via additive blending. *RSC Advances* **2018**, *8* (40), 22710-22728.
9. Pandele, A.; Serbanescu, O.; Voicu, Ş. I., Polysulfone Composite Membranes with Carbonaceous Structure. Synthesis and Applications. *Coatings* **2020**, *10*, 609.
10. Mangukiya, S.; Prajapati, S.; Kumar, S.; Aswal, V. K.; Murthy, C. N., Polysulfone-based composite membranes with functionalized carbon nanotubes show controlled porosity and enhanced electrical conductivity. *J. Appl. Polym. Sci.* **2016**, *133* (32).
11. Matsumoto, K.; Takahashi, T.; Ishii, S.; Jikei, M., Investigation of Dispersibility of Multi-Walled Carbon Nanotubes Using Polysulfones with Various Structures. *Int. J. Soc. Mater. Eng. Resour.* **2014**, *20* (1), 77-81.
12. Amini, M.; Jahanshahi, M.; Rahimpour, A., Synthesis of novel thin film nanocomposite (TFN) forward osmosis membranes using functionalized multi-walled carbon nanotubes. *J. Membr. Sci.* **2013**, *435*, 233-241.
13. Hwang, T.; Oh, J.-S.; Yim, W.; Nam, J.-D.; Bae, C.; Kim, H.-i.; Kim, K. J., Ultrafiltration using graphene oxide surface-embedded polysulfone membranes. *Sep. Purif. Technol.* **2016**, *166*, 41-47.
14. Kwon, O.; Choi, Y.; Choi, E.; Kim, M.; Woo, Y. C.; Kim, D. W., Fabrication Techniques for Graphene Oxide-Based Molecular Separation Membranes: Towards Industrial Application. **2021**, *11* (3), 757.
15. Ionita, M.; Pandele, A. M.; Crica, L.; Pilan, L., Improving the thermal and mechanical properties of polysulfone by incorporation of graphene oxide. *Composites Part B* **2014**, *59*, 133-139.
16. Meng, N.; Wang, Z.; Low, Z.-X.; Zhang, Y.; Wang, H.; Zhang, X., Impact of trace graphene oxide in coagulation bath on morphology and performance of polysulfone ultrafiltration membrane. *Sep. Purif. Technol.* **2015**, *147*, 364-371.
17. Liu, L.; Tong, C.; He, Y.; Zhao, Y.; Lü, C., Enhanced properties of quaternized graphenes reinforced polysulfone based composite anion exchange membranes for alkaline fuel cell. *J. Membr. Sci.* **2015**, *487*, 99-108.

18. Rezaee, R.; Nasser, S.; Mahvi, A. H.; Nabizadeh, R.; Mousavi, S. A.; Rashidi, A.; Jafari, A.; Nazmara, S., Fabrication and characterization of a polysulfone-graphene oxide nanocomposite membrane for arsenate rejection from water. *J. Environ. Health Sci. Engineer.* **2015**, *13*, 61.
19. Huang, Z.-Q.; Cheng, Z.-F., Recent advances in adsorptive membranes for removal of harmful cations. *J. Appl. Polym. Sci.* **2020**, *137* (13), 48579.
20. Qalyoubi, L.; Al-Othman, A.; Al-Asheh, S., Recent progress and challenges on adsorptive membranes for the removal of pollutants from wastewater. Part I: Fundamentals and classification of membranes. *Case Stud. Chem. Environ. Eng.* **2021**, *3*, 100086.
21. Badrinezhad, L.; Ghasemi, S.; Azizian, Y.; Nematollahzadeh, A., Preparation and characterization of polysulfone/graphene oxide nanocomposite membranes for the separation of methylene blue from water. *Polym. Bull.* **2018**, *75*, 469-484.
22. Zambianchi, M.; Durso, M.; Liscio, A.; Treossi, E.; Bettini, C.; Capobianco, M. L.; Aluigi, A.; Kovtun, A.; Ruani, G.; Corticelli, F.; Brucale, M.; Palermo, V.; Navacchia, M. L.; Melucci, M., Graphene oxide doped polysulfone membrane adsorbers for the removal of organic contaminants from water. *Chem. Eng. J.* **2017**, *326*, 130-140.
23. Jiang, L.; Liu, Y.; Liu, S.; Zeng, G.; Hu, X.; Hu, X.; Guo, Z.; Tan, X.; Wang, L.; Wu, Z., Adsorption of Estrogen Contaminants by Graphene Nanomaterials under Natural Organic Matter Preloading: Comparison to Carbon Nanotube, Biochar, and Activated Carbon. *Environ. Sci. Technol.* **2017**, *51* (11), 6352-6359.
24. Rathi, B. S.; Kumar, P. S.; Show, P.-L., A review on effective removal of emerging contaminants from aquatic systems: Current trends and scope for further research. *J. Hazard. Mater.* **2021**, *409*, 124413.
25. Meffe, R.; de Bustamante, I., Emerging organic contaminants in surface water and groundwater: A first overview of the situation in Italy. *Sci. Total Environ.* **2014**, *481*, 280-295.
26. Murray, K. E.; Thomas, S. M.; Bodour, A. A., Prioritizing research for trace pollutants and emerging contaminants in the freshwater environment. *Environ. Pollut.* **2010**, *158* (12), 3462-3471.
27. Petrie, B.; Barden, R.; Kasprzyk-Hordern, B., A review on emerging contaminants in wastewaters and the environment: Current knowledge, understudied areas and recommendations for future monitoring. *Water Res.* **2015**, *72*, 3-27.
28. Tröger, R.; Ren, H.; Yin, D.; Postigo, C.; Nguyen, P. D.; Baduel, C.; Golovko, O.; Been, F.; Joerss, H.; Boleda, M. R.; Polesello, S.; Roncoroni, M.; Taniyasu, S.; Menger, F.; Ahrens, L.; Yin Lai, F.; Wiberg, K., What's in the water? – Target and suspect screening of contaminants of emerging concern in raw water and drinking water from Europe and Asia. *Water Res.* **2021**, *198*, 117099.
29. Gagliano, E.; Sgroi, M.; Falciglia, P. P.; Vagliasindi, F. G. A.; Roccaro, P., Removal of poly- and perfluoroalkyl substances (PFAS) from water by adsorption: Role of PFAS chain length, effect of organic matter and challenges in adsorbent regeneration. *Water Res.* **2020**, *171*, 115381.
30. Glüge, J.; Scheringer, M.; Cousins, I. T.; DeWitt, J. C.; Goldenman, G.; Herzke, D.; Lohmann, R.; Ng, C. A.; Trier, X.; Wang, Z., An overview of the uses of per- and polyfluoroalkyl substances (PFAS). *Environmental Science: Processes & Impacts* **2020**, *22* (12), 2345-2373.
31. Liu, L.; Liu, Y.; Gao, B.; Ji, R.; Li, C.; Wang, S., Removal of perfluorooctanoic acid (PFOA) and perfluorooctane sulfonate (PFOS) from water by carbonaceous nanomaterials: A review. *Crit. Rev. Environ. Sci. Technol.* **2020**, *50* (22), 2379-2414.
32. McCleaf, P.; Englund, S.; Östlund, A.; Lindegren, K.; Wiberg, K.; Ahrens, L., Removal efficiency of multiple poly- and perfluoroalkyl substances (PFAS) in drinking water using granular activated carbon (GAC) and anion exchange (AE) column tests. *Water Res.* **2017**, *120*, 77-87.

33. Saleh, N. B.; Khalid, A.; Tian, Y.; Ayres, C.; Sabaraya, I. V.; Pietari, J.; Hanigan, D.; Chowdhury, I.; Apul, O. G., Removal of poly- and per-fluoroalkyl substances from aqueous systems by nano-enabled water treatment strategies. *Environ. Sci. Water Res. Technol.* **2019**, *5* (2), 198-208.
34. Valsecchi, S.; Rusconi, M.; Mazzoni, M.; Viviano, G.; Pagnotta, R.; Zaghi, C.; Serrini, G.; Polesello, S., Occurrence and sources of perfluoroalkyl acids in Italian river basins. *Chemosphere* **2015**, *129*, 126-34.
35. Franke, V.; McCleaf, P.; Lindegren, K.; Ahrens, L., Efficient removal of per- and polyfluoroalkyl substances (PFAS) in drinking water treatment: nanofiltration combined with active carbon or anion exchange. *Environ. Sci. Water Res. Technol.* **2019**, *5* (11), 1836-1843.
36. Lu, D.; Sha, S.; Luo, J.; Huang, Z.; Zhang Jackie, X., Treatment train approaches for the remediation of per- and polyfluoroalkyl substances (PFAS): A critical review. *J. Hazard. Mater.* **2020**, *386*, 121963.
37. Pooi, C. K.; Ng, H. Y., Review of low-cost point-of-use water treatment systems for developing communities. *npj Clean Water* **2018**, *1* (1), 11.
38. Peter-Varbanets, M.; Zurbrügg, C.; Swartz, C.; Pronk, W., Decentralized systems for potable water and the potential of membrane technology. *Water Res.* **2009**, *43* (2), 245-65.
39. Westerhoff, P.; Alvarez, P.; Li, Q.; Gardea-Torresdey, J.; Zimmerman, J., Overcoming implementation barriers for nanotechnology in drinking water treatment. *Environ. Sci.: Nano* **2016**, *3* (6), 1241-1253.
40. Mukherjee, R.; De, S., Novel carbon-nanoparticle polysulfone hollow fiber mixed matrix ultrafiltration membrane: Adsorptive removal of benzene, phenol and toluene from aqueous solution. *Sep. Purif. Technol.* **2016**, *157*, 229-240.
41. Zahri, K.; Wong, K. C.; Goh, P. S.; Ismail, A. F., Graphene oxide/polysulfone hollow fiber mixed matrix membranes for gas separation. *RSC Advances* **2016**, *6* (92), 89130-89139.
42. Sainath, K.; Modi, A.; Bellare, J., In-situ growth of zeolitic imidazolate framework-67 nanoparticles on polysulfone/graphene oxide hollow fiber membranes enhance CO₂/CH₄ separation. *J. Membr. Sci.* **2020**, *614*, 118506.
43. Dreyer, D. R.; Ruoff, R. S.; Bielawski, C. W., From Conception to Realization: An Historical Account of Graphene and Some Perspectives for Its Future. *Angew. Chem. Int. Ed.* **2010**, *49* (49), 9336-9344.
44. Peng, W.; Li, H.; Liu, Y.; Song, S., A review on heavy metal ions adsorption from water by graphene oxide and its composites. *J. Mol. Liq.* **2017**, *230*, 496-504.
45. Ahmad, S. Z. N.; Wan Salleh, W. N.; Ismail, A. F.; Yusof, N.; Mohd Yusop, M. Z.; Aziz, F., Adsorptive removal of heavy metal ions using graphene-based nanomaterials: Toxicity, roles of functional groups and mechanisms. *Chemosphere* **2020**, *248*, 126008.
46. Briñas, E.; Jehová González, V.; Herrero, M. A.; Zougagh, M.; Ríos, Á.; Vázquez, E., Submitted. **2022**.
47. Khaliha, S.; Marforio, T. D.; Kovtun, A.; Mantovani, S.; Bianchi, A.; Luisa Navacchia, M.; Zambianchi, M.; Bocchi, L.; Boulanger, N.; Iakunkov, A.; Calvaresi, M.; Talyzin, A. V.; Palermo, V.; Melucci, M., Defective graphene nanosheets for drinking water purification: Adsorption mechanism, performance, and recovery. *FlatChem* **2021**, *29*, 100283.
48. Ateia, M.; Maroli, A.; Tharayil, N.; Karanfil, T., The overlooked short- and ultrashort-chain poly- and perfluorinated substances: A review. *Chemosphere* **2019**, *220*, 866-882.
49. Vu, C. T.; Wu, T., Adsorption of short-chain perfluoroalkyl acids (PFAAs) from water/wastewater. *Environ. Sci. Water Res. Technol.* **2020**, *6* (11), 2958-2972.

50. Jin, T.; Peydayesh, M.; Mezzenga, R., Membrane-based technologies for per- and poly-fluoroalkyl substances (PFAS) removal from water: Removal mechanisms, applications, challenges and perspectives. *Environ. Int.* **2021**, *157*, 106876.
51. Jin, T.; Peydayesh, M.; Joerss, H.; Zhou, J.; Bolisetty, S.; Mezzenga, R., Amyloid fibril-based membranes for PFAS removal from water. *Environ. Sci. Water Res. Technol.* **2021**, *7* (10), 1873-1884.
52. Kancharla, S.; Jahan, R.; Bedrov, D.; Tsianou, M.; Alexandridis, P., Role of chain length and electrolyte on the micellization of anionic fluorinated surfactants in water. *Colloids Surf., A* **2021**, *628*, 127313.
53. de Pablo, L.; Chávez, M. L.; Abatal, M., Adsorption of heavy metals in acid to alkaline environments by montmorillonite and Ca-montmorillonite. *Chem. Eng. J.* **2011**, *171* (3), 1276-1286.
54. Srivastava, P.; Singh, B.; Angove, M., Competitive adsorption behavior of heavy metals on kaolinite. *J. Colloid Interface Sci.* **2005**, *290* (1), 28-38.
55. Lackovic, K.; Angove, M. J.; Wells, J. D.; Johnson, B. B., Modeling the adsorption of Cd(II) onto Muloorina illite and related clay minerals. *J. Colloid Interface Sci.* **2003**, *257* (1), 31-40.
56. Shi, M.; Min, X.; Ke, Y.; Lin, Z.; Yang, Z.; Wang, S.; Peng, N.; Yan, X.; Luo, S.; Wu, J.; Wei, Y., Recent progress in understanding the mechanism of heavy metals retention by iron (oxyhydr)oxides. *Sci. Total Environ.* **2021**, *752*, 141930.
57. Trivedi, P.; Axe, L.; Dyer, J., Adsorption of metal ions onto goethite: single-adsorbate and competitive systems. *Colloids Surf., A* **2001**, *191* (1), 107-121.
58. Zhang, P.; Gong, J.-L.; Zeng, G.-M.; Deng, C.-H.; Yang, H.-C.; Liu, H.-Y.; Huan, S.-Y., Cross-linking to prepare composite graphene oxide-framework membranes with high-flux for dyes and heavy metal ions removal. *Chem. Eng. J.* **2017**, *322*, 657-666.
59. Chong, W. C.; Choo, Y. L.; Koo, C. H.; Pang, Y. L.; Lai, S. O., Adsorptive membranes for heavy metal removal – A mini review. *AIP Conf. Proc.* **2019**, *2157* (1), 020005.
60. Wang, X.; Chen, Z.; Yang, S., Application of graphene oxides for the removal of Pb(II) ions from aqueous solutions: Experimental and DFT calculation. *J. Mol. Liq.* **2015**, *211*, 957-964.
61. Kovtun, A.; Bianchi, A.; Zambianchi, M.; Bettini, C.; Corticelli, F.; Ruani, G.; Bocchi, L.; Stante, F.; Gazzano, M.; Marforio, T. D.; Calvaresi, M.; Minelli, M.; Navacchia, M. L.; Palermo, V.; Melucci, M., Core-shell graphene oxide-polymer hollow fibers as water filters with enhanced performance and selectivity. *Faraday Discuss.* **2021**, *227* (0), 274-290.
62. Fiedler, H.; Kallenborn, R.; Boer, J. d.; Sydes, L. K., The Stockholm Convention: A Tool for the Global Regulation of Persistent Organic Pollutants. *Chem. Int.* **2019**, *41* (2), 4-11.

CONCLUSIONS & PERSPECTIVES

Water purification is a fundamental subject and its importance is growing every year. Modern difficulties and menaces add to the long-standing ones. Research on innovative materials offers new perspectives on which kind of solutions can be found. Nanotechnologies, with graphene and related materials on front line, open scenarios unavailable to traditional technologies, and the market of point-of-use purification devices allow to test these solutions at a comparable rate with the speed at which new pollutants emerge.

In this thesis, we saw two different strategies to create graphene-based composite materials for the development of multifunctional filters, which perform filtration and adsorption simultaneously. The first strategy (core-shell strategy) involves the coating of polymeric hollow fibers with graphene oxide. This permits the insurgence of a synergic effect, which exploits the totality of the surface area of graphene oxide for adsorption. This system has been studied to deepen our knowledge of water and ion mobility inside a graphene oxide membrane. We demonstrated that it is possible to modulate the ionic selectivity of the device through the application of an electric field. The second strategy (coextrusion strategy) exploits the embedding of graphene oxide inside the polymeric matrix of the hollow fibers. This causes the loss of a fraction of the exploitable surface area of graphene oxide, but keeps unaltered the water permeability of the pristine fibers. We demonstrated that this composite is suitable for industrial scale up and can remove from water organic molecules, heavy metals and, partially, perfluoroalkyl substances.

The choice of which feature has priority between efficiency and water permeability decreases the best application fields of these two materials: research for the core-shell system, and industry for the coextruded system.

This research line can advance in several ways. Biopolymers, such as polycaprolactone or polylactic acid, can substitute polysulfone and polyethersulfone as bases for hollow fibers, in order to break down their environmental impact. Another engaging subject is the covalent modification of graphene oxide aimed at the tuning of its selectivity toward specific pollutants. This can be exploited both for selective remediation and high precision sensing. In addition to this, there is the aspect of the industrial scale up, from point-of-use to point-of-entry, and from point-of-entry to water treatment plants.

One day, this scene happened. I am working in the lab. Suddenly, it comes Claudia, the cleaning lady for our institute, and notices a stain on the floor. “What is this?” she asks with attitude. With the typical arrogance of those who want to show off their expertise, I answer: “We are in an organic synthesis lab, Claudia. It could be literally anything”. She stares me directly in the eyes and replies, counting on two fingers: “Nope, it’s either water or grease! If it’s water, it is enough to clean it with the mop; if it’s grease, I should use a bit of acetone, before using the mop”. “In this case – I say, a bit startled – It has to be grease”. Then, she pours a drop of acetone on the floor, and cleans that mysterious stain out of existence.

I like to joke on this episode by saying that Thales of Miletus found the *arché*, the origin of the cosmos, in water, while Claudia of Bologna found it in grease, but the reality is that she was right in solving the problem, while I was wrong pontificating about it. Unfortunately, the water issue that afflicts our world is not this easy to solve. Some “stains” are extremely dangerous, some are extremely difficult to remove, and the worst ones are both. Having clean water all over the world is something that will require all to roll up their sleeves and truly work toward that objective, while stopping denigrating it as a secondary matter, or worse, working against its resolution. Research is necessary, but cannot solve the problem on its own. Mathematicians would say it is a necessary but not sufficient condition. It needs both the means of industry to apply the solutions it researched to solve the already existing problems, and needs education to avoid people perpetrating the same mistakes. Research must *understand how to*, industry must *do it*, and society must *wish for it*. As long as these three realities are not perfectly coordinated, no definitive solution to the water issue may be found. I hope for my work to contribute toward this, even if it is a drop of water in the ocean of grease.



ACKNOWLEDGMENTS

My initial intent was to avoid writing any acknowledgments at the end of this document. Official acknowledgments are stated in the title page or at the end of the articles, and I prefer to express my gratitude in person (specifically with hugs). The disclosure of how much I loved and was I loved by whom during these years would require way more pages than the rest of this thesis. Yet, I feel the need to make an exception.

Due to the rules by which this document must be produced, in no official instances (except for the articles authorships) the name of Manuela Melucci stands out.

I truly despise this fact, because if any is to be thanked for my ability to write *PhD* after my signature, that is Manuela. She accepted me in her group in a very difficult period of my life, giving me a work-family to take care of and from which being taken care of. The debates I had with her, both on the professional level and the personal level, taught me a lot about who I am and who I am not. It is a great pride of mine to call her a colleague, a mentor, and a friend, and I am utterly thankful to her for all she has done for me.

APPENDIX 1

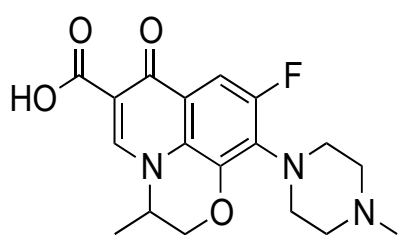
Supplementary Information for:

Core-shell graphene oxide-polymer hollow fibers as water filters with enhanced performance and selectivity

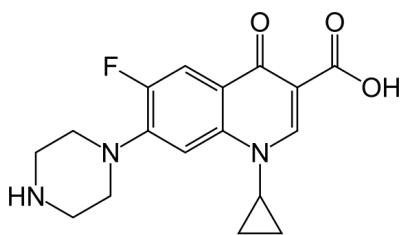
Contents:

1. Molecular structure of target Emerging organic contaminants (EOCs) and PES/PVS polymers
2. HF-GO cartridges preparation
3. Coating stability, filtered water potability
4. Optical microscopy
5. Scanning Electron Microscopy (SEM)
6. Micro-Raman
7. XRD analysis
8. Water permeability test
9. Gas permeability test
10. BSA Filtration experiments and analytical method
11. Nanoparticles filtration
12. Ofloxacin, Ciprofloxacin and Rhodamine B filtration experiments and analytical details
13. Simultaneous filtration of proteins and Ofloxacin from water and bovine plasma matrixes
14. Molecular modelling
15. Bibliography

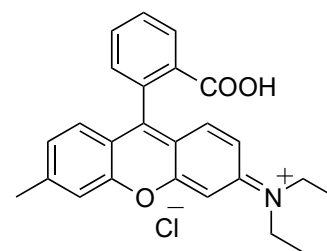
1. Chemical structures of Target EOCs and Polyethersulfone-polyvinylpyrrolidinone fibers



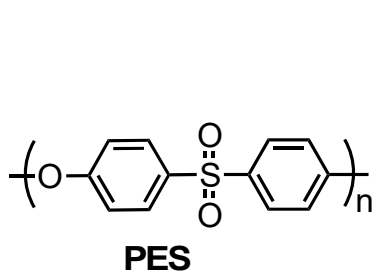
Ofloxacin



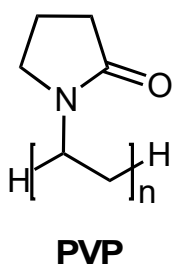
Ciprofloxacin



Rhodamine B



PES



PVP

Figure S1. Molecular structure of the target EOCs and of the Versatile™ PES polymeric components.

2. HF-GO cartridges preparation

GO powder (Abalonyx) was suspended in Milli-Q water (2mg/mL) and sonicated for 4 h. A volume of 5ml of GO suspension was filtered through PES cartridges (in-out or out-in configuration) then the cartridge was kept in oven at 80°C for 12 hs to give samples HF-GOo/i 1% (total weight of PES in the cartridge is about 700 mg). After cooling to room temperature, the filtration/fixation sequence was repeated a few times to give HF-GOo about 5% w/w (two further filtration/fixation cycles, for a total of three) and about 10% w/w in GO respectively (five further filtration/fixation cycles, for a total of six).

Cartridges nomenclature is:

HF-GO1e (out 1% GO),

HF-GO1i (in 1% GO),

HF-GO5e (out 5% GO),

HF-GO5i (in 5% GO),

HF-GO10e (out 10% GO),

HF-GO10i (in 10% GO).

3. Coating stability, filtered water potability

250 ml of tap water were filtered through a HF-GO5i cartridge (15mL/min).

Risultati analitici				
Parametro Metodo	U.M.	Risultato	Incertezza	Limiti
* Torbidità APAT CNR IRSA 2110 Mar 29 2003	NTU	< 0,02		
* Odore APAT CNR IRSA 2050 Mar 29 2003		Inodore		
* Sapore APAT CNR IRSA 2080 Mar 29 2003		Insapore		
* Colore APAT CNR IRSA 2020 Mar 29 2003		Incolore		
pH APAT CNR IRSA 2060 Mar 29 2003	upH	8,3	±0,4	6,5-9,5
Conducibilità APAT CNR IRSA 2030 Mar 29 2003	microS/cm	824	±62	< 2500
* Durezza totale APAT CNR IRSA 2040 Mar 29 2003	°F	45,20	±6,78	15-50
* Residuo fisso a 180 °C APAT CNR IRSA 2090 B Mar 29 2003	mg/l	741,6		< 1500
* Carbonio organico totale (TOC) IRSA Q100 - 3030	mg/l	11		
* Azoto ammoniacale (come NH4+) APAT CNR IRSA 4030 A1 Mar 29 2003	mg/l	< 0,1		
Cloruri APAT CNR IRSA 4020 Mar 29 2003	mg/l	31,8	±2,9	
Solfati APAT CNR IRSA 4020 Mar 29 2003	mg/l	85	±8	
Ferro (ICP-MS) EPA 6020B 2014	ug/l	24,0	±2,2	< 200
Alluminio (ICP-MS) EPA 6020B 2014	ug/l	72,4	±6,5	< 200
Manganese (ICP-MS) EPA 6020B 2014	ug/l	19,0	±1,7	< 50
* Sodio EPA 6010D 2018	mg/l	26,536	±2,388	< 200
* Cromo (ICP-MS) EPA 6020B 2014	ug/l	1,2		< 50
* Rame (ICP-MS) EPA 6020B 2014	ug/l	0,8		< 1,0
* Zinco (ICP-MS) EPA 6020B 2014	ug/l	1840,3		
* Mercurio (ICP-MS) EPA 6020B 2014	ug/l	< 0,1		< 1,0

Bologna Il: 10/10/2019

Il presente Rapporto di Prova si riferisce esclusivamente ai campioni sottoposti a prove ed è valido per tutti i casi previsti dalla legge come da R.D. 1/3/28 n. 842, art 16. Questo Rapporto di Prova non può essere riprodotto parzialmente salvo approvazione scritta del Laboratorio. Analisi eseguite presso la sede di Bologna

Pagina 2 di 4



LAB N° 1051 L

Risultati analitici				
Parametro	U.M.	Risultato	Incertezza	Limiti
* Selenio (ICP-MS) EPA 6020B 2014	ug/l	< 0,1		< 10
* Vanadio (ICP-MS) EPA 6020B 2014	ug/l	0,6		< 50
* Arsenico (ICP-MS) EPA 6020B 2014	ug/l	0,1		< 10
* Cobalto (ICP-MS) EPA 6020B 2014	ug/l	0,29		
* Bario (ICP-MS) EPA 6020B 2014	ug/l	71,22		
* Berillio (ICP-MS) EPA 6020B 2014	ug/l	< 0,01		

Limiti: » D. Lgs. 31/01 Agg. D.M. 14/06/2017

Table S1. Chemical potability parameters of filtered tap water (municipal Bologna network).

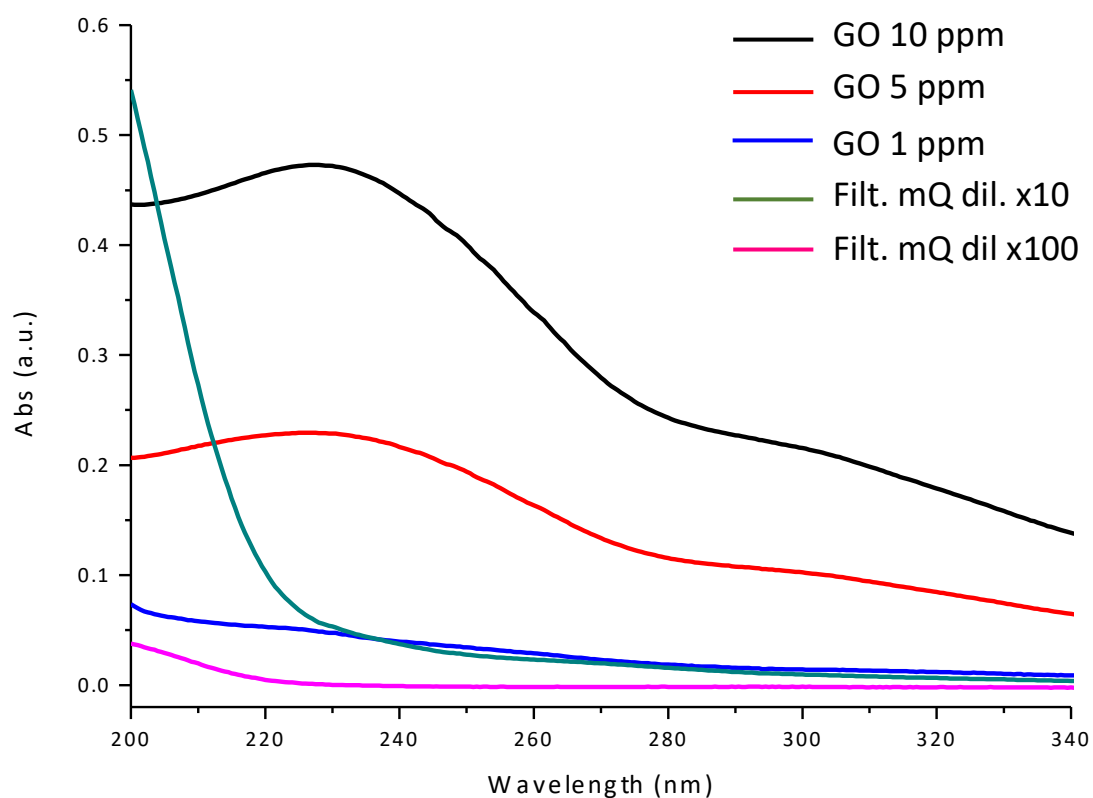


Figure S2. UV spectra of Milli-Q water filtered on HF-GO5e cartridge compared to calibrating solutions of GO.

4. Optical microscopy

HF-GO fibers were extracted from the cartridges and some cut samples (length about 1 cm) were put on a slide. Surface and section of the fibers were evaluated through optical microscopy under white light illumination with a Nikon Eclipse 80i microscope. Digital images were captured at 40x magnification with a Nikon camera (Digital Sight DS-5M) at a resolution of 1600 x 1200 pixels.

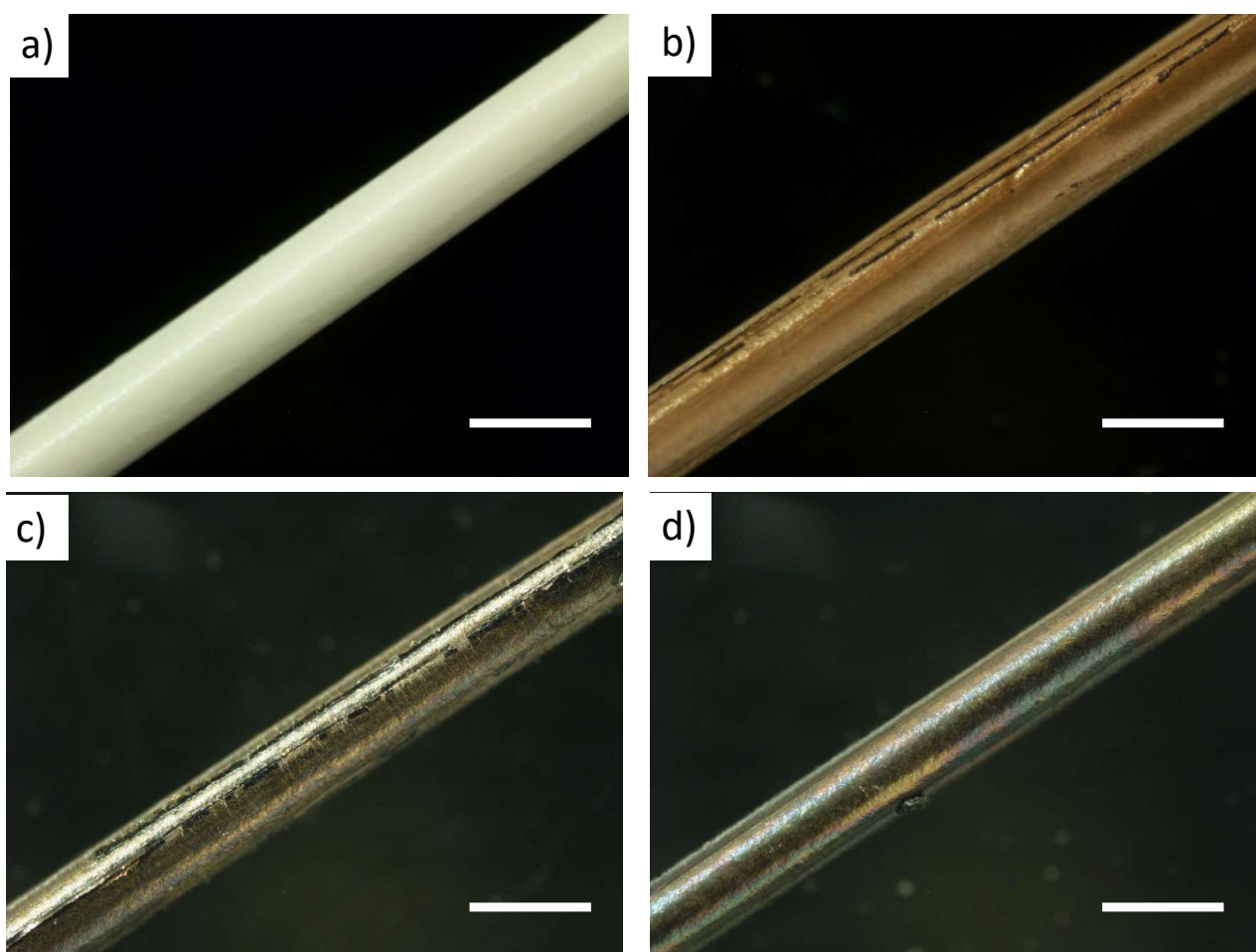


Figure S3. Optical microscopy of a) commercial PES (Versatile™ PES), b) HF-GO1e, c) HF-GO5e and d) HF-GO10e. Bar size: 800 μm .

5. Scanning Electron Microscopy (SEM)

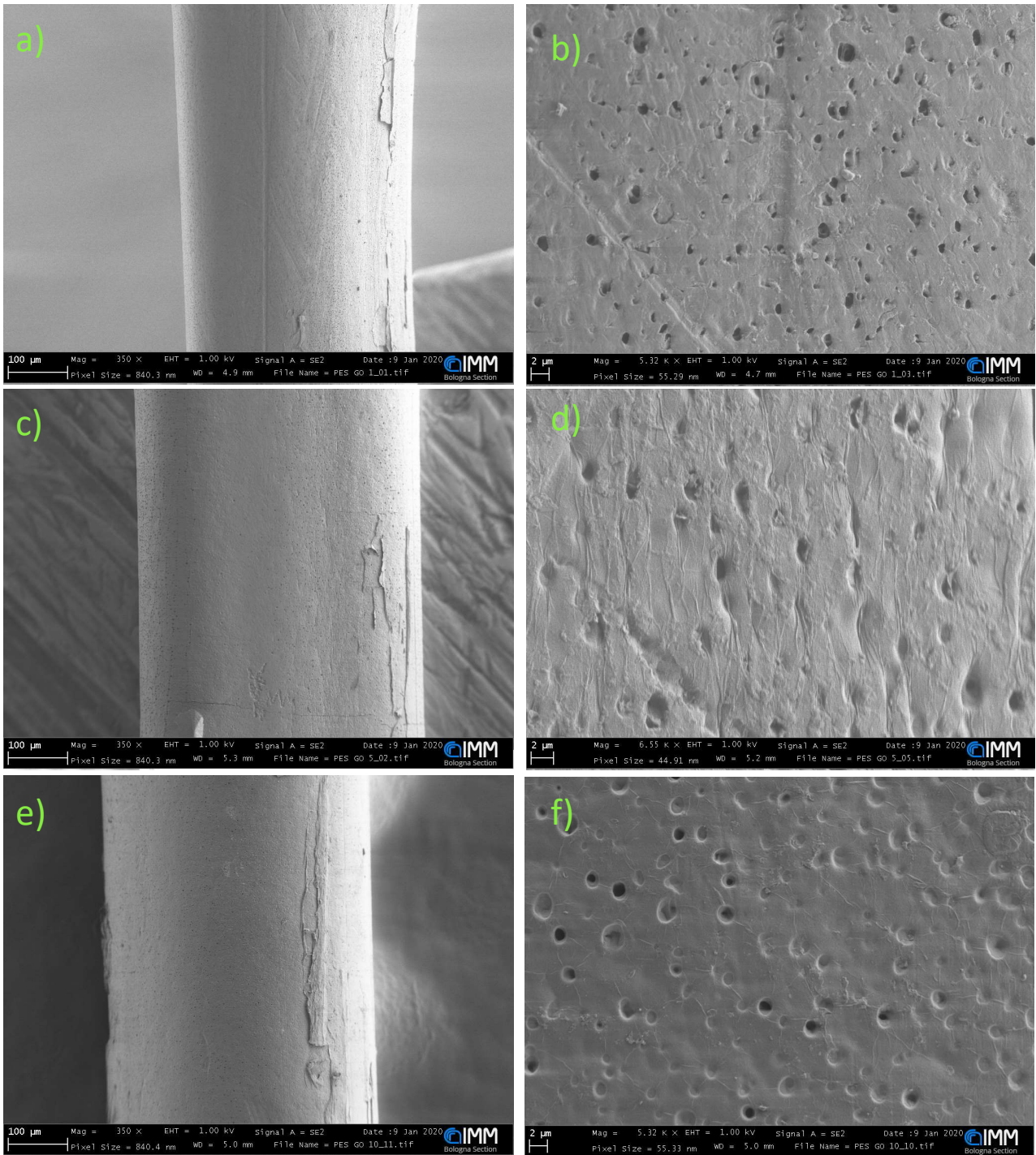


Figure S4. SEM images (at 1KV) of HF-GO1e (a,b)- HF-GO5e (c,d), HF-GO10e (e, f) at different magnification.

6. Micro-Raman

Micro-Raman spectra in the $1\,000\text{--}1\,800\text{ cm}^{-1}$ range were recorded in the unpolarized backscattering geometry through a Renishaw 1\,000 system (50x microscope objective) using the He-Ne excitation wavelength (632.8 nm).

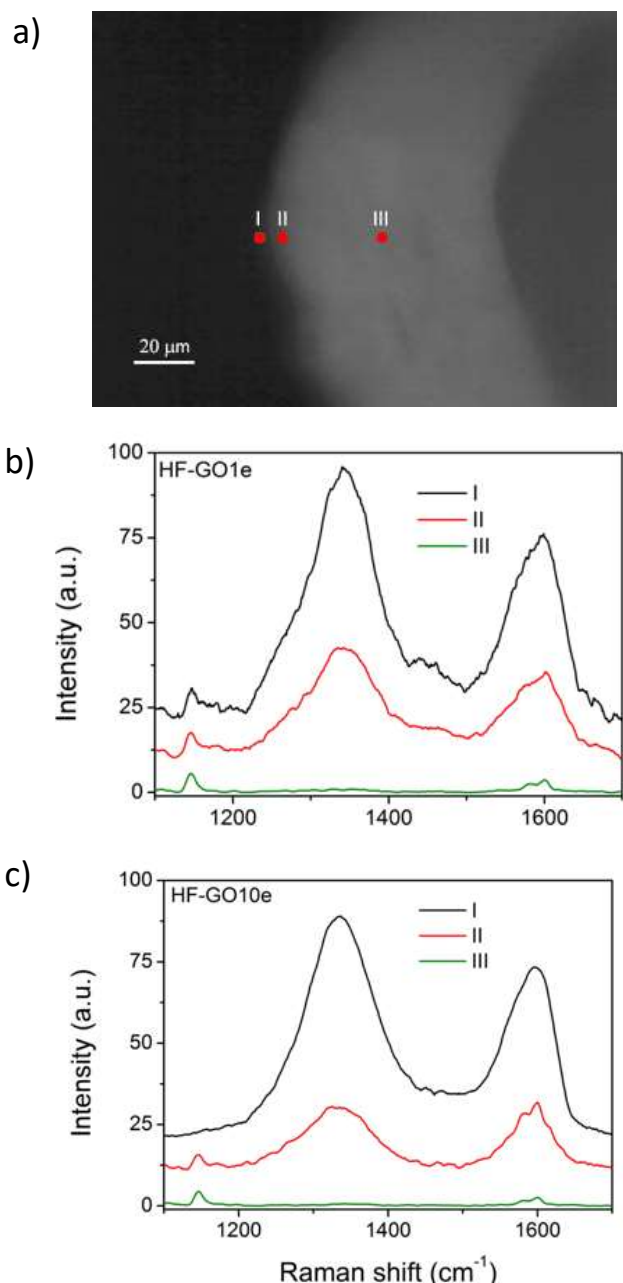


Figure S5. A) Optical microscope image of HF-GO10e cross section. Red dots indicate the Raman measurement points I) external wall; II) 5 μm from the external wall; III) centre of the wall. B) Raman spectra of HF-GO1e collected, as indicated in figure S5, in different point of the HF-GO wall. The spectra have been renormalized with respect to the intensity of the PES Raman band at $1\,535\text{ cm}^{-1}$. Raman PES peak at $1\,535\text{ cm}^{-1}$ is more intense in the uncoated inner region.

7. XRD analysis

The fibers were extracted from the cartridges and dried over night for 2 h at 80 °C, before the analysis. The same treatment was performed on cartridges already used for filtering 250 mL of solution 5mg/L of oflox, ciproflox, and RhB contaminants.

The analysis of cartridges already used for filtering 250 ml of solution 5 mg/L of oflox, ciproflox, and RhB contaminants,

PANalyticalX’Pert Pro X-ray diffractometer with nickel-filtered Cu K α radiation and fast X’Celerator detector was used for recording the powder X-ray diffraction (XRD) patterns of all samples. Scherrer equation was used to calculate the crystal size (length of coherent domains):

$$L = (K*\lambda) / (\beta*\cos\theta) \quad (S1)$$

where L is a measure of the dimension of the particle in the direction perpendicular to the reflecting plane, λ is the X-ray wavelength, K is a constant (here, taken as 1), β is the peak width; and θ is the scattering angle.¹

	FWHM (°)	L (nm)	GO layers
HF-GO1e	1.22±0.05	7.3±0.3	9
HF-GO5e	1.43±0.05	6.2±0.2	7
HF-GO10e	1.75±0.05	5.1±0.1	6
GO	0.66±0.03	13.5±0.6	16

Table S2: Crystal size (L) calculated from width of the $0\ 0\ 1$ peak (FWHM) by Scherrer equation, and estimated number of GO layers ($d=0.84$ nm), rounded to closest unit.

8. Water permeability test

Pumping osmotic ultrafiltered water at room temperature in a pressurized tank performed pure water permeability of the GO-coated cartridges. Filtration was performed in dead-end mode; pressure values were recorded at filter inlet with a pressure transducer and permeate was collected for 1 min and weighted. The effective membrane filtrating area of modules was 0.016 m². Three pressure values (between 100 and 300 mmHg) and three permeates were collected for each sample.

Water permeability (or filtration coefficient) was then calculated as:

$$K_f = \frac{Q_{uf} \text{ (ml/min)}}{\Delta P \text{ (mmHg)} \times A \text{ (sqm)}} \quad (S2)$$

The average of the 3 values for each sample was reported as filtration coefficient.

9. Gas Permeability test

Air permeability tests were carried out on the complete set of membrane modules aiming at an indication of the resulting porous structure of the PES membrane system after coating by GO dispersions. Tests are carried out with dry compressed air at room temperature (20 °C) and considering atmospheric pressure on the downstream side of the membrane. The measurements involved the determination of pressure drop given by the membrane systems by a differential manometer (resolution 0.1 mmH₂O), at constant flow rate obtained by a flow meter. The measured air permeance (or Transfer rate T.R.) of the coated membranes, or permeability of the GO layer only, provides an indication of the obtained structure, together with an estimation on the blocking effect given by the deposited GO layers. Interestingly, the results are not affected by any specific water/GO interaction, or even swelling effect on the GO stacking.

Gas permeance (T.R.) is obtained from the measured volumetric flux \dot{V} and the pressure drop:

$$\dot{n} = \dot{V} \frac{p}{RT} = T.R. \frac{\Delta p}{A} \quad (S3)$$

The results allowed the determination of the membrane permeance values reported in Table S3. As one can see, the transmembrane flux decreases significantly due to the presence of the GO coatings, and the more GO is deposited, the lower is the permeance. A large difference can be observed between membranes coated in the inner or in the external fiber layers, and it is very significant especially for lower concentration coatings; in particular, air permeance in HF-GO1i resulted to be 2 orders of magnitude higher than that in HF-GO1e, as a consequence of an incomplete coverage of the PES membrane fibers. The difference, however, disappears at the highest concentration, for which the air permeance becomes comparable.

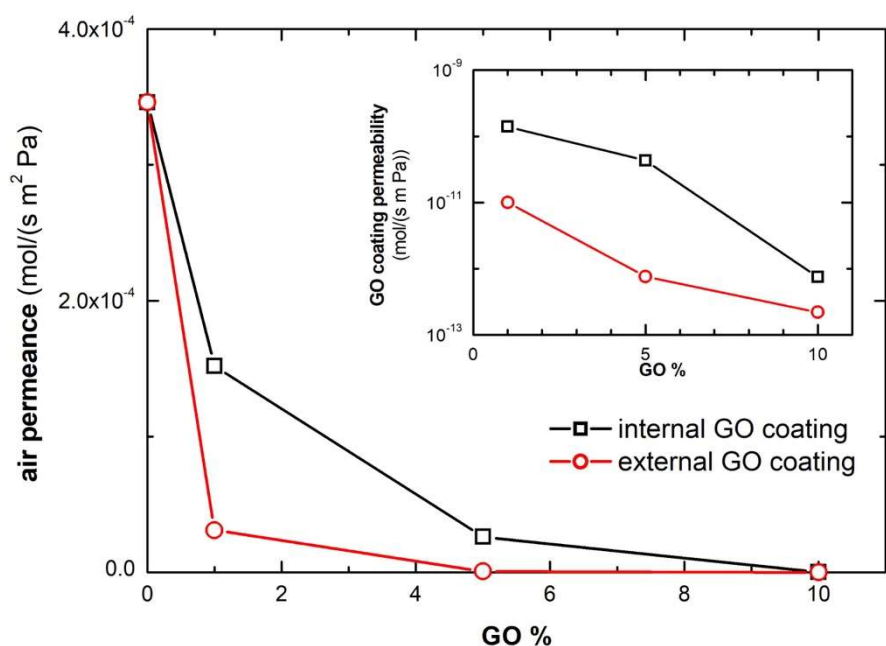


Figure S6. Air permeance in GO coated membranes.

Relevantly, based on the amount and the concentration of graphene oxide dispersion employed, it is possible to evaluate the average coverage of the membrane as mass of GO deposited per unit area. Furthermore, relying on literature data for stacked GO layers in graphene oxide paper, $\rho_{GO} = 1.8 \text{ g/cm}^3$,² an effective thickness value for the coating layer has been determined and also included in Table 1.

	grammage [g/m ²]	eff. thick. [μm]	permeance [mol/(s m ² Pa)]	GO permeability [mol/(m s Pa)]	D_{eff} [m ² /s]
Neat PES	-	-	$3.5 \cdot 10^{-4}$	-	-
HF-GO1i	0.89	0.5	$1.5 \cdot 10^{-4}$	$1.4 \cdot 10^{-10}$	$3.4 \cdot 10^{-7}$
HF-GO5i	2.66	1.5	$2.6 \cdot 10^{-5}$	$4.3 \cdot 10^{-11}$	$1.1 \cdot 10^{-7}$
HF-GO10i	5.32	3.0	$2.4 \cdot 10^{-7}$	$7.5 \cdot 10^{-13}$	$1.8 \cdot 10^{-9}$
HF-GO1e	0.68	0.7	$3.1 \cdot 10^{-5}$	$1.1 \cdot 10^{-11}$	$2.5 \cdot 10^{-8}$
HF-GO5e	2.03	2.0	$8.6 \cdot 10^{-7}$	$7.6 \cdot 10^{-13}$	$1.9 \cdot 10^{-9}$
HF-GO10e	4.06	4.1	$1.2 \cdot 10^{-7}$	$2.2 \cdot 10^{-13}$	$5.3 \cdot 10^{-10}$

Table S3. Air permeation properties in the coated membranes.

From simple resistance in series and relying on the estimated thickness, it is possible to evaluate the intrinsic (air) permeability of the GO coating only, assuming a uniform thickness (l_{GO}) of such coating on top of the microfiltration PES membrane.

$$\frac{1}{T.R.} = \frac{1}{T.R._0} + \frac{l_{GO}}{P_{GO}} \quad (S4)$$

Results obtained are also included in Table S3.

The resulting gas permeabilities can be interpreted from a phenomenological point of view, aiming to retrieve some information about the coating structure. Based on XRD measurements, the interlayer distance in the GO has been determined equal to $d = 0.89$ nm, which suggests a Knudsen diffusion mechanism in the GO coating ($K_n > 10$) to describe air molecules transport. The interlayer distance is expected to be the narrowest pore in the structure, and it is expected to be the controlling resistance. In these conditions, one can evaluate the diffusion coefficient from:

$$D_K = \frac{d}{3} \sqrt{\frac{8RT}{\pi M_i}} \quad (S5)$$

Therefore, Knudsen diffusivity in the slit results $D_K = 4.1 \cdot 10^{-7}$ m²/s.

$$D_{eff} = P \cdot R T \quad (S6)$$

The calculated effective diffusion coefficient, included in Table S3, compared with the value of D_K in the GO slit, is very explicative in the understanding of the transport mechanism occurring in the GO coating, thus providing an idea about the coating structure.

The calculated diffusion coefficients at the lower concentration value (1%) are very large and not compatible with a Knudsen diffusion, and such effect has to be ascribed to an incomplete coverage of the hollow fibers, likely due to imperfect deposition in the small interstices. This is indeed apparent not only for HF-GO1i and HF-GO1e, but also for HF-GO5i. From simple calculations, one can obtain that about 44% of the surface of is not covered in the HF-GO1i membrane, such that a negligible barrier effect can be associated to that portion of the area. Indeed, the deposition of well-staked and overlapped GO layers leads to a significant barrier effect, definitely not comparable with the T.R. associated to a microporous membrane. Similarly, HF-GO1e and HF-GO5i can be considered as not fully covered, with about 9% and 5%, respectively, of uncovered surface.

The other membranes with a thicker coating (HF-GO5e, HF-GO10e and HF-GO10e) shows an effective diffusion coefficient significantly lower than D_K , and basically of the same order of magnitude, between 10^{-9} and $8 \cdot 10^{-10}$ m²/s. That represents a clear indication that these structures are basically equivalent (only thicker at the higher concentrations) and large by-passing holes are not present and there exists only a compact layer of GO sheets. The quite low value of D_{eff}/D_K , in the order of 10^{-3} , reveals that diffusing molecules are forced to travel around the GO sheets, thus leading

to a tortuosity effect that depends on the in-plane distance between two near GO sheets and the intrinsic aspect ratio of the 2D materials.

10. BSA Filtration experiments and analytical method

Bovine serum albumin (BSA, 66KDa) was supplied by Sigma-Aldrich and used without any further purification. 10 mL of tap water solution of BSA (10 g/L) were loaded on a syringe and manually pushed into HF-GO cartridges with different GO content as well as a PES cartridge for comparison. The eluate was analysed by HPLC in order to evaluate BSA removal.

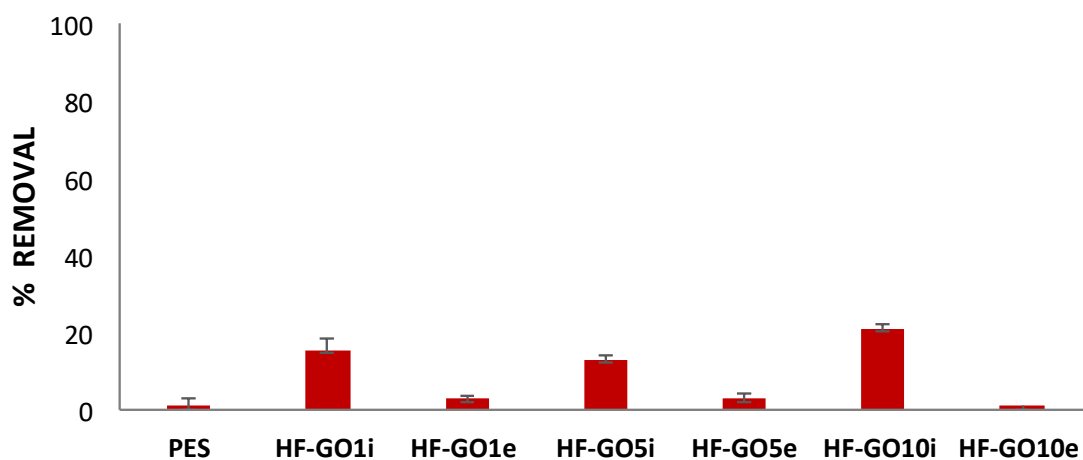


Figure S7. BSA removal efficiency by filtration on PES and HF-GO cartridges.

HPLC analyses were performed on a Dionex Ultimate 3000 system equipped with a diode array detector. 0.5 mL samples were used as sources for the automated injection. LC-MS grade acetonitrile was purchased from Sigma-Aldrich in the highest available purity and were used without any further purification. Ultrapure water (resistivity 18.2 M Ω /cm at 25 °C) was produced in our laboratory by means of a Millipore Milli-Q system. The chromatographic separation was performed on a reverse phase Zorbax C8 column 4.6 x 150 mm, 5 μ m, at flow rate of 1.0 mL/min, detection at λ 285 nm (details in table S4). In each experiment, the removal of BSA was determined by comparison with that of the initial untreated solution. Results are expressed as the mean of three independent experiments \pm SD.

Filters were filled with a saline solution before the test. One sample of each type was assayed for in-out filtration (Fig. S8a) and one for out-in filtration (Fig. S8b). 10 mL of bovine plasma were loaded on a syringe and manually pushed into the filter. Three samples of filtrates were consecutively collected and the amount of TP and BSA was measured in the samples by BT1500 a clinical chemistry automatic analyser.

Time (min)	H ₂ O (0.05% TFA)	Acetonitrile	RT (min)
0	70	30	2.60
2	20	80	
3	20	80	
4	70	30	

Table S4. LC method for determination of BSA.

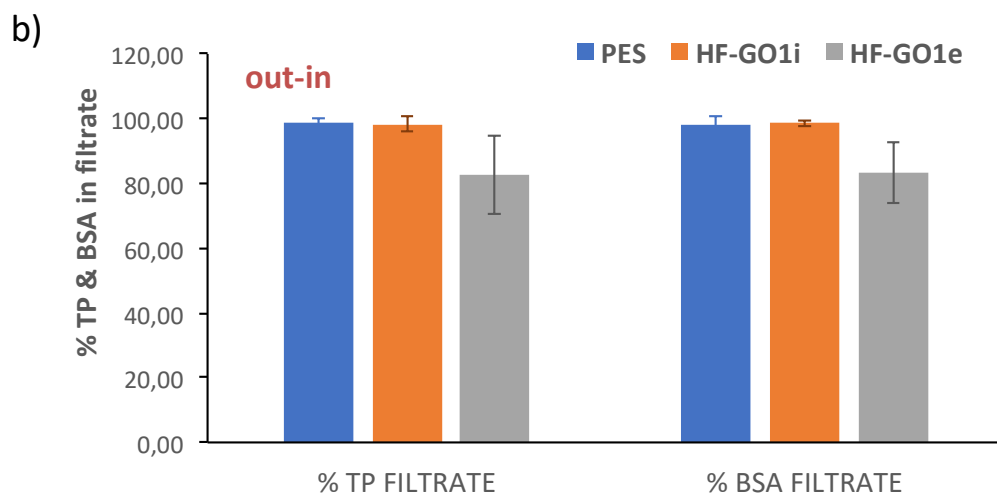
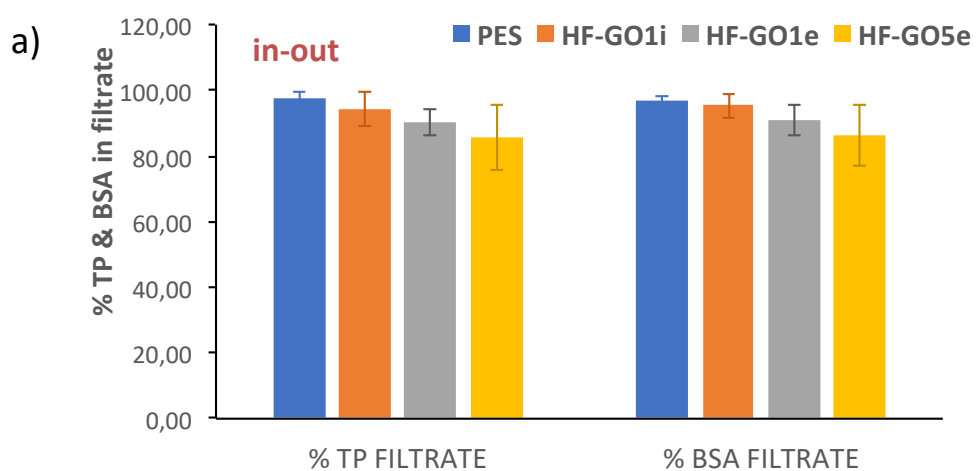


Figure S8. Filtration efficiency of total proteins (TP) and BSA (4 g/dL) for PES and HF-GO cartridges. Total proteins in plasma consist of albumin, globulines and fibrinogenes with a total concentration of 6-8 g/dL (60-80 g/L).

11. Nanoparticles filtration

Polystyrene Latex Particles Size 303 nm, (PS 303) conc. 0.1% w/v (Agar Scientific Ltd, UK), 0.1% = 1.000 ppm in water and Size 52 nm (PS 52), conc. 10% w/v (Magsphere Inc., USA), 10% = 100.000 ppm in water were used for determining the cut-off.

The nanoparticles (NPs) were sonicated for 30 min and diluted in Milli-Q water (1:10 PS 303, 1:100 PS52) and filtered through the cartridges. The concentration of NPs was determined by the absorbance intensity at 232 nm for the PS 303 and 213 nm for the PS 52, after a routine control of linearity of absorbance vs known concentration of nanoparticles.³

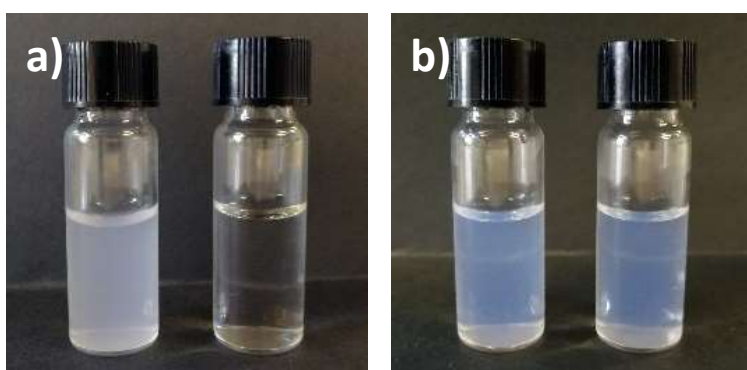


Figure S9. a) PS303 NPs and b) PS52 NPs suspensions before (left) and after (right) filtration on HF-GO1i cartridge.

12. Ofloxacin, Ciprofloxacin and Rhodamine B filtration experiments and analytical details

Ofloxacin (OFLOX), ciprofloxacin (Ciproflox), rhodamine B (RhB) were supplied by Sigma-Aldrich and used without any further purification. LC-MS grade acetonitrile was purchased from Sigma-Aldrich in the highest available purity and were used without any further purification. Ultrapure water (resistivity 18.2 M Ω /cm at 25 °C) was produced in our laboratory by means of a Millipore Milli-Q system.

A tap water solution of OFLOX, Ciproflox and RhB in mixture at 5 mg/L concentration of each compound was prepared. Filtration experiments were performed on 250 mL of 5 mg/L solution fluxed at 15 mL/min flow. The fluxed solution was analyzed by HPLC in order to evaluate the removal efficiency for each EOC.

HPLC analyses were performed on a Dyonex Ultimate 3'000 system equipped with a diode array detector. 0.5 mL samples were used as sources for the automated injection. The chromatographic separation was performed on a reverse phase Zorbax C8 column 4.6 x 150 mm, 5 μ m, at flow rate of 1.0 mL/min, detection at λ of maximum UV absorption of the selected analyte (details in table S5-

6). In all experiments the removal of analytes was determined by comparison with that of the initial untreated solution. Results are expressed as the mean of three independent experiments \pm SD.

Time (min)	H ₂ O (0.05% TFA)	ACN
0	100	0
15	30	70
17	0	100
19	100	0

Table S5. LC method for determination of OFLOX, Ciproflox and RhB in mixture.

Compound	RT (min)	λ (nm)
OFLOX	12.30	285
Ciproflox	12.60	285
RhB	18.50	540

Table S6. Retention time and maximum absorption wavelength of OFLOX, Ciproflox and RhB.

Figure S10 shows the removal efficiency of different chemicals analysed in present work, the removal efficiency depends from the interaction between GO and adsorbates. Ciproflox has a better affinity with GO respect to the OFLOX and RhB. Figure S11 compares the removal efficiency of the different EOC studied for HF-GO1e, HF-GO5e and HF-GO1e filters. The removal is close to 90% only with 10% GO load.

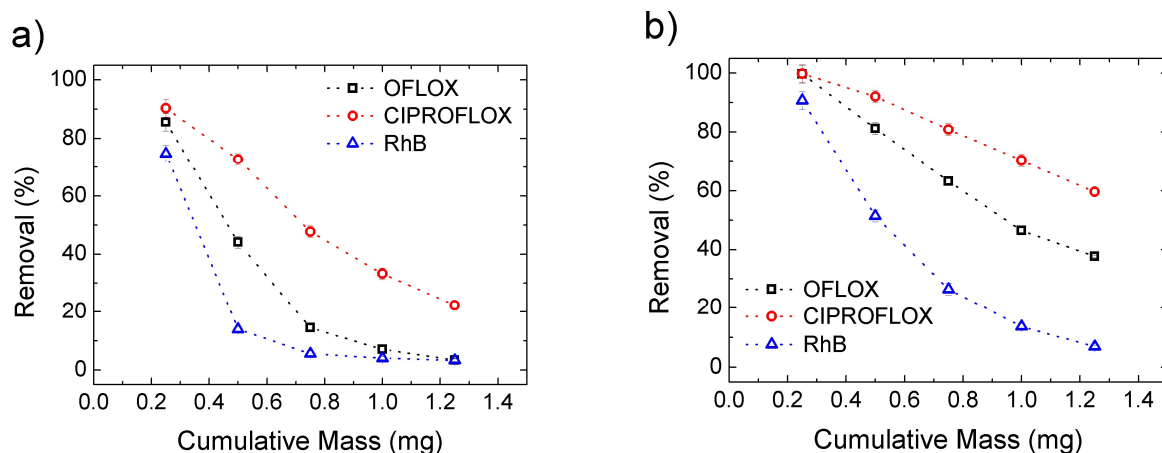


Figure S10. Removal efficiency for OFLOX, Ciproflox and RhB in case of a) HF-GO1i and b) HF-GO5i. Solution with fixed concentration (5 mg/L) and flow (15 mL/min).

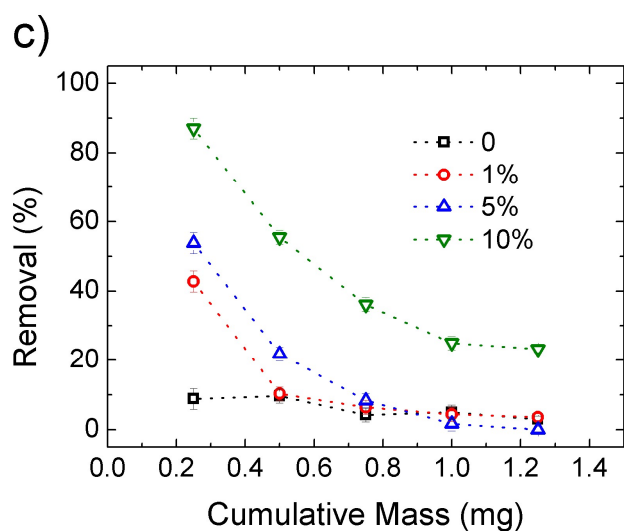
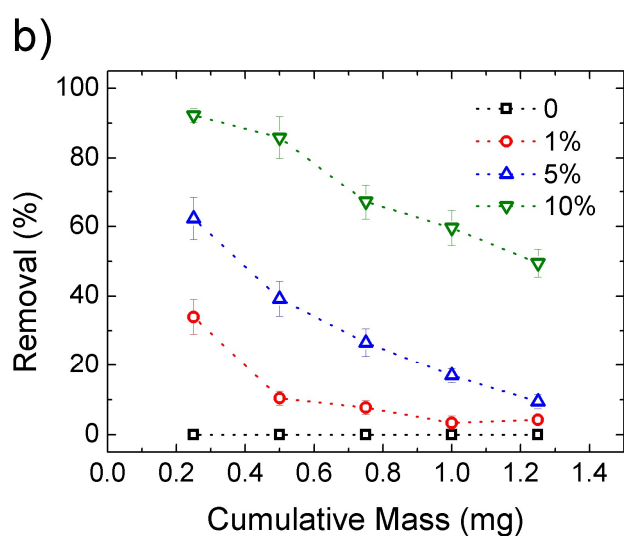
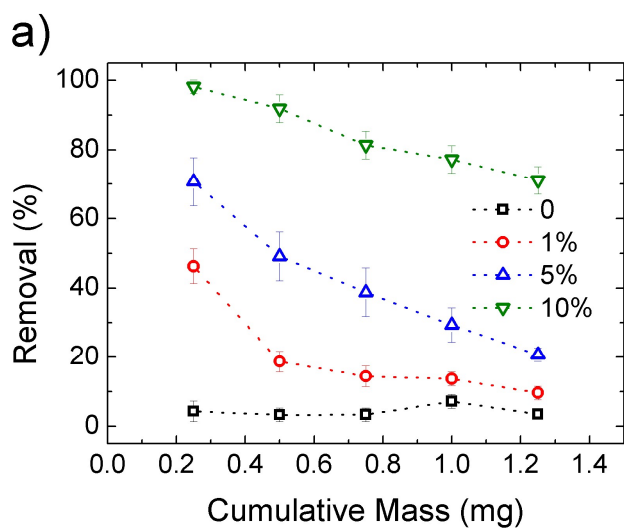


Figure S11. a) Removal efficiency for Ciproflox, b) OFLOX, and c) RhB, for PES and increasing GO loading in HF-GOe. The cumulative initial mass is obtained with fixed concentration (5 mg/L) and flow (15 mL/min).

The amount of EOC captured by GO ($\text{mg}_{\text{EOC}}/\text{g}_{\text{GO}}$) was determined for the sample HF-GO5i by selecting the EOC mass with a removal close to 90%. The WWT-P usually operate at sub-ppb concentration of EOC (C_{wwt}), and the overall efficiency can be intuitively expressed by the volume V of water filterable by a cartridge: $V = M_i/C_{\text{wwt}}$, where the M_i is the total mass of EOC fluxed through the filter. The volume of filterable water is reported in table S7. The efficiency of different active material should be compared by the ratio of the removed mass of EOC (M_R) over the mass of active material (M_{GO}), higher ratio corresponds to a more performing process. M_R/M_{GO} ratio has the same units of monolayer coverage mass (Q_m in mg/g) in Langmuir and BET isotherms, but is a completely different value, since it is measured out of thermodynamic equilibrium and at extremely low concentrations, when almost all the adsorption sites are available.

EOC	Removal %	M_i Initial (mg)	M_R removed mass (mg)	M_R/M_{GO} (mg/g)	C_{wwt} (ppb)	C_{wwt} (mg/L)	$V=M_i/C_{\text{wwt}}$ (L)
Ciproflox	91.6	0.5	0.458	15	0.2 *	$0.2 \cdot 10^{-3}$	2500
OFLOX	81.8	0.5	0.409	14	0.4 *	$0.4 \cdot 10^{-3}$	1250
RhB	89.1	0.25	0.2228	7	1	$1 \cdot 10^{-3}$	250

Table S7. Values used for the estimation of filterable volume of water (V) by a single filter with a 90% c.a. of removal. *The C_{wwt} values were taken from ref. 4.

In order to compare the M_R/M_{GO} with other materials, like Powdered Activated Carbons (PAC), we used the data of ref. 4 on pilot WWT-P in Paris, that claims a removal efficiency close to 90% for c.a. 6 million L of water in 6 days with a material cost of 40 Kg of PAC. This means that 0.887 g of ciproflox was removed ($C_{\text{WWT}}=0.172$ ppb, $M_i=1.02$ g) with a M_R/M_{PAC} of c.a. 20 $\mu\text{g}/\text{g}$.

13. Simultaneous filtration of proteins and OFLOX from water and bovine plasma matrixes

A tap water mixture solution of OFLOX and Bovine Serum Albumine (BSA) (50 mg/L and 10 g/L respectively) was prepared. 50 mL of OFLOX and BSA mixture were loaded on a syringe pump (1 mL/min) into HF-GO cartridges as well as a PES cartridge for comparison. We consider only HF-GO_i cartridges because of the better permeability values. The eluates were analysed by HPLC in order to evaluate OFLOX and BSA removal. HPLC analyses were performed on a Dyonex Ultimate 3000 system equipped with a diode array detector following the method previously described (table S4). Typical chromatograms with estimated removals are shown in fig. S12.

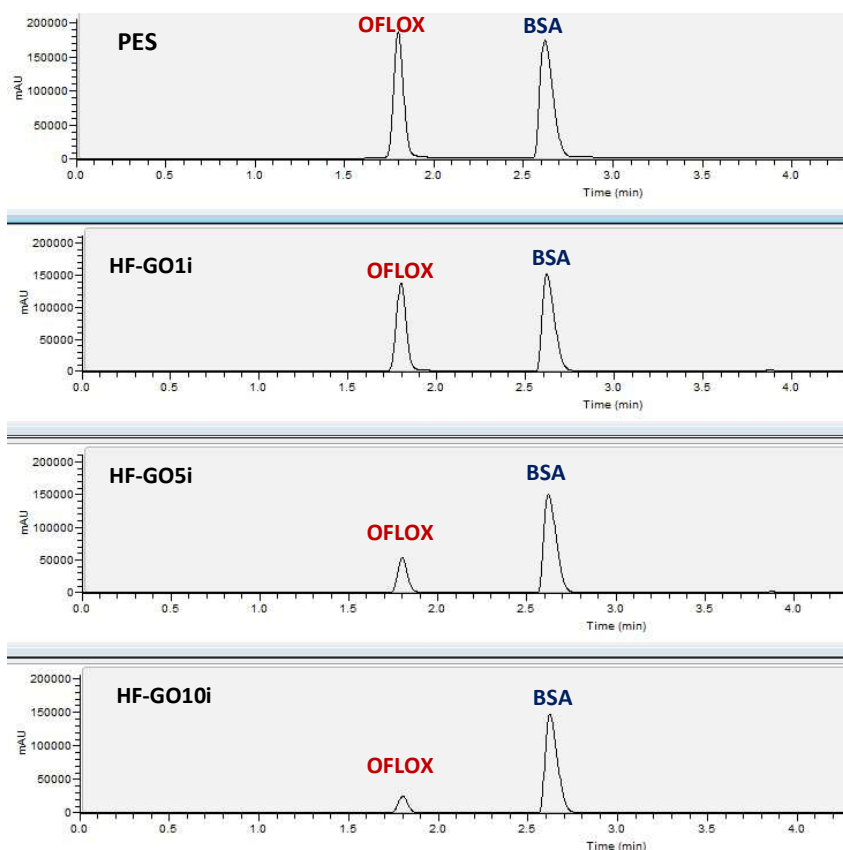


Figure S12. HPLC profile of OFLOX and BSA removal from water by filtration on PES and HF-GO_i cartridges.

A similar experiment was performed in bovine plasma. Two stock solutions of OFLOX in water at 0.5 and 2 g/L were prepared. Bovine serum (9 mL) was spiked with 1 mL of the proper OFLOX stock solution to obtain 50 and 200 mg/L OFLOX final concentration. 10 mL of plasma/OFLOX (50 and 200 mg/L) solution was loaded on a syringe and manually pushed into HF-GO_{1i}. OFLOX was quantified by HPLC analysis following the method previously described (table S4). Prior to the HPLC analysis the eluate was treated as following described. 200 μ L of the filtered solution was treated with equivalent amount of a trichloroacetic acid 5% and MeOH solution 3:1. After centrifugation (10'000 rpm for 10 min) 3 μ L of NaOH 0.1% were added then the resulting solution was injected in HPLC. Figure S13 show the percentage of removal of bovine plasma and total plasma proteins on HF-GO cartridges.

We used as case study HF-GO_{1i} cartridges because of the higher permeability towards protein rich matrix like plasma.

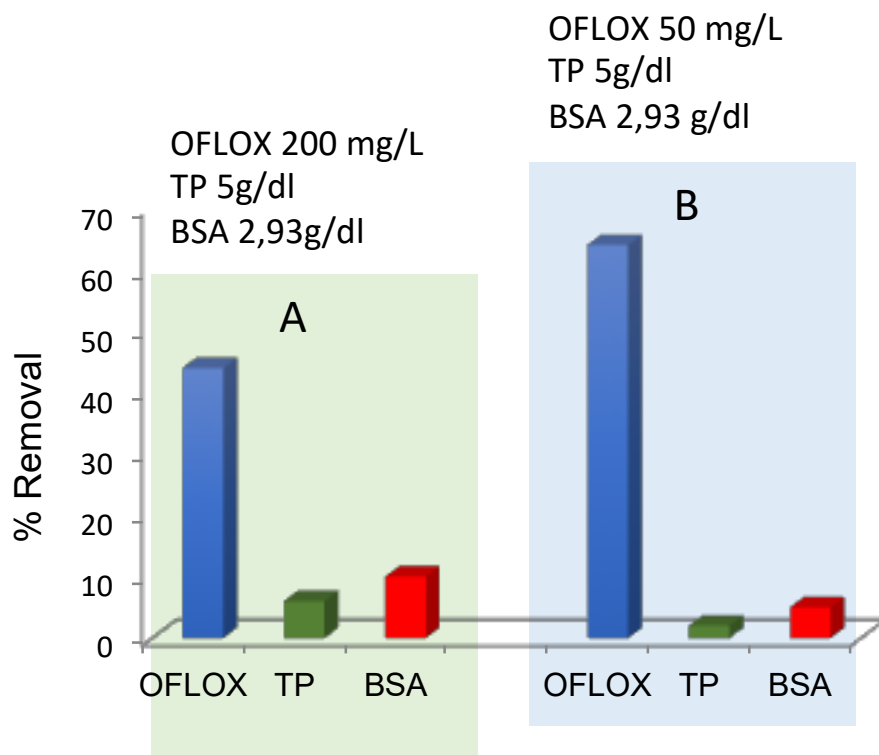


Figure S13. Simultaneous removal of BSA, TP, and OFLOX from plasma by using HF-GO1i cartridges (one cartridge for each experiment, three repetitions). TP concentration in plasma is about 5 g/dL, BSA concentration is 2.93 g/dL.

14. Molecular modelling

To obtain structural information on the effect of OFLOX intercalation on the spacing of GO layers, we carried out molecular mechanic studies using Gaussian 16.⁴ UFF force field⁵ was used to describe GO layers, water molecules and OFLOX. Charges were assigned to all atoms using the QEq method.⁶ Initial configurations of the GO nanoflakes were obtained by CSIRO Data Collection.⁷ An initial spacing of 1 nm was used in the starting GO bilayer structure. Geometry optimizations were performed using Gaussian 16.⁸

15. Bibliography

1. J.I. Langford, A.J.C. Wilson *J. Appl. Cryst.*, **1978**, *11*, 102-113.
2. D. A. Dikin, S. Stankovich, E. J. Zimney, R. D. Piner, G. H. B. Dommett, G. Evmenenko, S. T. Nguyen, R. S. Ruoff, *Nature*, **2007**, *448*, 457–460.
3. J. Shang, X. Gao, *Chem. Soc. Rev.*, **2014**, *43*, 7267-7278.
4. R. Mailler, J. Gasperi, Y. Coquet, S. Deshayes, S. Zedek, C. Cren-Oliv, N. Cartiser, V. Eudes, A. Bressy, E. Caupos, R. Moilleron, G. Chebbo, V. Rocher, *Water Research*, 2015, *72*, 315-330.
5. A. K. Rappé, C. J. Casewit, K. S. Colwell, W. A. G. III, W. M. Skiff, “ *J. Am. Chem. Soc.* **1992**, *114*, 10024-10035.
6. A. K. Rappé, W. A. Goddard III, *J. Phys. Chem.* **1991**, *95*, 3358-3363.
7. A. Barnard, **2018** Graphene Oxide Structure Set. v1. CSIRO. Data Collection.
<https://doi.org/10.25919/5b91c8b150944>
8. Gaussian 16, Revision C.01, M. J. Frisch, G. W. Trucks, H. B. Schlegel, G. E. Scuseria, M. A. Robb, J. R. Cheeseman, G. Scalmani, V. Barone, G. A. Petersson, H. Nakatsuji, X. Li, M. Caricato, A. V. Marenich, J. Bloino, B. G. Janesko, R. Gomperts, B. Mennucci, H. P. Hratchian, J. V. Ortiz, A. F. Izmaylov, J. L. Sonnenberg, D. Williams-Young, F. Ding, F. Lipparini, F. Egidi, J. Goings, B. Peng, A. Petrone, T. Henderson, D. Ranasinghe, V. G. Zakrzewski, J. Gao, N. Rega, G. Zheng, W. Liang, M. Hada, M. Ehara, K. Toyota, R. Fukuda, J. Hasegawa, M. Ishida, T. Nakajima, Y. Honda, O. Kitao, H. Nakai, T. Vreven, K. Throssell, J. A. Montgomery, Jr., J. E. Peralta, F. Ogliaro, M. J. Bearpark, J. J. Heyd, E. N. Brothers, K. N. Kudin, V. N. Staroverov, T. A. Keith, R. Kobayashi, J. Normand, K. Raghavachari, A. P. Rendell, J. C. Burant, S. S. Iyengar, J. Tomasi, M. Cossi, J. M. Millam, M. Klene, C. Adamo, R. Cammi, J. W. Ochterski, R. L. Martin, K. Morokuma, O. Farkas, J. B. Foresman, and D. J. Fox, Gaussian, Inc., Wallingford CT, 2016.

APPENDIX 2

Supplementary Material For:

Graphene oxide-polysulfone hollow fibers membranes with synergic ultrafiltration and adsorption for enhanced drinking water treatment

Contents:

1. Ultrafiltration modules production
 - 1.1 PSU-GO HF extrusion
 - 1.2 Modules assembly
2. PSU-GO morphology
 - 2.1 Pore size analysis
 - 2.2 Optical and SEM imaging
 - 2.3 Contact angle
 - 2.4 Confocal Raman microscopy
3. CIPRO adsorption experiments
4. MWCO determination and ultrafiltration
5. PFASs experiments
 - 5.1 Experimental conditions for PFASs quantification in water
 - 5.2 Removal experiments
6. Heavy metals experiments
7. Water potability tests
8. SERS experiments on GO release
9. Preliminary real conditions POU test

1. Ultrafiltration modules production

1.1 PSU-GO HF extrusion

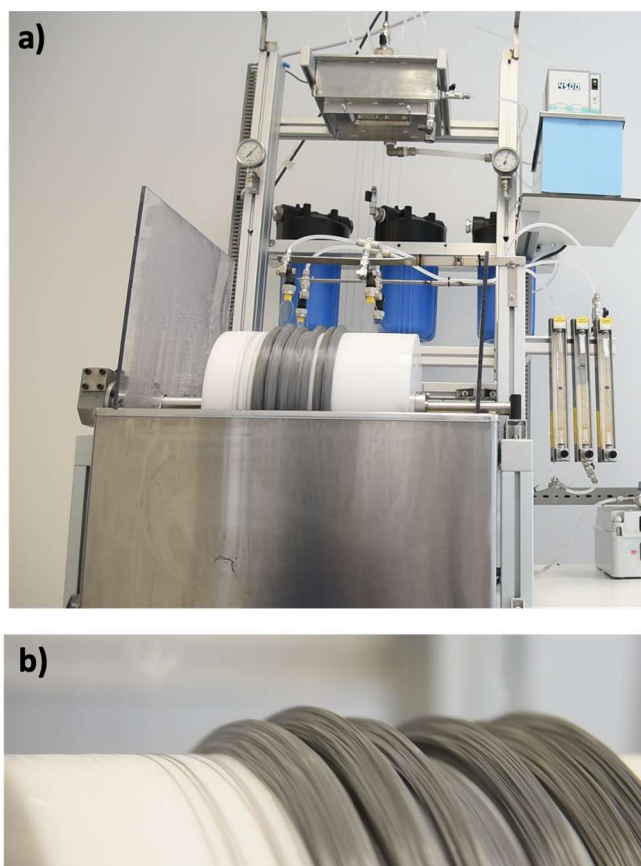


Fig. S1. a) Spinning plant pilot for hollow fiber fabrication. b) Collection wheel with hollow fibers bundle.

The dope solution is prepared adding PSU granules to a GO solution in NMP, obtained after 24-36 h of sonication. PSU is mixed with the GO solution alternating propeller immersion mixing and sonication, while viscosity is checked periodically. The resulting dope solution is extruded with a lab scale benchtop spinning plant, with a maximum dope solution capacity of 3 kg. During extrusion in the spinneret, the dope solution enters in contact with a precipitation solution composed of water and NMP. The PSU-GO HF then freely fall in a coagulation bath, are collected by a bobbin system, moved into a washing bath, and finally collected onto a collection wheel. Fibers are stocked in bundles and then kept in water for solvent extraction and glycerinization, and ultimately dried at open air. 1 kg of material corresponds approximately to 20 km of fibers.

1.2 Modules assembly

Small bundles of closed fibers are obtained cutting the dried stocked bundles with a hot wire. Fibers are then potted in polyurethane resin at the edges inside a module scaffold and then centrifuged. The potting is ultimately cut (to open the fibers) and ferrules are welded to give the final device.

2. PSU-GO morphology

2.1 Pore size analysis

	39BU36500NG211_60_07122 1_7 b...	39BU36500NG211_60_07122 1_7 b...	39BU36500NG211_60_07122 1_7 b...
Measuring mode	"Full porometry"		
Start time	"2021-12-09 15:22:50 +01:00"	"2021-12-10 10:19:13 +01:00"	"2021-12-10 11:44:03 +01:00"
Error	"0"		
Operator	"DP"		
Material	"MEDISULFONE - UF (PSU)"		
Sample ID	"39BU36500NG211, 3 horizontal fibers"	"39BU36500NG211, 2 horizontal fibers"	"39BU36500NG211, 1 horizontal fiber"
FFP method	Size for flow rate above 1,5 ul/min	Size for flow rate above 1,5 ul/min	Size for flow rate above 1 ul/min
FFP filter	X		
FFP pressure (bar)	5,739	6,544	6,218
FFP flow (ul/min)	2,342	11,35	1,125
FFP pore size (nm)	6,969	6,113	6,433
MFP pressure (bar)	5,801	6,59	6,299
MFP size (nm)	6,896	6,07	6,351
Smallest pore pressure (bar)	6,148	6,958	6,411
Smallest pore size (nm)	6,506	5,749	6,239
Smallest pore convergence (%)	99		
Mean pore pressure (bar)	5,897	6,704	6,376
Mean pore diameter (nm)	6,783	5,966	6,273
Corrected prevalent effective pore	1,411	0,681	0,638

length (um)			
Total pore number	7,44E+09	1,65E+10	5,61E+09
Total pore area (mm^2)	0,2685	0,4617	0,1732
Total pore area (%)	0,5701	1,47	1,103
Calculated permeability (um^2)	8,28E-09	1,64E-08	1,33E-08
Sample holder	"47,1"	"31,4"	"15,7"
Sample area (mm^2)	47,1	31,4	15,7
Sample thickness (um)	50		
Min. temp. (°C)	24,37	23,68	23,86
Max. temp. (°C)	24,58	23,98	24,14
Liquids	"Water-Isobutanol"		
Interfacial tension (dyn/cm)	2		
Contact angle (°)	60		

	PS31 - GO_2 horizontal fiber	PS31 - GO_2 horizontal fiber	PS31 - GO_2 horizontal fiber	PS31 - GO_1 horizontal fiber	PS31 - GO_1 horizontal fiber	PS31 - GO_1 horizontal fiber
Measuring mode	"Full porometry"					
Start time	"2021-12-13 13:58:21 +01:00"	"2021-12-16 15:55:43 +01:00"	"2021-12-20 10:28:06 +01:00"	"2021-12-13 15:28:36 +01:00"	"2021-12-15 10:16:01 +01:00"	"2021-12-16 09:30:55 +01:00"
Error	"0"	"5007 (Flow too high)"	"0"	"5007 (Flow too high)"	"0"	"0"
Operator	"DP"					
Material	"PS31 - GO"					
Sample ID	"2 horizontal fibers"	"2 horizontal fibers"	"2 horizontal fibers"	"1 horizontal fiber"	"1 horizontal fiber"	"1 horizontal fiber"
FFP method	Size for flow rate above 1,5 ul/min					
FFP filter	X					
FFP pressure (bar)	2,79	2,78	1,18	3,603	2,798	3,199
FFP flow (ul/min)	2,019	2,048	1,869	2,268	1,802	1,57
FFP pore size (nm)	18,43	18,5	43,57	14,27	18,38	16,07
MFP pressure (bar)	3,999	4,041	3,214	5,052	4,249	5,463
MFP size (nm)	12,86	12,73	16	10,18	12,1	9,413
Smallest pore pressure (bar)	4,39	5,195	3,983	5,108	4,304	5,523
Smallest pore size (nm)	11,71	9,898	12,91	10,07	11,95	9,311
Mean pore pressure (bar)	3,757	3,954	2,599	5,058	4,274	5,438
Mean pore diameter (nm)	13,69	13,01	19,78	10,17	12,03	9,456
Corrected prevalent effective pore length (um)	2,9	3,074	3,929	0,2411	0,2598	0,2416
Total pore number	2,90E+09	4,37E+09	1,72E+09	8,86E+10	7,37E+10	8,84E+10
Total pore area (mm ²)	0,3971	0,5248	0,3521	7,147	8,342	6,136
Total pore area (%)	0,843	1,114	0,7475	15,17	17,71	13,03
Calculated permeability (um ²)	4,20E-08	5,26E-08	6,57E-08	4,75E-07	7,84E-07	3,48E-07
Sample holder	"47,1"					
Sample area (mm ²)	47,1					
Sample thickness (um)	50					
Min. temp. (°C)	23,47	23,63	22,47	23,61	23,2	23,06
Max. temp. (°C)	23,72	23,88	22,79	23,81	23,75	23,7
Liquids	"Water-Isobutanol"					
Interfacial tension (dyn/cm)	2					
Contact angle (°)	50					

Table S1. Pore size and pore distribution analyses.

2.2 Optical and SEM imaging

PSU-GO HF samples were freeze-fractured in liquid nitrogen to obtain cross section. The cross section was coated with gold (Lecia EM ACE600) and observed by SEM (JEOL JSM-7800F Prime) at an acceleration voltage of 8 kV.

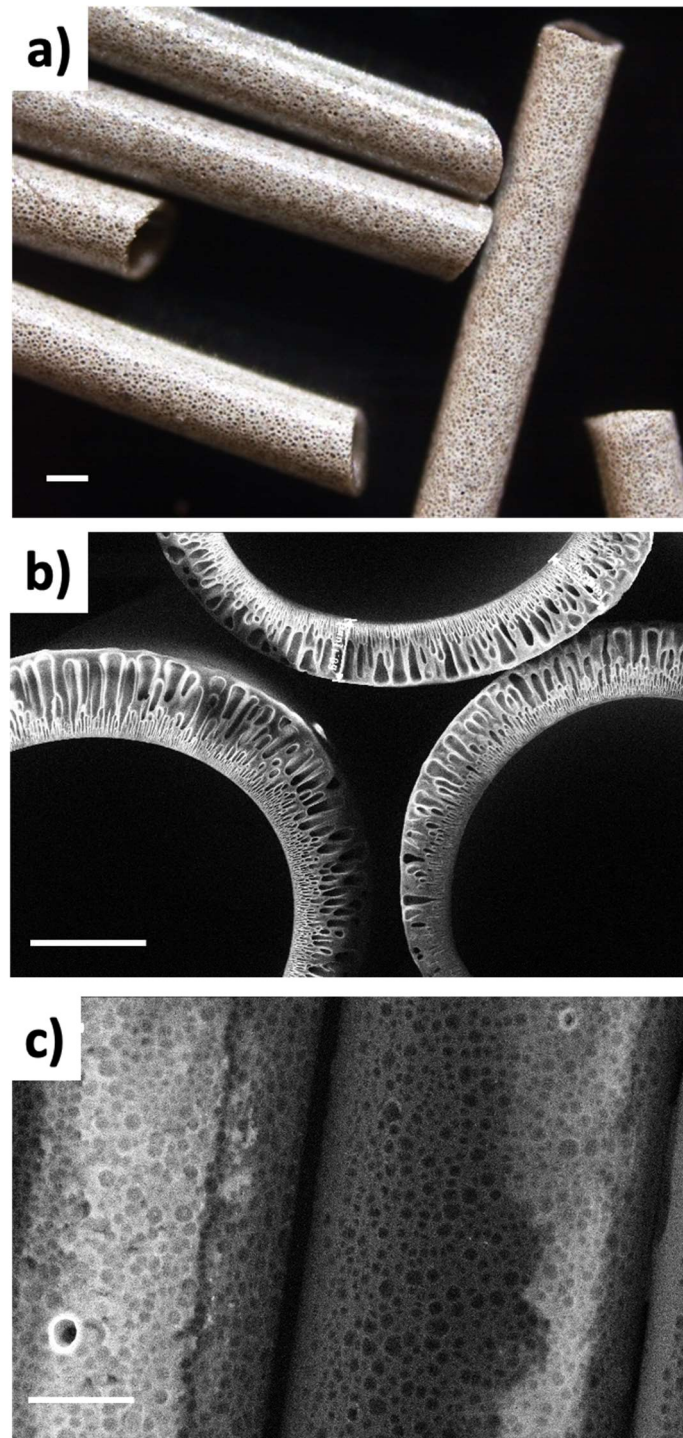


Fig. S2. Morphology of PSU-GO 5% taken as reference system. a) Optical microscopy image, b) SEM images of the section and c) of the HF surface. Bars size 100 μm .

2.3 Contact Angle

Contact angle of PSU-HF and PSU-GO 3.5% HF were measured with OCA Dataphysics instrument.

Fibers were flattened before measurement to remove the outer porosity of the fiber and allow the measurement of the contact angle of the material.

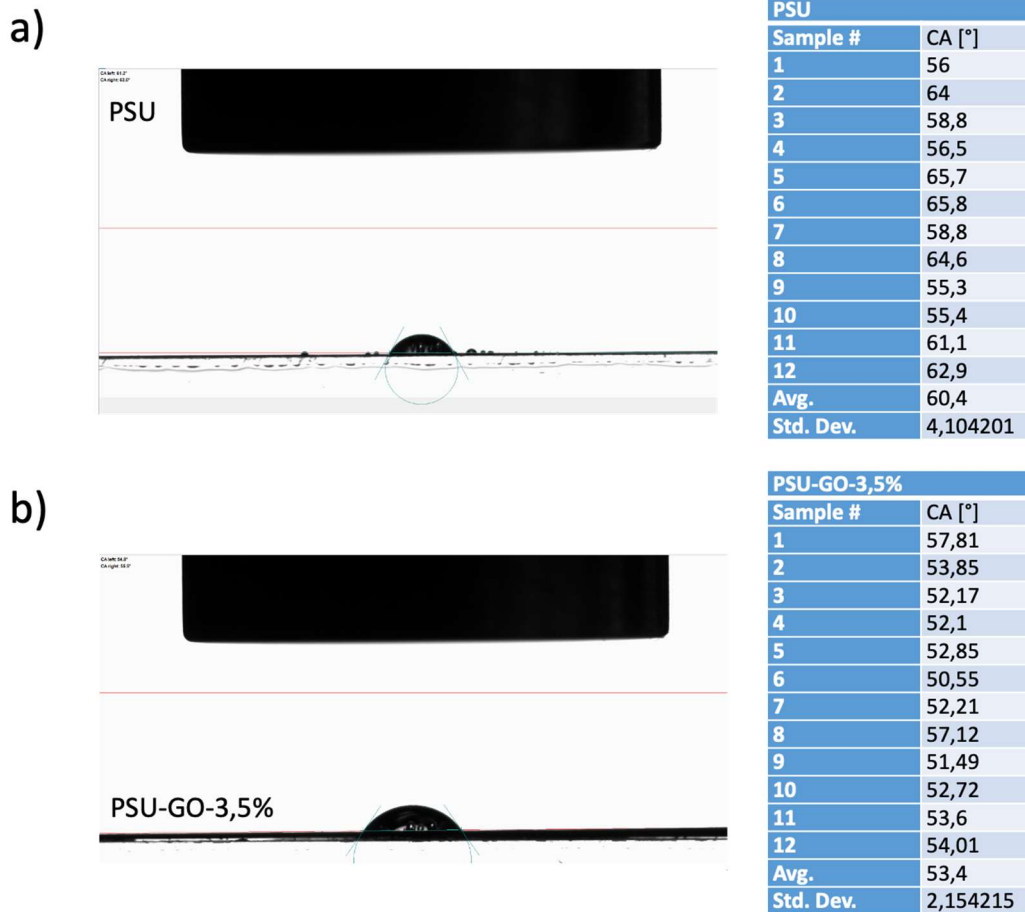


Fig. S3. Contact angles values and images of PSU and PSU-GO 3.5% HF.

2.4 Confocal Raman microscopy

Raman stack mapping was performed on a confocal Raman micro-spectroscope (Alpha300R, WITec, Germany). The light source used was a 532 nm laser with the output power of around 0.7 mW cm^{-2} . The diffraction grating of 600 g/mm was employed together with a 50x microscope objective. Fibers were imaged by collecting Raman images from 5 layers of 2.5 mm increment in the z direction. A 2 mm step size was used in the x and y direction for each Raman image with 0.5 s integration time and a spectral range from 0 to 3600 cm^{-1} .

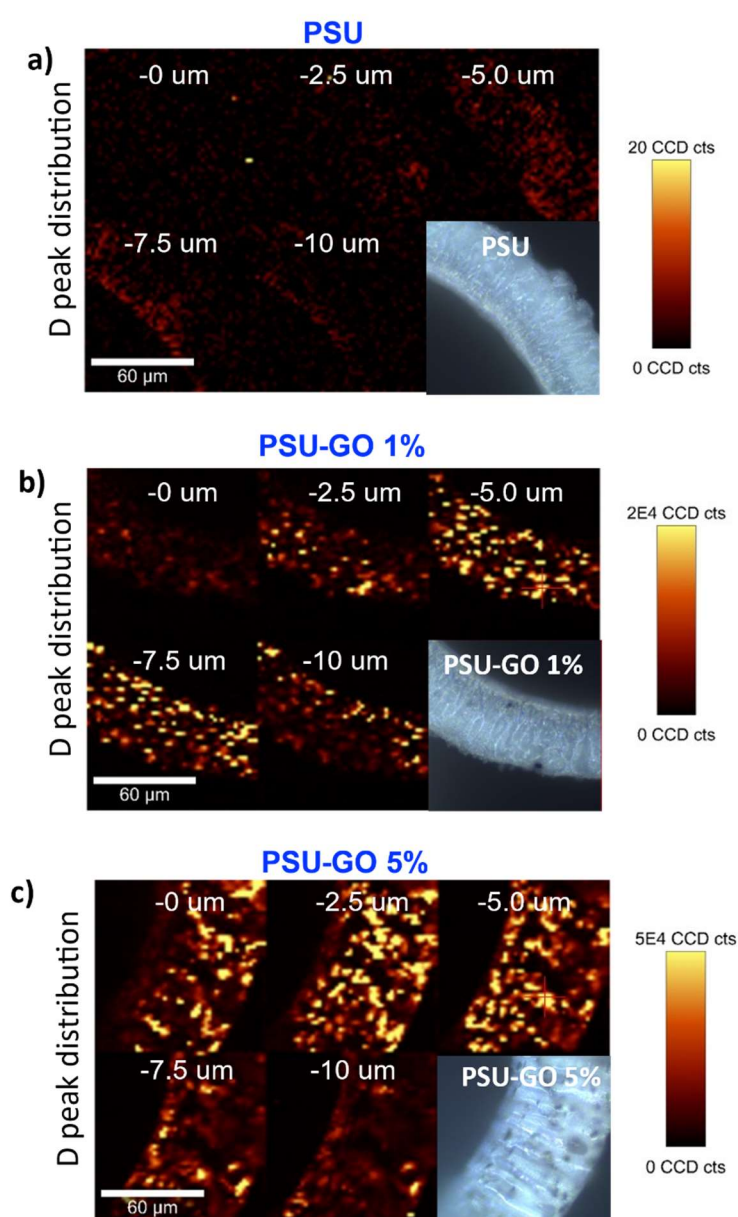


Fig. S4. Z stack of Raman maps and the relative optical images of original PSU, PSU-GO 1% and PSU-GO 5%, constructed by mapping the D-band region.

3. CIPRO adsorption experiments

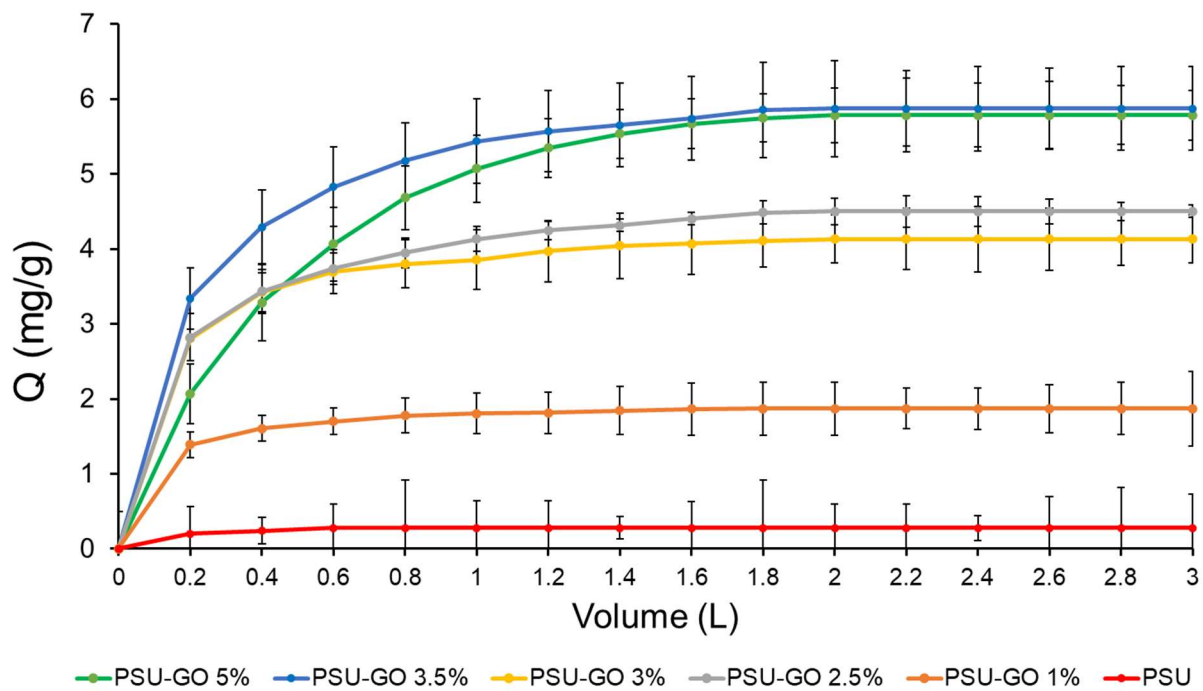


Fig. S5. Comparison between the Ciprofloxacin adsorption efficiency of PSU and PSU-GO materials at five different GO (percentage mg/g composite).

4. Flow-rate vs. pressure curve

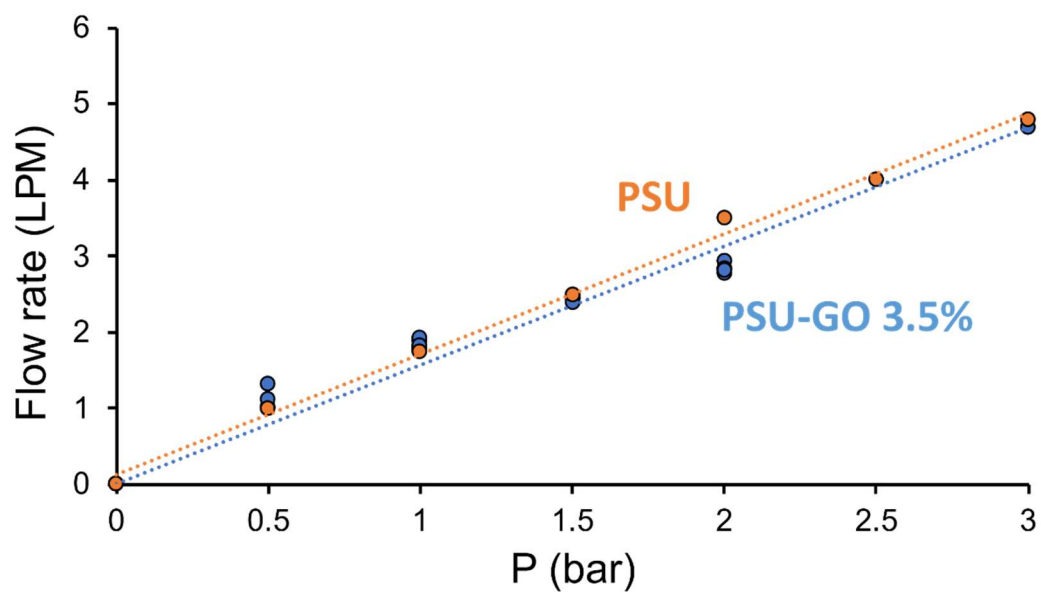


Fig. S6. Pressure/flow rate correlation of PSU and PSU-GO 3.5%, expressed as litres per minute (LPM).

5. PFASs experiments

5.1 Experimental conditions for PFASs quantification in water

Analyses were performed by using a UPLC-MS/MS Waters ACQUITY UPLC H-Class PLUS – XEVO TQS Micro mass detector. 0.5 mL samples were used as sources for the automated injection. The chromatographic separation was performed on a reverse phase Waters Acquity UPLC CSH Phenyl-Hexyl (1.7 μm , 2.1x100 mm) and Waters Isolator Column 2.1x50 mm, column temperature 34 °C, linear gradient from 100:0 to 5:95 mobile phase A (MeOH: aqueous NH_4OAc 2 mM 95:5)/mobile phase B (NH_4OAc 2 mM in MeOH), flow rate 0.3 mL/min. The mobile phase composition varied according to the gradient program reported in Table S2. Mass details and limits of quantitation (LOQ) for each analyte are reported in Table S3.

Time (min)	Analytical pump		
	Flow(mL min^{-1})	A%	B%
0	0.3	100	0
1	0.3	80	20
6	0.3	55	45
13	0.3	20	80
15	0.35	5	95
17	0.35	5	95
18	0.3	100	0
21	0.3	100	0

Table S2. Elution gradients used by the analytical pump. Mobile phases: (A) MeOH: aqueous NH_4OAc 2 mM 95:5; (B) NH_4OAc 2 mM in MeOH.

The calibration curves were calculated by using the average value of 2 subsequent UPLC-MS/MS injections. Calibration curve solutions (0.01, 0.05, 0.1, 0.5, 1.0, 2.5, 5.0 $\mu\text{g/L}$) were freshly prepared diluting methanolic PFASs stock (5'000 $\mu\text{g/L}$) solution with laboratory phase A and injected before

each analytical batch. Regression equations of calibration curves were linear in the range of 10-0.01 or 0.05 or 0.1 µg/L depending on the analyte (see Table S3 LOQ). The results are expressed as the mean of $2 \pm$ SD. Laboratory drinking water was checked for PFASs contamination: no PFASs compounds were detected above LOD value.

		ES(-)	Collision energy (eV)	LOQ
PFBA	Perfluorobutanoic acid	212.97→168.99	8	0.01
PFPeA	Perfluoropentanoic acid	263.09→218.93	6	0.01
PFBS	Perfluorohexanoic acid	299.03→79.84	32	0.01
PFHxA	Perfluoroheptanoic acid	312.90→269.02	6	0.01
PFHpA	Perfluorooctanoic acid	262.90→168.98	6	0.01
PFHxS	Perfluorononanoic acid	398.96→79.90	38	0.01
PFOA	Perfluorodecanoic acid	412.98→168.98	18	0.01
PFNA	Perfluoroundecanoic acid	462.96→218.97	16	0.01
PFOS	Perfluorododecanoic acid	498.90→79.90	54	0.01
PFDA	Perfluorotridecanoic acid	513.12→469.00	10	0.01
PFUnDA	Perfluorotetradecanoic acid	562.96→519.06	10	0.05
PFDODA	Perfluorobutanesulfonic acid	613.06→569.04	14	0.05
PFTrDA	Perfluorohexanesulfonic acid	622.90→168.97	28	0.05
PFTA	Perfluorooctanesulfonic acid	712.96→168.96	32	0.1

Table S3. LC/MS/MS parameters for all PFASs target analytes using UPLC-MS/MS ACQUITY UPLC H-Class PLUS – XEVO TQS Micro MS.

5.2 Removal experiments

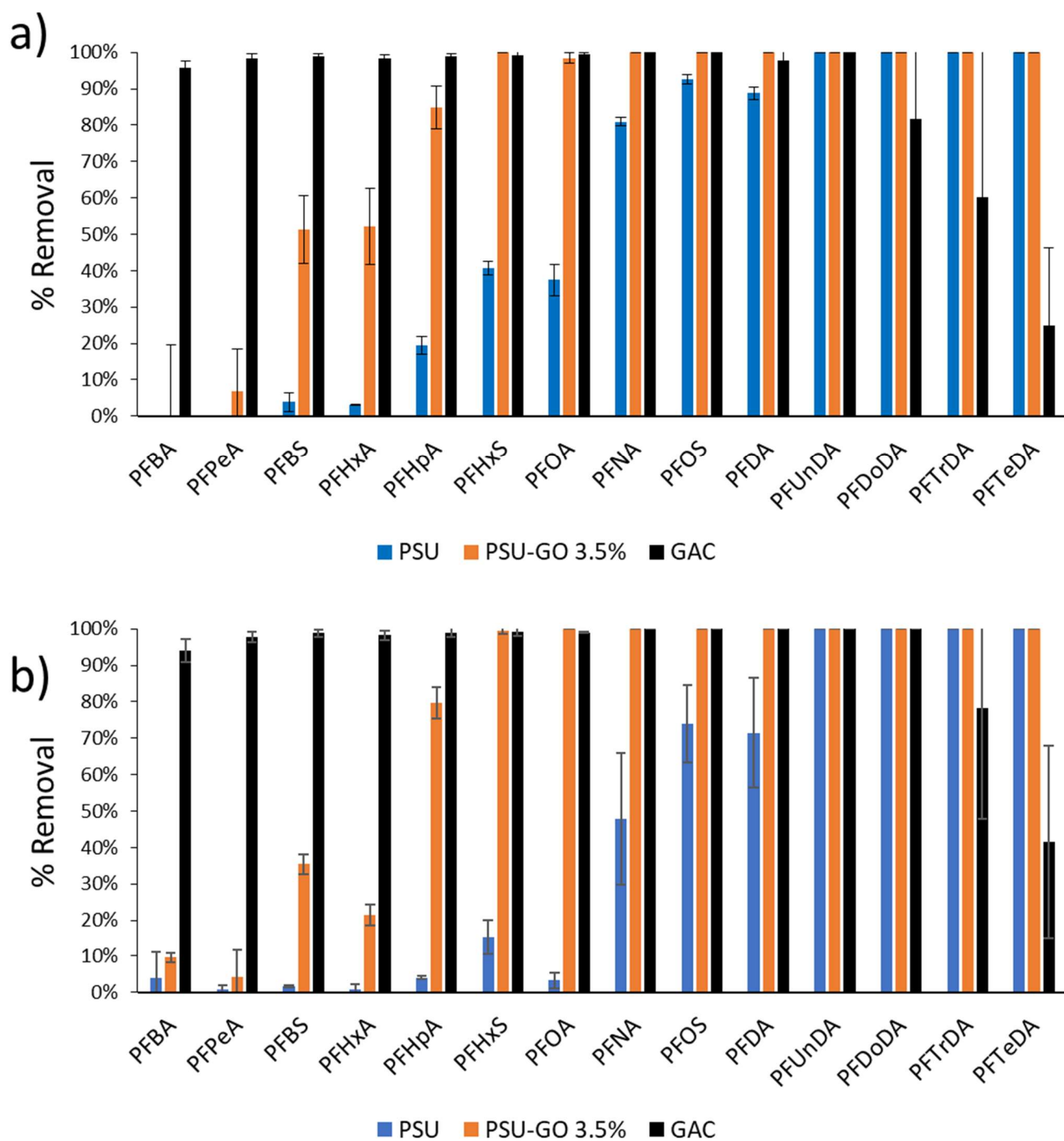


Fig. S7. Removal of a mixture of fourteen PFASs in tap water, a) total volume=0.5 L and b) 1 L, C_{IN} = 0.5 μ g/L, flow rate= 5 mL/min. Amount of material in the module: PSU 0.26 g, PSU-GO 3.5% 0.27 g, GAC 2.3 g.

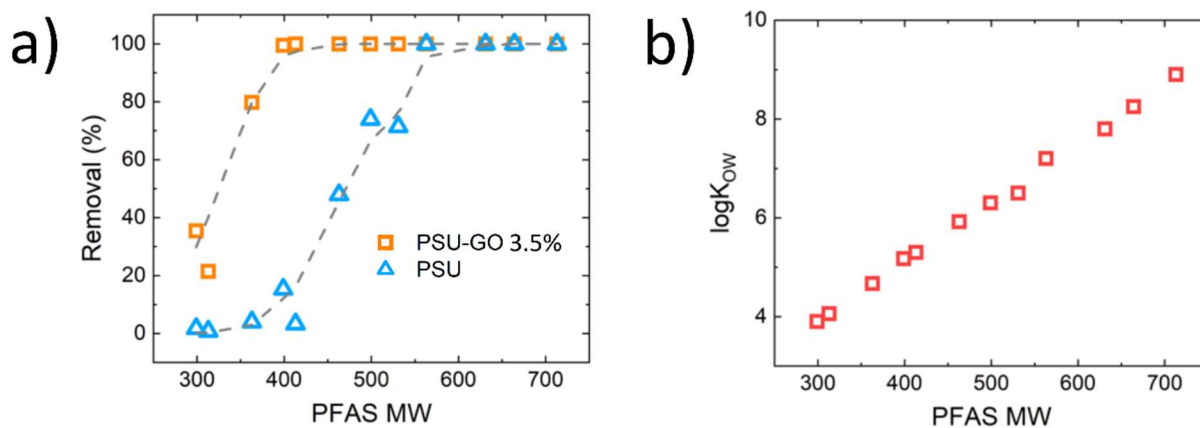


Fig. S8. a) Removal of a mixture of fourteen PFASs in tap water by PSU (blue) and PSU-GO 3.5% (orange) vs the molecular weight of PFASs. b) LogK_{ow} of fourteen PFASs vs their molecular weight.

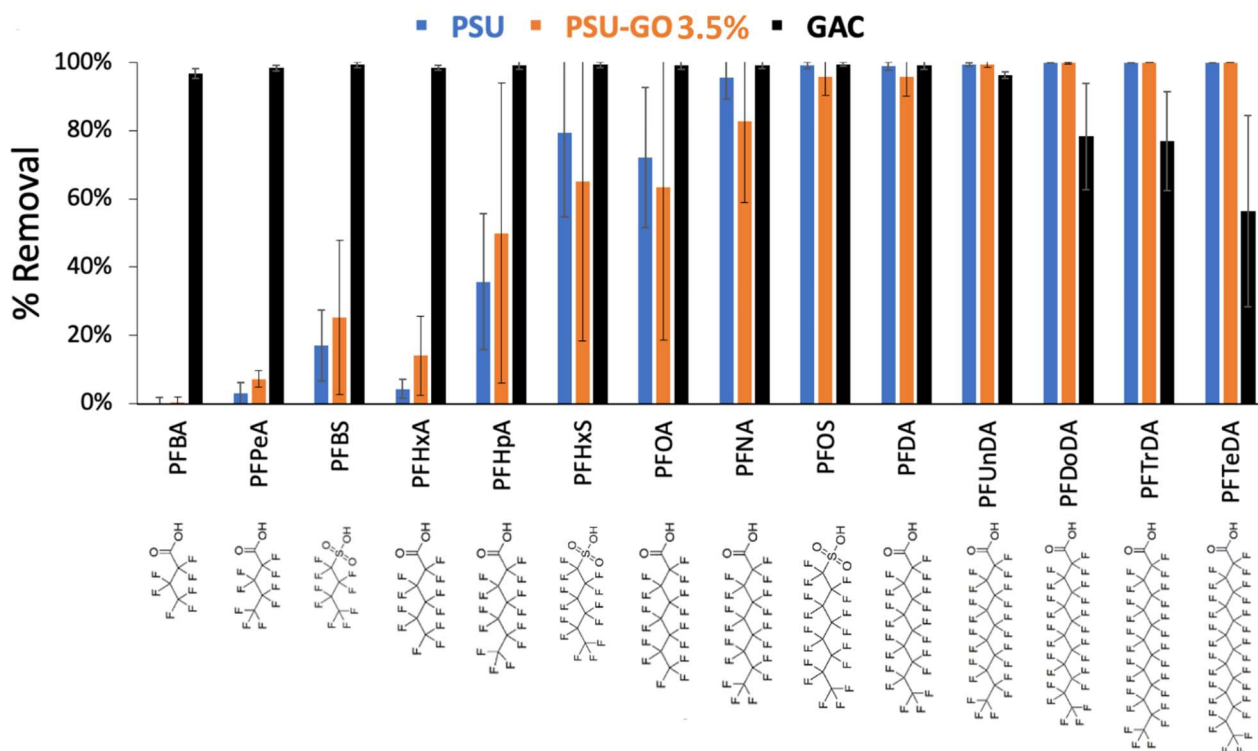


Fig. S9. Removal of a mixture of fourteen PFASs in tap water, total volume=250 mL, C_{IN}= 10 μg/L, flow rate= 5 mL/min. Amount of material in the module: PSU 0.26 g, PSU-GO 3.5% 0.27 g, GAC 2.3 g.

6. Heavy metals experiments

Parameter	Value
EC ($\mu\text{S}/\text{cm}$)	495
Fixed residue (mg/L)	275
pH	7.38
Ca^{2+} (mg/L)	95
Na^{+} (mg/L)	3.2
Mg^{2+} (mg/L)	1.3
K^{+} (mg/L)	0.65
HCO_3^{-} (mg/L)	289
SO_4^{2-} (mg/L)	2.5
Cl^{-} (mg/L)	5.1
F^{-} (mg/L)	0.05
NO_3^{-} (mg/L)	7.7
SiO_2 (mg/L)	7.2

Table S4. Natural water parameters. Natural water is the commercialized bottle water “Nocera Umbra”.

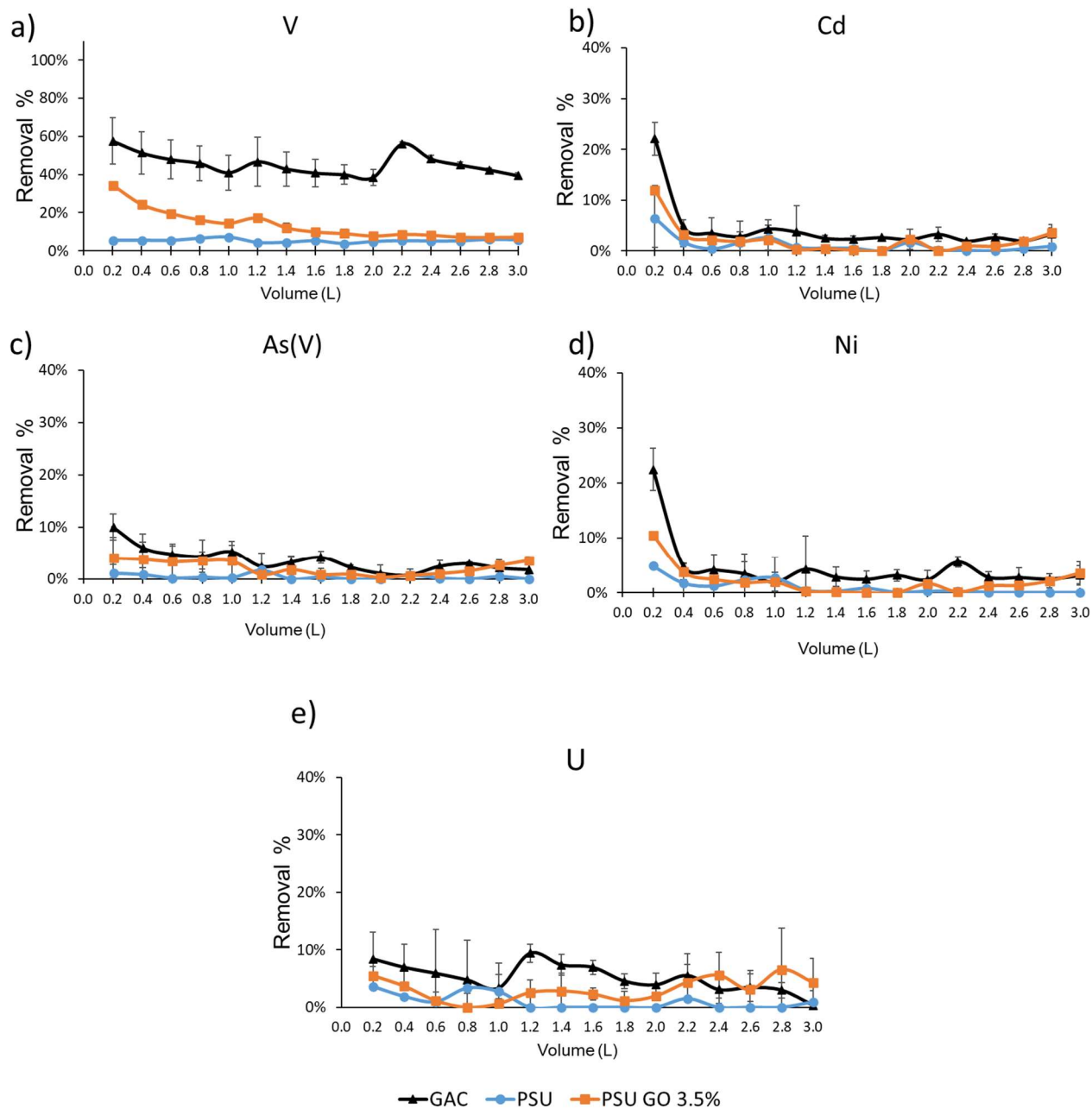


Fig. S10. Removal efficiency of selected heavy metals and metalloids in mix. Initial mix concentration 100 $\mu\text{g/L}$, Flow rate 5 mL/min, treated volume 3 L. A comparison of three different modules is reported: PSU (blue), PSU-GO 3.5% (orange), and GAC (black). Experiments were repeated in duplicate, reported mean value and standard deviation.

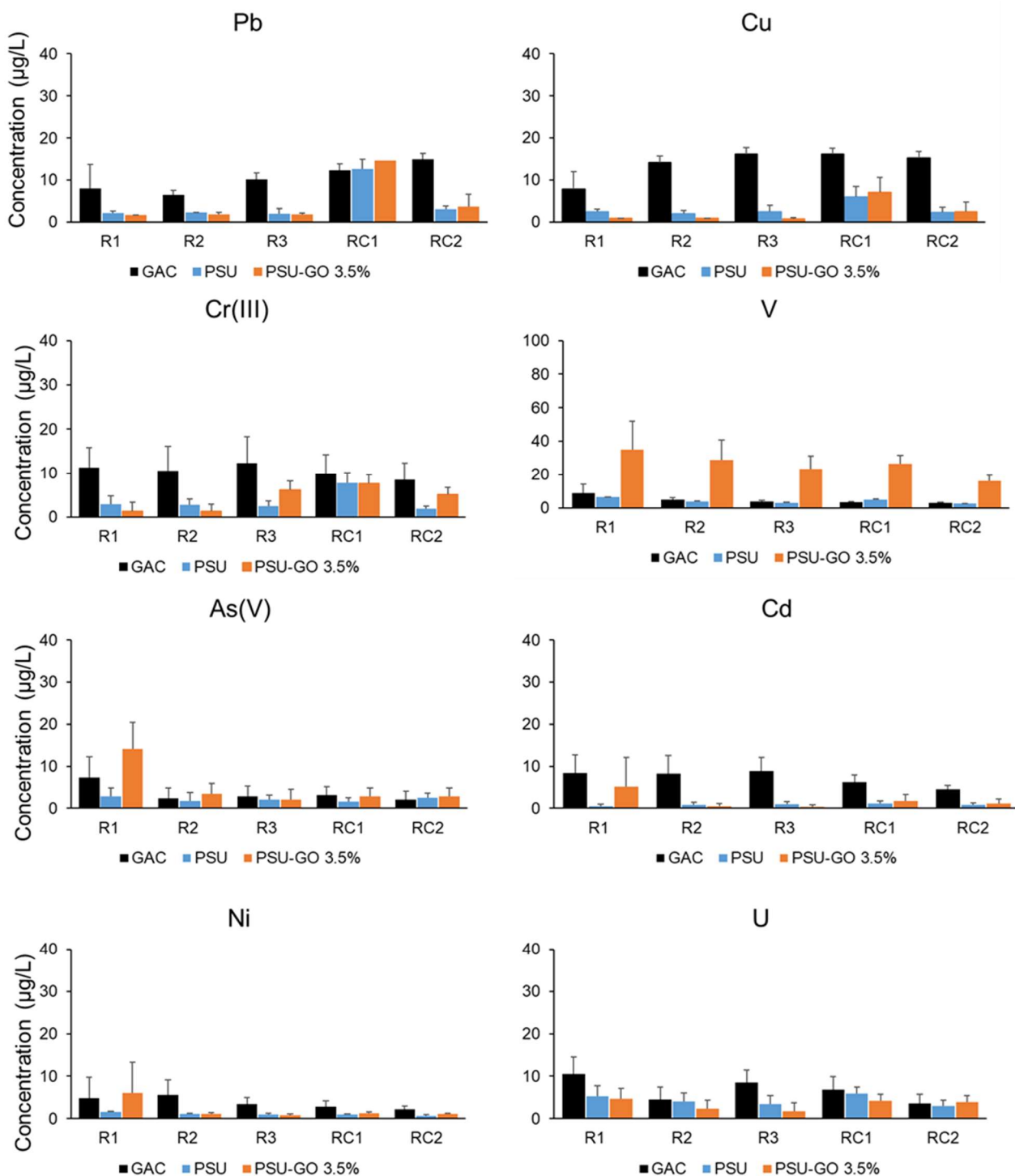


Fig. S11. Released concentration after washing modules (PSU, PSU-GO 3.5% and GAC) after adsorption tests. Flow rate = 20 mL/min. Three fractions (R1, R2 and R3) of 50 mL Milli-Q water in direct flow (in-out) and 2 more fraction (RC1 and RC2) of 50 mL in reverse flow (out-in).

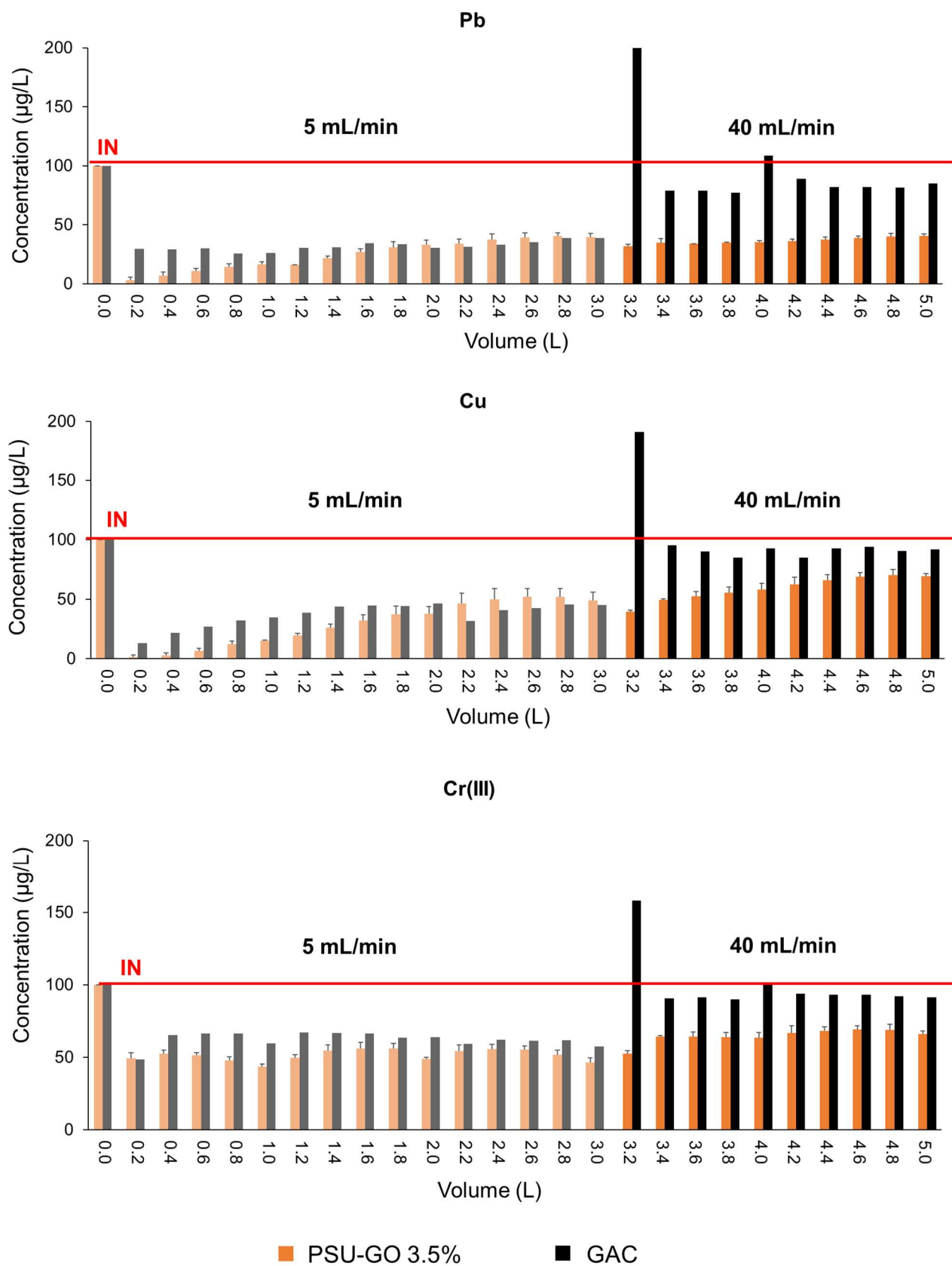


Fig. S12. Treated water concentration comparison of PSU-GO 3.5% (orange) and GAC (black) performance at two different flow rate (5 and 40 mL/min). Reported trend for selected heavy metals with higher removal efficiency (Pb, Cu and Cr (III)).

Element	GAC	PSU	PSU-GO 3.5%
As	9%	58%	19%
Cd	14%	7%	7%
Cr	3%	2%	1%
Cu	2%	2%	0%
Ni	7%	10%	8%
Pb	1%	1%	1%
U	9%	39%	9%
V	1%	10%	16%

Table S5. Total release (percentage) of adsorbed heavy metals at end of experiments (flow 20 mL/min, 150 mL passed in-out and 100 mL out-in).

7. Water potability tests

Risultati analitici				
Parametro <i>Metodo</i>	U.M.	Risultato	Incertezza	Limiti
ATTIVITA' DI LABORATORIO				
* Torbidità APAT CNR IRSA 2110 Man 29 2003	NTU	< 0,02		
Odore APAT CNR IRSA 2050 Man 29 2003		Inodore		
Sapore APAT CNR IRSA 2080 Man 29 2003		Insapore		
Colore APAT CNR IRSA 2020 A Man 29 2003		Incolore		
pH APAT CNR IRSA 2060 Man 29 2003	upH	8,0	±0,4	6,5-9,5
* Carbonio organico totale (TOC) UNI EN 1484:1999	mg/l	< 1		
Conducibilità APAT CNR IRSA 2030 Man 29 2003	microS/cm	508	±38	< 2500
Durezza totale (da calcolo) APAT CNR IRSA 3010 B + APAT CNR IRSA 3020 Man 29 2003	°F	55	±11	15-50
* Residuo fisso a 180 °C APAT CNR IRSA 2090 B Man 29 2003	mg/l	389,0	±31,1	< 1500
Azoto ammoniacale (come NH4+) UNI 11669:2017	mg/l	< 0,02		
Cloruri APAT CNR IRSA 4020 Man 29 2003	mg/l	38,50	±3,85	< 250
Solfati APAT CNR IRSA 4020 Man 29 2003	mg/l	117,1	±14,1	< 250
Nitriti APAT CNR IRSA 4020 Man 29 2003	mg/l	0,07	±0,01	< 0,5
Ferro (ICP-MS) EPA 6020B 2014	ug/l	9,2	±0,8	< 200
Alluminio (ICP-MS) EPA 6020B 2014	ug/l	7,6	±0,7	< 200
Manganese (ICP-MS) EPA 6020B 2014	ug/l	< 0,1		< 50
Sodio APAT CNR IRSA 3010 B + APAT CNR IRSA 3020 Man 29 2003	mg/l	38,81	±5,59	< 200
Conta Escherichia coli UNI EN ISO 9308-1:2017	UFC/100 ml	0		< 0
Conta Enterococchi intestinali UNI EN ISO 7899-2:2003	UFC/100 ml	0		< 0

Bologna Il: 30/03/2021

Il presente Rapporto di Prova si riferisce esclusivamente ai campioni sottoposti a prove ed è valido per tutti i casi previsti dalla legge come da R.D. 1/3/28 n. 842, art 16. Questo Rapporto di Prova non può essere riprodotto parzialmente salvo approvazione scritta del Laboratorio. Analisi eseguite presso la sede di Bologna

Pagina 2 di 4



LAB N° 1051 L

segue Rapporto di prova n°: **21BO04571** del **30/03/2021**

Risultati analitici				
Parametro	U.M.	Risultato	Incertezza	Limiti
Metodo				
Conta coliformi totali UNI EN ISO 9308-1:2017	UFC/100 ml	0		< 0
Microrganismi vitali a 22°C UNI EN ISO 6222:2001	UFC/ml	0		< 100

Limiti: » D. Lgs. 31/01 Agg. D.M. 14/06/2017
Il simbolo "<" riportato nei limiti sopra elencati va inteso come "inferiore o uguale".

Table S6. Water potability tests results.

8. SERS experiments on GO release

The SERS-active substrate was prepared in the following way: gold nanoparticles (AuNPs; 20 μ L of a 10.7 nM solution) were deposited dropwise on a Si/SiO₂ substrate. Subsequently, 120 drops (1200 μ L) of analytical solution were added to the center of the SERS substrate. The sample was analyzed by SERS detection using an InVia Renishaw microspectrometer equipped with a 532 nm point-based laser. The power density was kept below 10% and a 1 s acquisition time was employed to avoid laser heating effects. SERS measurements were acquired for 400 μ m² surfaces located in the middle of the drops with an average of 3000 spectra measurements. The baseline was removed using Windows®-based Raman Environment (WiRE) software. The 3000 spectra were then averaged to give a single spectrum for each replica, using a program generated in MATLAB R2020a with our own code. The spectrum of AuNPs was used as the control and was subtracted in all the samples to avoid the interferences.

Sample	Filtered Volume (mL)	Intensity 1350 cm ⁻¹ (a.u.)	RSD% ^a
WPSU_1	250	21.17	5.35
WPSU_2	500	18.75	4.08
WPSU_3	750	19.98	2.45
WPSU_4	1000	20.45	5.05
WPSU_5	500 in recycle for 2h	15.33	4.71
WPSUGO_1	250	34.62	2.89
WPSUGO_2	500	35.91	5.47
WPSUGO_3	750	32.87	3.17
WPSUGO_4	1000	27.09	3.88
WPSUGO_5	500 in recycle for 2h	41.34	3.83
TAP water (reference)	Nonfiltered	14.11	3.32

Table S7. Filtered water samples and intensity values (1350 cm⁻¹) measured on SERS substrates.
^aRelative standard deviation (RSD) of intensity values (3000 points per sample).

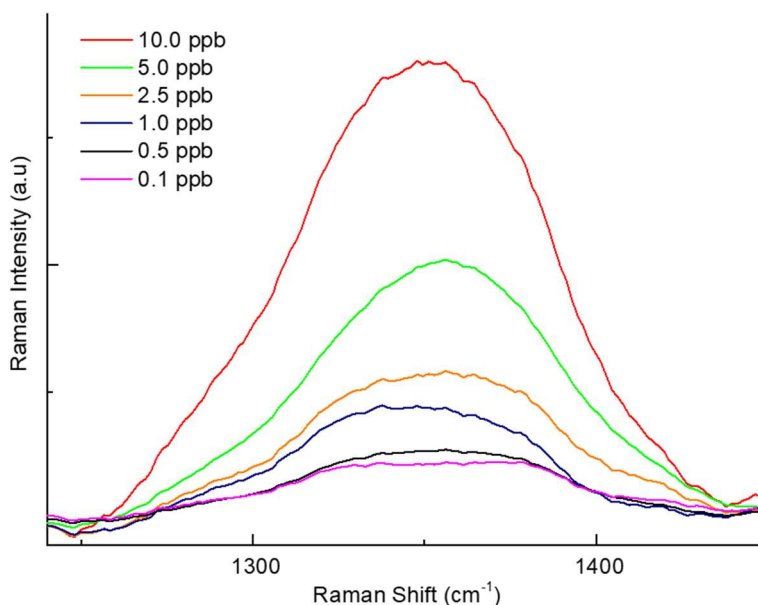


Fig. S13. Average Raman spectra of different concentration of GO (0.1- 10 ppb) measured on SERS substrates ($R^2 = 0.995$; LOD (ppb) = 0.11; P-LOQ (ppb) = 0.10).



Fig. S14. PSU-GO 3.5% HF module opened with a hacksaw.

Samples		Weight (mg)	Intensity 1350 cm ⁻¹ (a.u.)	RDS%	Concentration detected (ppb)	%GO release
FPSUGO Used_1	A	1.32	285.95	3.86	2.77	0.12
	B	1.32	296.08		2.90	0.13
	C	1.32	308.80		3.06	0.13
FPSUGO Used_2	A	2.18	549.39	2.71	6.12	0.16
	B	2.18	568.53		6.37	0.17
	C	2.18	539.01		5.99	0.16
FPSUGO Used_3	A	4.00	671.10	3.77	7.67	0.11
	B	4.00	629.49		7.14	0.10
	C	4.00	628.72		7.13	0.10
FPSUGO New_1	A	1.24	239.88	5.10	2.18	0.10
	B	1.24	239.17		2.17	0.10
	C	1.24	261.31		2.46	0.11
FPSUGO New_2	A	2.21	351.37	4.32	3.60	0.09
	B	2.21	383.00		4.00	0.10
	C	2.21	369.84		3.84	0.10
FPSUGO New_3	A	3.99	547.31	0.43	6.10	0.09
	B	3.99	546.25		6.08	0.09
	C	3.99	542.82		6.04	0.09

Table S8. Data obtained from water samples prepared from sonication of different weights of fibers. RSD is the relative standard deviation from the average intensity values of three replicates (A, B and C) for sample. All the intensities result from the subtraction of the control intensity from the intensity obtained from PSU-GO samples.

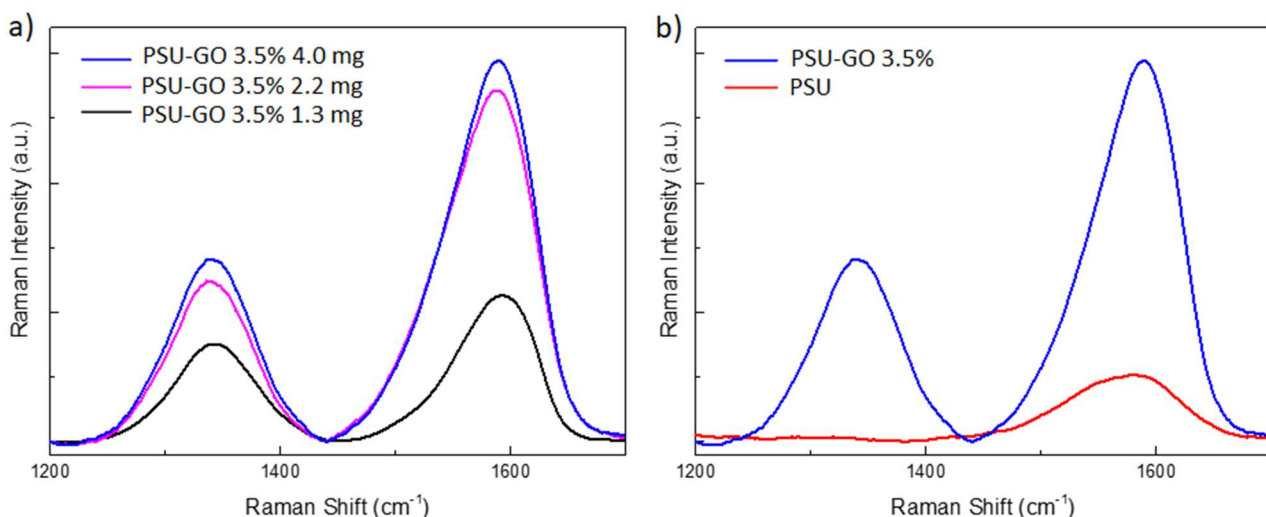


Fig. S15. SERS spectra of water samples prepared from 30 min of sonication of different quantities of PSU-GO 3.5% HF scraps: a) 1.3 mg (black), 2.2 mg (pink), and 4 mg (blue). b) Comparison of the same amount (4 mg) of PSU HF (red) and PSU-GO 3.5% HF (blue) scraps after 30 min of sonication.

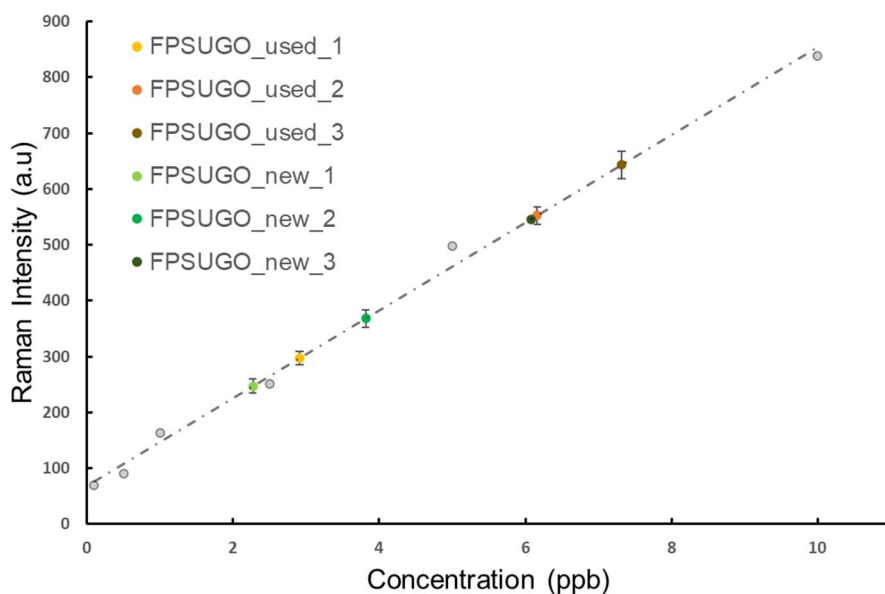


Fig. S16. Calibration line and measurements of water samples prepared by sonication of different quantities of fibers.

9. Preliminary real conditions POU test

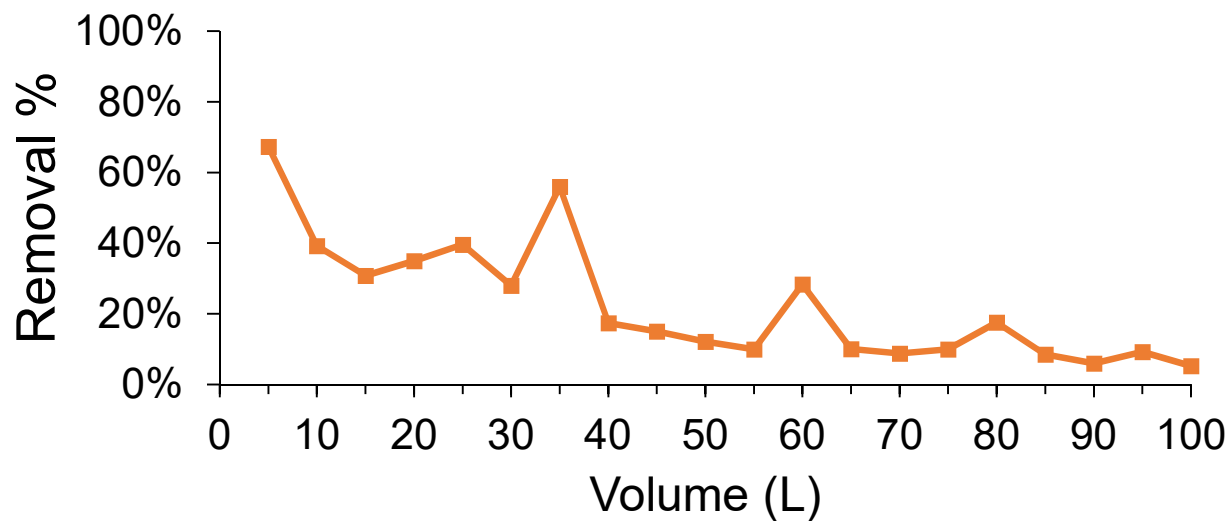


Fig. S17. Removal of CIPRO (1 mg/L) from PSU-GO 3.5% HFs (FS 0.28m², U-shaped HF) connected at the tap (at 2.8 bar). Composite weight in each module about 6 g, with 210 mg of GO.

